UiT
THE ARCTIC
UNIVERSITY
OF NORWAY

Department of Physics and Technology

Simulating and characterizing carbon based solar thermal absorbers

—

Amitap Jain

FYS-3900 Master's Thesis in Physics

May- 2014

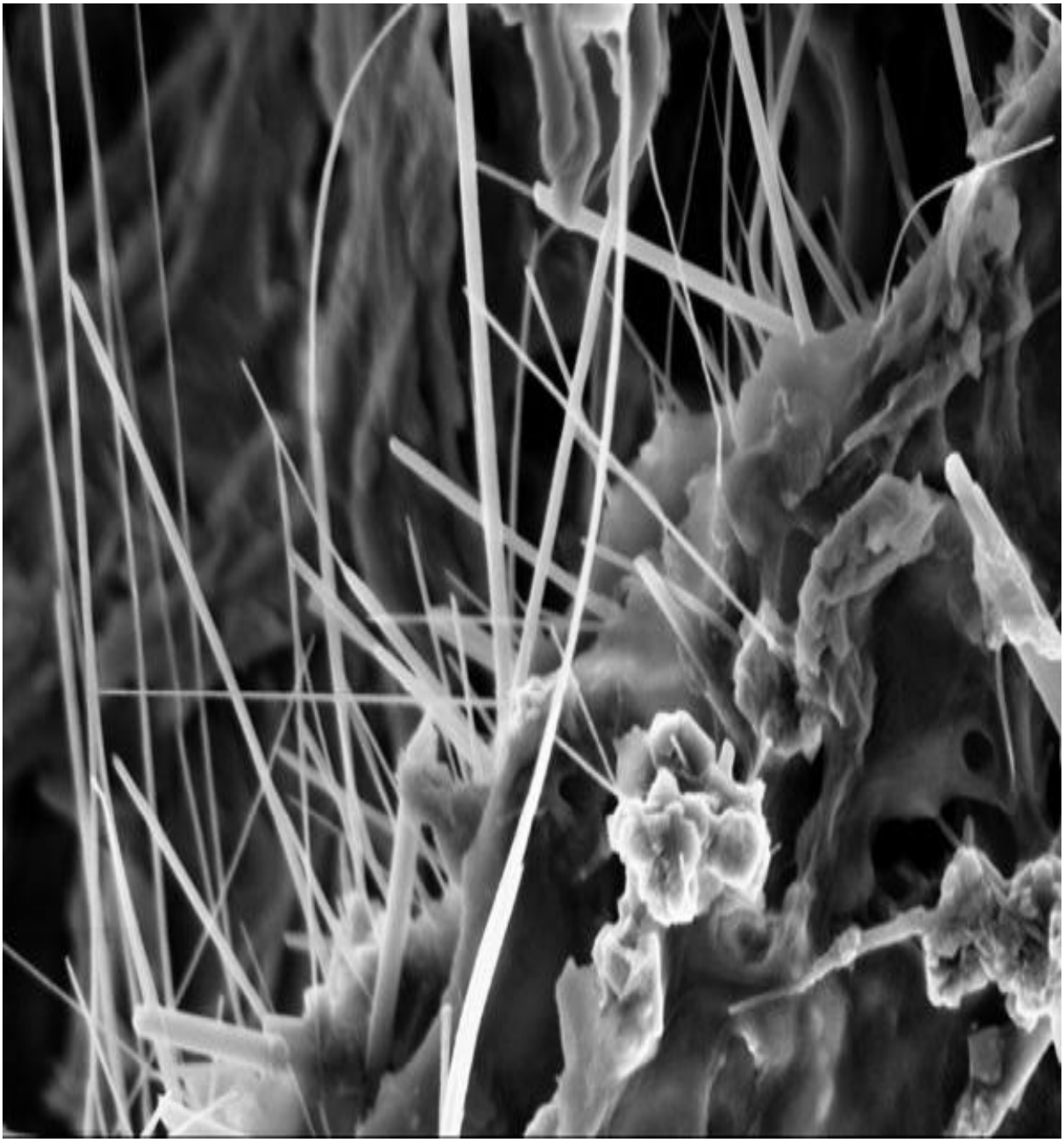

UNIVERSITY OF TROMSØ

Acknowledgment

First and foremost, I would like to express my huge gratitude to my supervisor, Professor Tobias Boström, for giving me the opportunity to study an exciting subject, both in terms of mathematics and renewable energy. He has been tremendously helpful in the development of this thesis by providing academic guidance as well as generous amounts of his own time and resources, from the initial concept to the final deliverance of this research. He has encouraged me to utilize my own perceptions and ideas while pursuing my own interests. I also owe my thanks to Dr. Jean Claude Tinguely, for the dedication of his time and his interest in continuous discussion and constructive criticism throughout this project. I would also like to thank Zhonghua Chen for allowing me to use his prepared samples for SEM and EDX, which were a crucial part of my experiments, as well as sharing details of his valuable lab experience.

Special thanks go to Thomas Kræmer, Adit Decharat and Muhammad Bilal for their continuous support and instruction throughout the writing of my master thesis. It would not have been possible without them. I would also like to thank friends and staff members at the Department of Physics and Technology for all of their help and inspiration in the completion of this project.

Finally, I would like to thank my family, especially Ashish Jain, and Tamara Karataeva for their support and encouragement throughout the duration of this Master thesis.

Abstract

The main objective of this project is to determine and characterize the optical and structural properties of carbon nanotube (CNT) coated aluminum substrates to facilitate better understanding regarding their suitability for solar absorption. In this way, it may be possible to utilize this material to produce improved and more efficient spectrally selective solar thermal absorbers in solar thermal collectors. The project started with a collaboration on characterization of Zhonghua's CNT samples and changed more to simulation of various carbon materials.

This project includes simulations for reflectance of seven different carbon materials at a variety of thickness levels in order to observe the variation of reflectance in visible and infrared wavelength regions, as well as their respective absorptance and emittance. An anti reflection coating was also added in order to increase the absorptance values. The samples prepared by Zhonghua Chen (PhD Candidate) were utilized in surface morphology by application of scanning electron microscopy to investigate the properties of an absorbing surface, such as structure, uniformity, porosity, CNT alignment and homogeneity. Energy dispersive x-ray spectroscopy was also conducted in the characterization of various elements.

Contents

List of Tables

List of Figures

Chapter 1

Introduction

Throughout the majority of the duration of mankind, renewable energy has been the only energy-source option available in forms such as mainly bioenergy, sun, wind and water. These natural resources are always available and can be harvested by humans as required. Renewable energy has been the main source of attainable energy in the past. Solar radiation provided the necessary heat for habitats to make life on Earth possible, as well as the high-quality energy needed to grow food. The food could then be converted by the human body into energy for maintenance and external work. Only during the last few centuries have fossil and (more recently) nuclear energy sources been used in a nonrenewable way. These moved to the forefront because of their availability in abundant quantities (in some particular areas), and seemed much cheaper than renewable sources. However, environmental problems on a local as well as global scale were always in existence, but are now becoming more apparent. This has raised such questions as: are the fossil and nuclear choices actually the cheapest way of producing primary energy? And have we considered the indirect costs of continuing to drain these sources? In any case, renewable-energy options have been developed in very few areas around the world, and the reasons behind their successes and failures must be evaluated for the better and safer future of forthcoming generations [1].

In this modern era, we cannot even dream of an existence without energy. Our reliance upon energy makes it considered one of the most vital elements to the economic stability, progress, prosperity and development of any country. It can also affect other sub-related fields with respect to the main concern of any nation, such as eradicating poverty, enhancing future development, and addressing security concerns. Obtaining an uninterrupted energy supply has been a vital issue for both developing and developed countries alike. Future economic growth of all countries depends on the long-term

availability of energy from sources that are more affordable, accessible, and environmentally amicable, and can sustain consumption for long time spans such as fossil fuels. Development, climate change, security and public health are significantly dependent upon energy. Profuse, continuous, cheap, and clean energy sources are required for modern and acceptable human living conditions, which in turn lead to a prosperous and healthy economy [2]. In the past few decades, a staggering increase in developmental activities across all sectors has triggered a growing demand for energy (which is often met by burning fossil fuels)that unfortunately results in further contributions to adverse effects on the climate. In fact, the world has already experienced its first and second energy crises due to the oil and gas scarcities in 1973 and 1978, respectively [3].

Human beings have come a long way from living in a completely uncivilized, unknown universe to the modern, fascinating and fast lifestyle that many of us experience today. There are many inventions that are common in current times that were unimaginable in previous centuries. Civilization has drastically changed our perception of life within a very short amount of time, and by actively engaging in long-term study we will continue to grow and learn. But this comes at a price. To maintain the pace of development and invention that we have become accustomed to, we must continue to use these energy-intensive techniques which lead to further energy demand [4].

We face many challenges for the future, such as the risk of our conventional sources of energy becoming depleted, and potential worsening of environmental issues such as global warming, ozone layer exhaustion, etc. Thus, we must constantly be searching for additional sources of energy, but in a way that will not deteriorate our future environment further and could be considered Eco-friendly. There are options that we can pursue such as non-conventional or renewable sources of energy. These are abundant and pollution free, and their nature is discrete. In the future, they will likely serve as a substitute for the problematic conventional sources that we rely upon today. But in order for this to be a viable option, we require much needed technological-development and intensive research work. The cost of renewable energy production per unit is higher and the efficiency is much lower than the energy coming from conventional sources. A staggering 1.6 billion people worldwide have no access to modern technology, mostly belonging to developing countries, and could greatly benefit from such energy sources. But access is only realistic if the source is cost-effective [4].

Nanotechnology may be the key to unlocking the future of energy production. Such scientific breakthroughs have brought us a new revolution in almost every field of research, and provide us with a great amount of internal information about all processes and materials. It also leads to much more

effective economical structures by reducing their cost, their size, the quantities of materials used, and by improving their efficiency. It is a steady and strong tool that may be used to build sustainable development in the energy sector. Nanotechnology is an option with an inherent ability to improve power production, its storage and more efficient usage. This technology is able to handle any size of nanostructure, from microscopic to molecular. It has introduced us to the study of nanoscale ranges regarding materials, and with its use we can manipulate the properties of any material in the range of atoms to molecules to improve design and widen the range of potential applications [5].

Renewable energy is the energy that is derived from natural processes that restore themselves constantly. There are various forms of renewable energy, derived directly or indirectly from the sun as well as from heat generated deep within the Earth. Renewable energy resources include solar, wind, biomass, geothermal, hydroelectric power and ocean resources, solid biomass, bio gas and liquid bio fuels.

Over the past millions of years, a long time decomposition of doomed plants and bones of animals and buried and compressed beneath of rock and sand. This pressure has turned them into organic materials which then formed fossil fuels. Since plants and animals originally use the energy of sunlight to grow and thrive while still alive, the sun's energy is stored in chemical form within the decomposing bodies which transition into fossil fuels.

Coal and crude oil were not usable as energy supplies at the end of the 18^{th} century. The burning of firewood and the harnessing of hydroelectric power were the only ways of meeting energy demands at that time. Watermills and windmills were common features of the countryside. In 1769, James Watt laid the foundation for industrialization by developing the steam engine. Later, the invention of the internal-combustion engine rapidly replaced most of the mechanical watermill and windmill installations. Due to the invention of the engine, coal emerged as the single most important source of energy during that period. However, in the beginning of 20^{th} century, the increased demand on the current energy supply made reliance upon a single source impossible, so crude oil was introduced to support the increasing popularity of motorized vehicles. Furthermore, due to large industrial growth and consumption, hydroelectric power plants came into the picture and made windmills nearly obsolete. Natural gas also came into existence after the second World War. During $1960s$, the new source called nuclear energy was added to conventional energy sources, but the role of nuclear energy remained low due to its volatile nature and need for heightened security. The dominant sources that meet the primary energy demand of nations worldwide are now coal, oil and

natural gas [3].

When the use of fossil fuels as energy became possible on a larger scale due to a higher focus on technological development, few renewable-energy techniques were taken seriously as competition. In the year 1900, solar power was estimated to cost about 10 times that of competing fossil power. Wind power was found to be similar to fossil fuels in terms of costs, but by then it was too late. Fossil energy systems were being developed and certain infrastructures were built around them, which were more suitable to firms of that time, making it difficult to switch to a different form of energy [6].

Non-conventional energies are especially useful in rural areas, where renewable resources abound and can play an extremely important role. They can significantly contribute to the improvement of quality of life for local populations. Rural areas may be the perfect place for brand new patterns of development to emerge, which may lead to natural resource preservation and their rational use and re-use. This will stem from a concern for environmental protection, energy independence and public participation in the management of new environmental supply systems. In rural areas, wind is used to produce energy by utilizing mini-grids and hybrid systems for entire villages. The use of wind and solar PV technologies in these kinds of systems is on the order of a thousand systems worldwide, mostly installed in China. India is another main location for village-scale power systems. Another possible use for wind power in rural areas is water pumping, both in terms of irrigation and as drinking water. Renewable energy, therefore, can be considered a contribution to access strategies in rural and remote areas. It helps to increase services for rural populations that do not have access to central electric power networks. Moreover, renewable-energy technologies represent a cost-effective alternative to grid-extension in remote areas and in developing countries. Renewable resources, in fact, are a convenient choice in respect to conventional fuels and traditional grid extension in terms of economic costs [7].

This report is structured as follows: Chapter 2 includes relevant theory regarding solar energy and solar radiation, followed by an economic and financial evaluation of solar energy. Chapter 3 provides information pertaining to solar thermal systems, such as design, components, classifications and an examination of various types of spectrally selective solar absorbers. Chapter 4 presents information regarding carbon nanotubes in terms of categorization, synthesis, characterization and the use of carbon nanotubes as solar thermal absorbers. Chapter 5 includes information pertaining to the optics of thin film, including the associated theoretical background. Chapter 6 covers the methodology applied in this research, including the optical and structural characterization tools utilized, as well as detailed information regarding the

simulation of carbon materials. Chapter 7 demonstrates sample preparation combined with details regarding substrates, carbon nanotubes and anti reflection solutions, as well as their individual deposition methods. In Chapter 8, the results of the experiments are discussed, including simulation of reflectance, further calculations of absorptance and emittance values, scanning electron microscopy and energy dispersive x-ray analysis and validation of the refractive index. Finally, a conclusion sums up this work, along with suggestions for further research in Chapter 9.

Chapter 2

Solar energy

Renewable energy is the energy generated from natural resources, which renews itself automatically. However, all renewable energies (aside from geothermal and tidal) derive their energy from the sun. Around the world, engineers are working hard to develop technologies to tap into the clean power of renewable-energy resources due to their enormous potential to produce huge quantities of energy without generating greenhouse gases or any kind of pollutants, which can negatively contribute to climate change. There are a wide range of renewable sources available with great possibilities for improving our future, if only we can learn how to best use them to our advantage.

Solar energy stored in the form of fossil fuels was probably used for the first time some 9000 years ago when prehistoric man began burning oil as a light source, although technically oil falls under the umbrella of nonrenewable resources. Fossil energy is not usually encompassed in the range of renewable energy forms. The photovoltaic (PV) effect was discovered by Edmond Becquerel in 1839, but solar cell applications did not gain considerable momentum until 1954. That is when Bell Laboratories developed successful photovoltaic panels in response to space program demands which presented favorable conditions for the use of photovoltaic (PV) panels [1].

Renewable energy is created by the biggest and strongest natural source available to us, which is the*Sun*. It is transformed into various forms of energy (e.g. solar radiation into wind or wave energy) and spread over the Earth's atmosphere with the help of several complex processes. These processes are essential for the general circulation occurring in the atmosphere and in the ocean. The energy system experienced by the inhabitants of the Earth is dominated by the environmental heat associated with the greenhouse effect, which captures solar energy and stores it within the upper sheets of topsoil and in the atmosphere around the Earth.

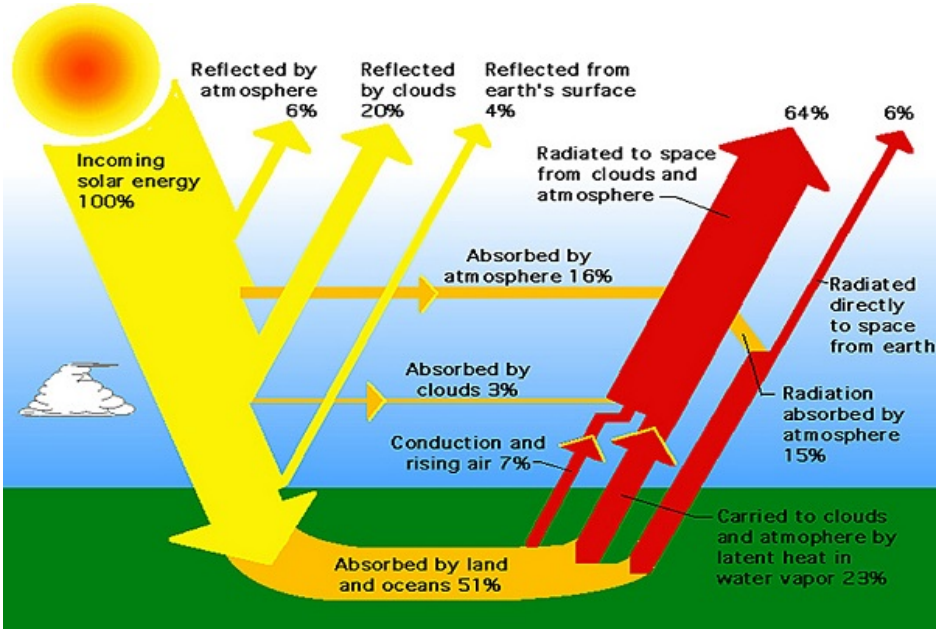

Figure 2.1: A typical view of global energy budget [9].

As previously mentioned, most of our energy comes from the sun, and it is called solar energy. This energy travels from the sun to the Earth in the form of rays. The sun radiates huge amounts of energy every day, and most of that energy is lost in space, as only a small part reaches the Earth. Sunlight turns into heat when it hits any surface. Solar energy circulation is a combination of many elements and internal processes. Figure 2.1, demonstrates how diverse and important that process can be [8].

It requires three main processes to transfer energy from the sun to the Earth: reflection, absorption and conduction. A large portion of the total incoming solar energy is absorbed by the land and ocean, which provides the necessary energy creatures require for survival by direct or indirect means. Another large portion is radiated back into space through the clouds and the atmosphere. A small amount of this energy is absorbed by the atmosphere to make the temperatures propitious for life on Earth. Therefore, without the sun we could not live on the Earth because the freezing temperatures would make it uninhabitable. Solar energy has enormous potential as a clean, abundant, and economical energy source, but it can be difficult to put that energy to use. First it must be captured and converted, and since solar energy is diffuse and intermittent, conversion must involve concentration and reliable storage [8].

We can transform this incoming solar energy into other kinds of useful

energy:

- Solar thermal: Incoming sunlight can be used directly for the heating of buildings and water, and also indirectly for inner space heating through windows.
- Solar photovoltaic: Converting sun radiation into electricity.
- Solar biomass: Using trees and plants, wooden blocks, anaerobic bacteria, algae, agriculture waste or oilseed to make energy fuels, biogas, methanol etc.
- Food: All plants and vegetation grow with the help of energy from the sun which is stored in their roots and leaves. That energy feeds every living thing on Earth in a variety of ways.

  This following paragraph is refer to source [10].

2.1 Energy conversion in the sun

The sun is giant nuclear fusion reactor, which generate it's power by conversion of hydrogen into helium at the rate of 4 million tons per second. It's high surface temperature is approximately 6000°C, which radiates energy outward. Of this radiation, approximately one-third is reflected back into space by the Earth's surface. The rest is absorbed and eventually retransmitted into deep space. The Earth without any atmosphere can re-radiate the same energy that it receives and remains in a stationary energy balance at a temperature that suitable for life [11].

2.2 Solar radiation

Sunlight is a part of electromagnetic radiation. As demonstrated in Figure 2.2, sunlight hits the Earth as infrared, visible and ultraviolet light. The light dribbles through Earth's atmosphere, is absorbed and then reflected by clouds into space. The sun is also the ultimate natural source of vitamin D for human beings. Radiation from the sun is more dense in the upper layers of the atmosphere than it is in the lower layers. All hot objects emit light and heat as electromagnetic radiation in regard to their temperature. A body at a certain temperature, that can emit the maximum quantity of radiation and can also transfer the identical radiation to it's surroundings, is known as a black body or the Planck spectrum. So, the sun spectrum is a spectrum that relies on the body temperature [12–14].

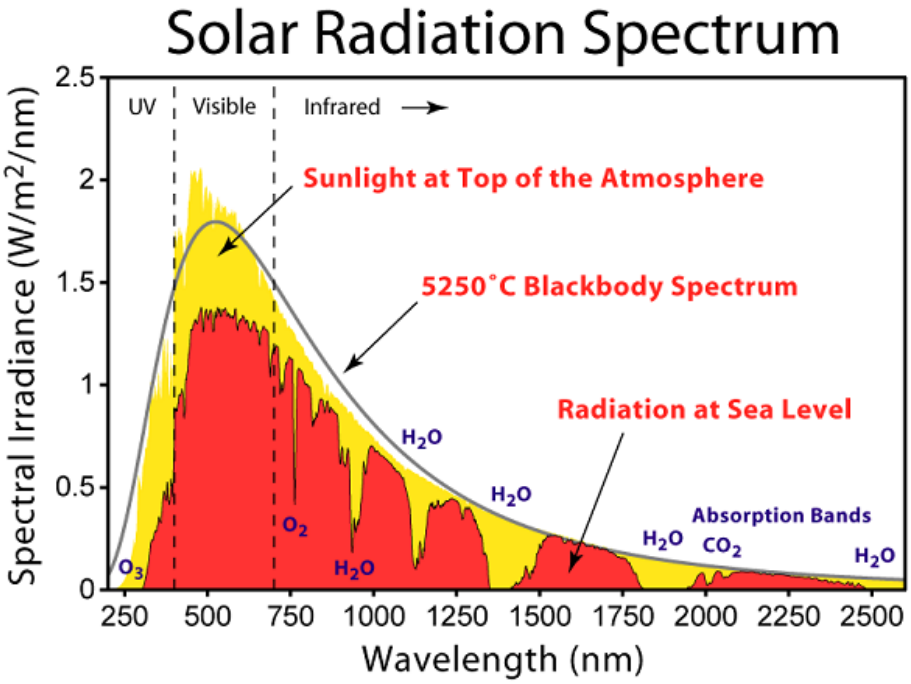

Figure 2.2: Solar irradiance spectrum above atmosphere and at sea surface with black body radiation [15].

The sun radiates energy in a wide spectrum that can range from ultraviolet(UV) to infrared radiation, but our eyes are sensitive to less than one octave of these, the visible region extending from 400 to 750 THz or 750 to 400 nm. The term power density is used to indicate watts per square meter(W/m^2), or the amount of solar power (instantaneous energy flux) falling on a unit of area per unit of time. We also have other technical terms that can define solar radiation in other ways; the amount of solar energy falling on a unit of area over a stated time interval. At the distance of one astronomical unit, the power density of solar radiation is about $1360W/m^2$, which is known as a solar constant. However, it is not really constant, as it varies throughout the year and the largest variation we notice is in January, while the Earth is nearest to the sun [16, 17].

Solar radiation incident on the Earth's surface is a result of multiple interactions of energy between the atmosphere and the surface. When the sun's rays come in contact with the atmosphere the light is then scattered, though it depends on the cloud cover at that particular point in time. Therefore, there are considered to be two kinds of radiation:

- Direct radiation: What is normally referred to as 'sunshine'(that of a part of the light that seems to come straight from the sun) is also known as direct radiation. In a day with clear skies, this can reach a power density of 1 kilowatt per square meter($1kW/m^2$) at earth surface.

- Diffuse radiation: The proportion of the light that still comes through after the process of scattering, known as diffuse radiation. In northern Europe it is common to experience diffuse radiation for over half of the year.

  This following paragraph refers to source [11].

2.3 Economic and financial scenario for solar energy

The most important problems that the world faces today is how to make solar energy economically and financially feasible. Conventional sources of energy are diminishing at a remarkable rate, and some researchers have already suggested a time horizon for their depletion. This means that the fossil fuel reserves that remain for future generations will not be adequate to meet their needs for modern life. It is possible that in the future people may find better uses for these energy sources as raw materials, rather than contaminating the atmosphere by burning them, as is currently the case. The

technology for the sustainable use of non-conventional energy or renewable-energy sources (RES) already exists and must continue to be improved, with the intent of slowing down our extraction and consumption rate of fossil fuels. Continuing to deplete these fossil fuels will only result in further destruction of the environment [18].

Finding new sources of energy is not the problem; the difficulty lies in making these energy sources economically attractive. Economic efficiency is the main concern when planning renewable power projects, as poor economic efficiency is one of the principal arguments against their development. That's why it is important to manipulate and estimate the cost of energy produced by different methods. The aim of economic calculations is to result in one outcome from various solutions that can provide the desired energy at the lowest cost. Therefore, the economic feasibility of various renewable-energy systems are compared and contrasted. Furthermore, renewable-energy systems are usually compared with conventional systems, but such comparisons do not take into consideration other harmful impacts or external costs. They are only concerned with economics. Typically the financing of such development is borne by the government, especially in the riskier, early stages of work, and is often a critical decision for any nation. However, most human activities consist of extensive fossil fuel consumption, which has led to undesirable phenomena such as global warming and environmental pollution, some of the most important challenges facing societies in recent decades. In addition, we are coping with one of the biggest threats to the future of humanity, which is how to provide an affordable, sustainable, and universally-available energy supply to all people of all nations. Renewable energy sources and energy efficiency improvements have the potential to provide the energy needed for human development. We currently have improved technologies which have reduced the cost of renewable energy production and seem feasible for the future promotion of renewable energy. Governments often try to influence the trade patterns of renewable energy technologies in order to support important national manufactures in international trade. By supporting research work and designing renewable energy parks, governments can help to educate people, raise awareness of renewable energy and also convey the importance of producing clean energy [19, 20].

Renewable energy sources are expected to become economically competitive, as their costs have already fallen significantly compared to conventional energy sources in recent years This will be of particular importance if the massive subsidies to nuclear and fossil forms of energy are phased out. Finally, new and independent renewable-energy sources offer huge benefits to developing countries, specifically in the provision of energy services to the people who currently lack them. In the past, renewable sources have been

completely discriminated against for economic reasons. However, the trend in recent years is in many cases to favor renewable sources over conventional sources. The advantages of renewable energy are that they are sustainable, available to every environment, and are essentially clean and environmentally friendly [21].

Chapter 3

Solar thermal system

The most common way to utilize solar thermal energy is for the heating of water and indoor spaces. But the collection and optimization of the Sun's rays could be handled in a much better and more efficient way. To attain this level of sophistication, complex physical systems must be utilized. Solar thermal systems use a combination of many accessories that make it feasible to harness solar thermal energy. These can vary from very simple to very complex structures. They also present the possibility to optimize natural, pollution-free energy sources for purposes of daily life while reducing the drain of primary energy sources.

The intermediate temperature potential offered by solar power is typically optimized by particular fields of interest such as food industries, clothing manufacturers and chemical markets. Around thirty percent of processing temperatures in most industries hover around 300°C or below, and such temperatures are conducive to new, advance solar thermal systems. These systems can play a great role in industrial manufacturing and processing. A favorable point for such systems is that the heat requirement in these sectors is more or less consistent throughout the year. A study conducted by the Energy Research and Development Administration (ERDA) suggests that 7.5 quadrillion Btu of fossil fuels are consumed to produce temperatures below 300°C for industrial process, and could easily be saved by the development of around 2000 systems utilizing solar thermal power. But the level of efficiency of solar thermal systems is still a big concern. Efficiency also plays a role in determining the size of the area needed to collect rays for a particular application, although the collector contributes more than 50 percent of the total cost for any type of solar system installation [22].

Usually the solar thermal collector is placed on the roof of the building in question in order to get the best exposure to sunlight. It works on a very simple and basic principle: whenever sunlight strikes the glass surface

of the collector, it is converted into heat and can be used for many purposes. The use of this heat-energy depends on the quantity of sunlight and energy system that derives its power from the collector, such as water heating, indoor heating and even to drive steam turbines for electricity generation.

3.1 Solar thermal system components and design

Solar activity is not consistent in all parts of the world due to the rotation of the Earth around the Sun. Solar radiation availability differs from place to place in regards to time, duration and intensity of activity. So to make optimum use of sunlight, solar thermal system designs should take local weather conditions and applications into consideration.

A solar thermal system can be viewed as one single unit, but it is actually a combination of several small components. The design and components of these systems vary according to the nature of expected application, such as domestic, commercial, personal, and or communal. Nevertheless, each has some basic common components which may vary in size and design in order to improve efficiency. These basic components are:

- Collector: A collector is a basic structure for capturing the radiation of the sun, which is a form of electromagnetic radiation. A collector is a necessary component of solar thermal systems, which captures incoming sunlight and transforms it into heat, which is then transferred into the water or working fluid in the system.

- Absorber plate: Absorber plate: This is an essential element of the collector, which absorbs the sunlight that falls onto the collector area and transforms it into heat. An absorber plate plays an important role in the design of the collector in terms of the absorption factor and efficiency levels. These elements predominately affect the total area used on a solar collector for a particular application.

- Insulation material: The transfer of thermal energy takes place from a higher to lower intensity and can be achieved by using a convection or a conduction or by radiation process. In the case of heat, it can be transferred by both processes. In order to prevent the undesired transfer of heat, the material must be designed with a shielding property called insulation material. Its basic function is to prevent heat transfer from inside solar thermal systems to the outside environment. The most commonly used insulating materials are:

  - Organic group: Cellular glass, glass wool with fibers.
  - Inorganic group: Polystyrene, sheep wool, cotton wool, polyester fiber.
  - Combined material: Glued Expanded polystyrene board, wool wood board, wood fiber board

    The section refers to source [23].

- Glass: Glass is a critical part of the solar thermal system and a main element in the collector. The function of the glass is to transmit and capture as much solar radiation as possible with the least amount of reflection. The glass also provides a shield of protection against seasonal variations and potential outer damage to the interior panel. Glass can be used in any size and shape, depending upon the required temperature for the area of interest.

- Water tubes: Water tubes located in a solar thermal system serve as an intermediate element which plays a role in transferring absorbed heat from the collector to a storage tank. In most cases copper is used for manufacturing the water tubes.

- Water storage tank: A water storage tank is a key element when it comes to storing and maximizing collected heat for later use. Especially in the case of solar radiation, it is useful to store excess heat whenever it's available, which is usually in the daytime. The water storage tank should have enough strength and insulation capacity to withstand the potentially damaging effects of the heat. It comes into direct contact with hot water through the collector, so the thermal strength must be high and the insulating capacity must be capable of holding the heat for a long period of time with minimum losses. Steel is the most favored material for storage tank manufacturers, but fiberglass is also often used due to its lighter weight, higher strength and cost-effectiveness.

- Valve: A valve is essentially a switch that controls and diverts the flow of water between the collector and the storage tank. It is also referred to as a safety switch in emergency situations to stop an excess flow of hot water to or from the storage tank.

- Pump: The requirements of a pump depend upon the type of solar heating system. In the case of an indirect or closed loop system, external force is needed for the circulation of cold water through the heat exchanger. Direct-current motor pumps are more common due

to lower starting voltage requirements, smoother functioning and less maintenance.

- Controller: This is a supervisory unit for the whole system making sure that working conditions are safe and efficient. It also plays an important role in addressing the failure of any interconnected components within the system by sensing the state of heat flow through these components.

- casing: The casing is the most outer part of the system which holds the collector assembly in place within its shell. It acts as a protective shield against normal weather conditions and also prevents any physical damage from extreme weather conditions. Casings are usually made from aluminum and steel with a coating of an anti-corrosive material, which protects against rain and moisture.

3.2 Classification of solar thermal system

Solar thermal systems can be classified in many ways. This section will cover some of the more popular classifications.

3.2.1 Direct solar thermal system

In a direct solar thermal system, the use of solar energy is of course direct. It captures the sun light directly through the collector and passes it on for a particular usage such as water or indoor heating. This is also called an open loop system. In this system the heat is transferred through a pipe to the water, and then this hot water goes to the connected storage tank where it is stored until it is used. Fresh water can be added to this system at any time. This kind of system much simpler in construction, more efficient and require less maintenance than an indirect system. The direct system, however, can only be used in warm weather conditions where the temperature is above zero degrees Celsius. A typical example of such a system is the thermosyphone solar water heater, which has a storage tank situated on the outside of the unit. It works by utilizing natural convection. The cold water is first heated and then rises from the collector into the storage tank, which is placed at a higher level than the collector. So in this way, the hot water circulates itself within the system.

3.2.2 Indirect solar thermal system

Unlike a direct solar thermal system, an indirect solar thermal system uses a heat exchanger to transfer the absorbed heat from sunlight into the end product. Indirect systems are also known as closed loop systems, because the same liquid heat exchanger circulates again and again through the system. The sunlight gathered through the collector passes into the heat exchanger and then is transferred into the water storage tank. Such systems are favorable in cold climate conditions where the temperatures are below freezing. Indirect systems can be a bit complicated, expensive and require more maintenance than direct systems. Water running outdoors in the indirect system also must be mixed with anti-freezing liquid, the glycol, in order to avoid blocking the pipes with ice formations.

3.2.3 Active solar thermal system

An active solar thermal system uses a combination of both solar collection and active design. In the case of active design, solar energy can be collected, stored, and then circulated into the desired place by using any external force such as a wind blower, central air conditioning system and so on. In this system, the heat absorbed by the heat exchanger can be circulated into the system by means of any mechanical mechanism (such as a pump) to release hot water and absorb cold water to and from the storage tank. This kind of system is more complex and more expensive than a passive system.

3.2.4 Passive solar thermal system

A passive solar thermal system does not rely on any kind of external force for heat circulation. It depends upon the natural convection of the rise and fall of hot and cold air respectively. A typical example of a passive system is the natural heating of any structure from incoming sunlight such as a solarium or a greenhouse. In such structures, sunlight passes through the glass and is trapped or absorbed by an interior structure to maintain a suitable temperature inside. The passive system can be improved and optimized by making certain changes to the design parameters to provide maximum exposure to solar radiation. Energy requirements from conventional sources can then be reduced for lighting and heating of the same area.

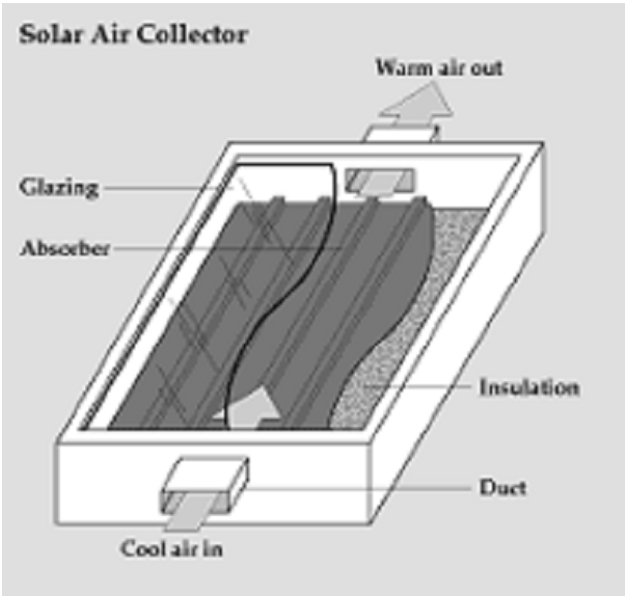

Figure 3.1: A classic view of flat plate solar air collector [24].

3.2.5 Basis on individual application

The solar thermal system can be categorized basis on the nature of application.

Air heaters: Air heaters are mostly optimized in two major fields providing hot air for the space heating and drying of crops, grains and textiles. They are simple in design and economical, requiring little maintenance. Their design can vary depending upon the combination of materials, the mode of application, the total cost and the temperature requirements. The basic components of an air heater are a collector, an absorbing plate, insulation, ducts and a casing unit to hold it all together. A simple flat plate solar collector is depicted in Figure 3.1. A solar air heater is a type of heat exchanger in which the absorbed heat is transferred into the incoming air. Solar radiation is absorbed by the absorbing plate and transferred into the flowing cold air from the inlet duct as the hot air flows out from outlet duct. Air heaters can be one of two types: either with glazing for space heating application with a recirculation system, or without glazing for agricultural purposes. A glazing layer is used to reduce convective and radiative losses, and also to hold the radiation between the glazing layer and the absorbing plate. It can further result in providing maximum opportunities to absorb most of the incoming radiation with the absorbing plate. Insulation prevents

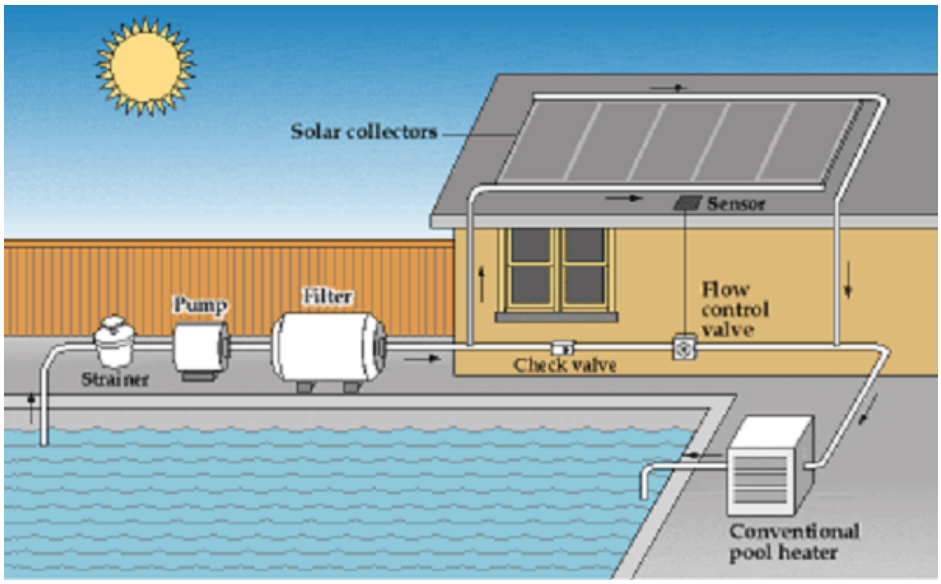

Figure 3.2: A typical view of a solar pool heater [27].

heat losses into the surrounding environment [25, 26].

Swimming pool heating: The concept of swimming pool heating is similar to that of indoor heating. In this case, a larger piece of unglazed plate solar collector is used to keep water just few degrees above the ambient temperature. Such solar heating systems are simpler in design and much cheaper in cost compared to traditional water heating systems. In addition, keeping the swimming pool covered can reduce the pool heating costs when not in use. Advanced versions of swimming pool solar water heaters consist of a flat plate collector, a pump, a filter, a control valve and a sensor, as evident in Figure 3.2. The working principle is quite simple: the water pump draws water from the swimming pool through a filter into the solar collector, where the water is heated before being sent back into the swimming pool again. The filter blocks any debris from reaching the collector area, such as rock, vegetation or animals. The control valve maintains the water allowed into the solar collector and can pass water directly into the swimming pool just past the filter. A sensor is typically used in more advanced versions of this system to check the water temperature variation between the solar collector and the swimming pool, which can trigger automatic control valve functions allowing it to be manually or automatically operated.

- Trombe wall: The concept behind a trombe wall was patented by Ed-

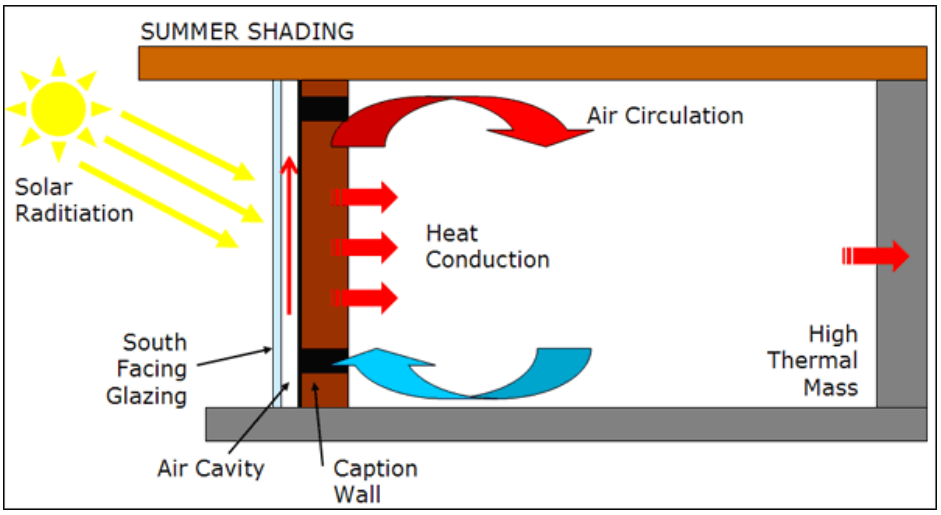

Figure 3.3: A simplified view of a trombe wall with air circulation [29].

ward S. Morse in 1881, but French architects Felix Trombe and Jacques Michel simplified it for public use in the 1960*s*. It operates as a passive solar thermal system and is very simple and useful for controlling indoor temperatures. A simplified diagram of a trombe wall can be observed in Figure 3.3, which shows the construction of a trombe wall and the circulation of the air within. A south-facing outer wall is constructed of glass next to an inner wall made of concrete, divided by a small pocket of air. This space between the two walls is called an air cavity, which acts as a natural solar collector for incoming radiation, and also plays a important role in hot and cold air circulation. The inner wall is fitted with upper and lower ducts for the intake of hot air and the outlet of cold air from the room. During the day this air cavity and the inner wall grow warm from the radiation of the sun, followed by the circulation of hot air throughout the room which forces out the cold air to provide additional heat. Even when the sun sets in the evening, the inner wall is filled with stored heat which keeps the circulation going until it finally grows cold. In order to stop the outside cold air from flowing into the room, the bottom duct can be closed so that the air can only flow in one direction throughout the night. The air cavity can be as wide as 3 to 6 *cm*, so frictional and heat losses can be minimized [28].

3.3 Collectors

A solar energy collector is the most important part of any solar thermal system. It has also been called the 'heart 'of the solar thermal system heat exchange process. The solar collector's basic function is to collect the incoming solar radiation and pass it into the working heat transfer fluid, such as water or air. Thus, this heat energy can be directly used for water heating or indoor heating, or stored for later use on cool nights and cloudy days [30,31].

3.3.1 Stationary collectors

A stationary collector is the simplest kind of collector, which does not have any tracking system to optimize the variation of incoming solar radiation during the day. This kind of solar collector is used for a low and medium applications.

3.3.1.1 Flat plate collectors

A flat plate collector is the most common, cost effective and available collector all around the world. It is a simple, rectangular structure that is easy to mount onto any surface. Due to its permanently fixed position, great care must be taken in regards to orientation, as it must be placed in such a way as to optimize the daylight in any season.

- Unglazed This type of collector consists of a black absorber plate, insulation and a water tube. The working principle for such a collector is straight-forward: incoming sunlight is collected by the absorber plate and it transfers the heat to the water tube in which cold water is circulating. An unglazed collector is suitable for such places where the water temperature can be lower than the ambient air temperature, making some heat loss of minor concern. A perfect application of this type of collector is swimming pool heating.

- Glazed In such a collector, glazing material is used to enhance the performance of the absorber plate. The property of the glass allows the transmission of most incoming short wavelength radiation to the absorber plate, and releases an almost negligible amount of emittance outwards in long wavelengths. Glazed collectors can be categorized on the basis of the medium used to collect heat, and these are described below:

Water flow: This is most common type of collector for water heating. In such a collector, water is used as a medium or end product to collect heat from the absorber. The water is circulated through the steel pipes in either a zigzag shape or through several pipes arranged in a parallel manner. While in such arrangements, the absorber must have a high thermal conductivity to transfer as much heat as possible into the water. The expected temperature gain is about 50 to 100°C.

Air flow: This type of collector is not as commonly used for air flow as it is for water flow, but it is still sometimes seen. Air is used as a source from which to collect and distribute heat for use. Construction-wise, this is a more simple design than for water flow, as it is composed of just one large duct allowing air flow to collect the absorbed heat. It is most commonly used for indoor heating. The possible temperature reached with this device is between around 50°C.

This subsection refers to source [11].

3.4 Analysis and performance of collector

The collector is a key component of the solar thermal system, which reflects the performance and efficiency of the entire system. To get a better understanding of each aspect, a collector analysis and performance evaluation should be carried out to ensure positive end results and future growth potential.

3.4.1 Thermal analysis of collector

Thermal analysis has a great deal of importance in many fields, especially in terms of heat flow, heat capacity, the thermal conductivity of a structure and heat transfer through a structure. Most of these factors are quite relevant and are related to the operating principles of the collector. The information available regarding the interaction of various materials with various temperatures is also detailed.

For a proper thermal analysis, we should consider a proper model of a flat plate solar collector with all important associated elements, as shown in Figure 3.4. The figure is modified from the original source [32], and the following mathematical expression also comes from this same source. Let suppose the solar radiation with intensity I in W/m^2, falls onto the surface of the collector area A, in m^2, and the radiation is perpendicular to the collector

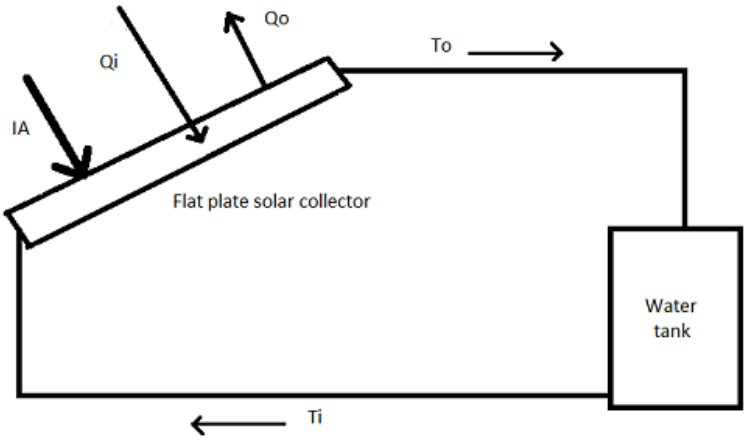

Figure 3.4: A schematic model of solar flat plate collector with water tank.

surface area. The quantity of solar radiation which strikes the surface of the collector is:

$$Q_i = I \cdot A \tag{3.1}$$

As demonstrated in Figure 3.4, part of the radiation labeled Q_i is absorbed by the glazing, and the rest is transmitted to the absorbing plate. The other part of the radiation, labeled Q_o, is reflected back into the atmosphere. The term conversion factor refers to the amount of radiation penetrating the glazed surface area as opposed to the amount being absorbed. So it can be defined as product of the rate of transmission from the glazed surface-area and the rate of absorption by the absorber. Then Equation 3.1, can be rewritten as:

$$Q_i = I(\tau\alpha) \cdot A \tag{3.2}$$

In Equation 3.2, τ is the rate of transmission through the glazing and α is the absorption efficiency of the absorber. As more and more solar radiation penetrates the collector's surface, it's temperature begins to increase higher than the surrounding around by means of convection and radiation. Thus, there will be heat losses, which is mostly dependent upon the overall collector heat transfer coefficient and the temperature of the collector.

$$Q_o = U_L A(T_c - T_a) \tag{3.3}$$

In Equation 3.3, Q_o represents heat loss in W, U_L, heat transfer coefficient

in W/m^2, T_c and T_a collector average temperature and ambient temperature respectively in Kelvin(K). Therefore, the useful energy generated by the collector is the difference between the energy absorbed by the collector and the direct and indirect heat loss from the collector surface into the surrounding area.

$$Q_u = Q_i - Q_o = I(\tau\alpha) \cdot A - U_L A(T_c - T_a) \tag{3.4}$$

In Equation 3.4, Q_u, is a useful energy in W. There is another way to examine the amount of extracted useful energy from the collector, by means of measuring the amount of heat that is carried away from the collector by the working fluid.

$$Q_u = mc_p(T_o - T_i) \tag{3.5}$$

In Equation 3.5, m is the mass flow rate of working fluid in Kg/s, c_p, is the specific heat capacity at constant pressure, and T_o and T_i represent the incoming and outgoing fluid temperature. By examining Equation 3.4, it becomes obvious that it is difficult to estimate the average temperature of the collector all of the time. So, it is useful to express the term, which creates a connection between the actual useful energy of the collector with the useful gain when the collector surface is at the same temperature as the incoming working fluid. The term is known as collector heat removal factor (F_R) or correction factor:

$$F_R = \frac{mc_p(T_o - T_i)}{I(\tau\alpha) \cdot A - U_L A(T_c - T_a)} \tag{3.6}$$

The optimum actual useful energy gain Q_u, can be attained from the solar collector, while the collector surface temperature is equal to that of the working fluid temperature. The expression for actual energy gain can be obtained by the multiplication of the collector heat removal factor and the useful extracted energy of the collector. It can be expressed as:

$$Q_u = F_R A[I(\tau\alpha) - U_L(T_c - T_a)] \tag{3.7}$$

The above equation is known as the "Hottel-Whillier-Bliss equation", which is the most commonly used expression for measuring solar collector energy gain.

3.4.2 Performance of the collector

The most common and widely used standard for a flat plate solar collector is ASHRAE Standard 93 : 1986($RA91$) [33], which was approved and reaffirmed

on September 9, 1991 by the American National Standard Institute ($ANSI$). The main objective of the standard is to provide a procedure to test the solar collector performance basis in many different combinations, such as thermal efficiency with regards to incident angle and time constant. Due to recent advancements in technology and the manufacturing process, there has been a need to update the standard once again. The new standard was approved on January 23, 2014 as ASHRAE Standard 93 : 2010($RA2014$) [34], which is an affirmation of ASHRAE Standard 93 : 2010.

- Thermal efficiency: Thermal efficiency is a measure of the thermal heat, which relates to the incoming and outgoing of thermal energy of any system. It is a dimensionless parameter. To get a fair idea of solar thermal collector performance, it can be defined in terms of thermal efficiency η, which is a ratio of extracted useful energy Q_u to the incident energy Q_i, in W. It can be expressed as instantaneous thermal efficiency:

$$\eta = \frac{Q_u}{AI} \tag{3.8}$$

  Equation 3.8 can be rewritten in terms of correction factor F_R, by using Equation 3.7, as follows:

$$\eta = \frac{F_R A[I(\tau\alpha) - U_L(T_i - T_a)]}{AI} \tag{3.9}$$

$$\eta = F_R\tau\alpha - F_R U_L \left(\frac{T_i - T_a}{I}\right) \tag{3.10}$$

  It is assumed that the factors F_R, τ, α and U_L in the above equation are constant for any particular collector. In that case, efficiency is dependent on the other three parameters, inversely proportional to the solar radiation I and directly proportional to the temperature difference of incoming fluid T_i, and ambient air T_a.

- Incident angle: In all of the previous expressions for a solar collector in this section, it is assumed that the solar radiation is perpendicular to the collector surface area, but this actually happens quite rarely. In such conditions, the rate of transmission and absorption of solar radiation factor($\tau\alpha$) will reduce due to specular reflection by the smooth glazing surface. To compensate for this phenomenon, it is preferable

to introduce the incident angle modifier, which is most commonly defined as a ratio of the factor $\tau\alpha$, at a particular angle to $\tau\alpha$ at normal incidence.

3.5 Spectrally selective solar absorber

The absorber is the most critical part of the solar thermal system, which initiates the conversion of solar radiation into useful heat. Most absorbers are designed as a thin surface or layer that sits on top of the system. In general, the absorber consists of a thin solar radiation absorbing layer over a metal surface, which is most commonly made from aluminum and copper. The working principle of the absorber is to transform solar radiation into heat, which is then passed through the metal surface and into the working fluids of the system. An important characteristic of an ideal absorber is to gather all incoming solar radiation while avoiding any loss of that captured energy.

There are several desired qualities which all absorbers should possess: the ability to efficiently transfer heat into a working fluid, great resistance against moisture and high temperatures and reasonable production costs. Solar thermal systems are the most encouraging source of potential heat production as the conversion of radiation to heat is environmentally beneficial. To make the environmental impact almost negligible for energy conversion by solar collectors, the production and destruction chain should be as environmentally friendly as possible.

The most common and basic use of a solar collector is to heat water at domestic and industrial levels. When they were first being manufactured, most absorbers were made from bulk materials which were too inflexible in terms of solar spectrum selectivity to reach a desired efficiency. In recent years research interest has shifted towards finding better combinations of materials that allow for more control. Tandem absorbers were then developed, composed of two different surfaces with unique optical properties such as a metal-semiconductor and a metal-dielectric. As a combined unit they can reach a higher spectral selectivity than the bulk material absorbers. Many also have a thin layer on the top of the substrate which allows for absorption and reflection within a selected spectrum. Materials with high infrared reflectance and low thermal emittance such as copper and aluminum are usually used as a substrate.

Solar radiation spectral distribution and solar thermal radiation are the basic fundamentals for the optical design of any absorber. The spectrum of terrestrial solar radiation is dominant with in the range of 0.3 to 2.5 μm,

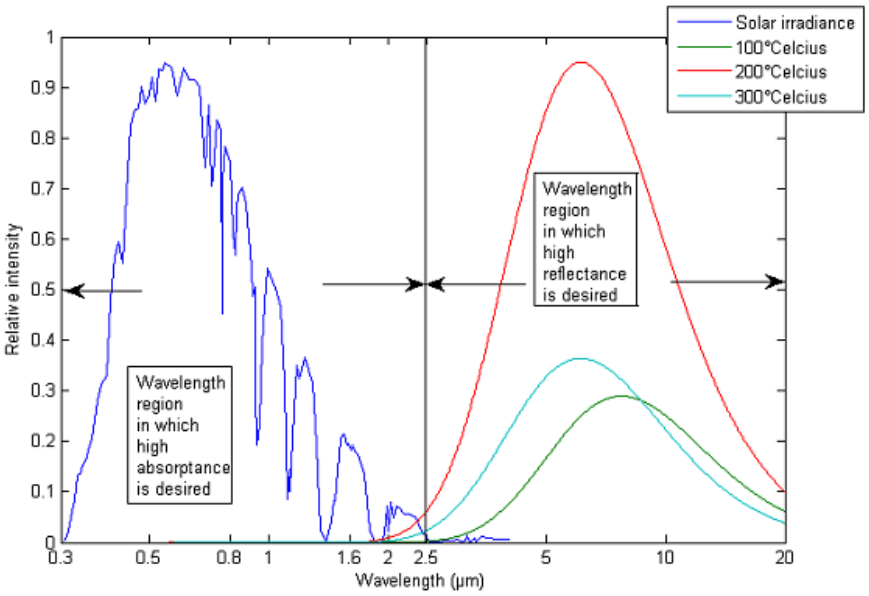

Figure 3.5: The solar spectral irradiance distribution,blue curve(ISO 9845-1), emitted radiation of blackbodies at three different temperatures 100, 200 and 300°C are in green, cyan and red respectively. Desired high absorptance and high reflectance for the wavelengths is also indicated in figure.

accounting for 98.5%, of the total incoming solar radiation. Maximum solar intensity can be found around at 0.55 μm. Therefore, it is necessary for any selective surface absorber to maximize absorptance in the solar region as well as minimize emittance in higher wavelength regions. The designed surface or absorber must have low reflectance in solar regions and higher reflectance with little thermal radiation emittance, known as a solar spectrally selective surface or absorber. The solar irradiation that hits the Earth's surface through a clear sky can be seen in Figure 3.5. The wavelength axis is in logarithmic scale. When the radiation continues to strike the Earth's surface, the surface increases in warmth and begins to re-radiate heat into its surroundings. The maximum radiation can be send out from a body at definite temperature, termed as thermal radiation. In common the thermal radiation is known as blackbody radiation. The emitted spectral distribution for blackbodies at temperatures 100, 200 and 300°C can also be seen in Figure 3.5. In normal conditions, the temperature of an absorber plate in operation is usually comparative within 100°C [12].

It is important to acquire a wide spectral selectivity. In some conventional applications the spectral selectivity is quite close to ideal, achieved by coating and painting techniques such as solar thermal and radiative cooling. This

was achieved due to intensive research over a 50 year time span. Painting and coating are quite common techniques used to achieve the desired spectrum selectivity, due to their economical cost and the simplicity of application as compared to other techniques [35].

3.5.1 Ideal

As discussed, the optical design of an absorber depends on the understanding of spectral distribution and blackbody radiation. But it is also essential to have criteria regarding the ideal surface for an absorber to compare with an actual surface. Electromagnetic theory states that any hot object tends to emit radiation, while the radiation spectrum and intensity levels are in respect to the temperature of the body emitting the radiation. Any surface is as an ideal one if it can absorb all of the radiation that falls onto it and re-radiate the same amount of radiation into its surroundings,. In the case of a solar thermal system, an ideal surface should absorb all the incoming radiation as well as minimize the thermal radiation [36]. An ideal surface emissive power can be calculated using **Planck's law**, which explains the spectral radiation distribution of blackbody as follows:

$$B(\lambda, T) = \frac{2\Pi hc^2}{\left(e^{\frac{hc}{\lambda k_B T}} - 1\right)\lambda^5} \tag{3.11}$$

In this equation $B(\lambda, T)$ is spectral distribution, λ is it's wavelength, T is absolute temperature, $h = 6.6260755 \cdot 10^{-34}$ in J is a Planck's constant, $c = 3 \cdot 10^8$ in ms^{-1} is the speed light of and $k_B = 1.3806488 \cdot 10^{-23}$ in JK^{-1} is the **Boltzmann's constant**. To calculate the total amount of emitted energy, the Planck's spectrum can be integrated over a particular wavelength period. Further calculations lead to **Stephan-Boltzmann's law**, which expresses the total emitted energy for a ideal surface:

$$B(T) = \sigma T^4 \tag{3.12}$$

In this equation, $B(T)$ is the total emitted energy and σ is a constant of proportionality or **Stefan-Boltzmann constant**. The temperature of the blackbody increases, thus the emitted energy and the peak power density is moved towards a shorter wavelength. To calculate the displacement in the peak wavelength λ_{max} using **Wien's displacement law** law can be expressed as:

$$\lambda_{max} T = b \tag{3.13}$$

Figure 3.6: A schematic diagram of an intrinsic solar absorber.

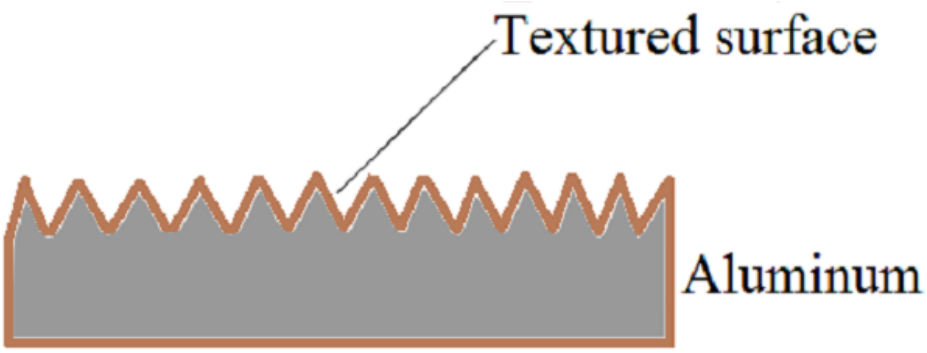

Figure 3.7: A schematic diagram of a textured surface solar absorber.

In this equation b is a constant, which is known as Wien's displacement constant and is equal to $b = 2.8978 \cdot 10^{-3}\ mK$. All above equations and their descriptions in this subsection referred to source [37]

3.5.2 Intrinsic absorber

This is the most straightforward type of absorber. It is made from a single material which has intrinsic properties that allow the absorber to be a spectrally selective. It is composed of a layer of intrinsic material over a conductive surface, as can be seen in Figure 3.6. The crossover from low to high reflectance must take place at exceedingly short wavelengths, or the slope will not be sufficiently steep at the transition wavelength. Unfortunately researchers have not determined any promising commercial application for intrinsic absorbers. The best currently known intrinsic materials are C_aF_2 and Z_rB_2 [38].

3.5.3 Textured surface absorber

Textured surfaces known as an optical trapping surface. These kinds of surfaces are usually rough and inlaid with a certain pattern. A textured surface absorber diagram can be seen in Figure 3.7. The main advantage of this kind of surface is the multiple reflections produced which are caused by dendrites or porous structures to enhanced the absorption ability of solar radiation [12].

Figure 3.8: A schematic diagram of a multilayer solar absorber.

The application of evaporated silicon on a molybdenum surface by reactive ion etching has produced a solar selective absorber with a sub micron textured surface [39].

3.5.4 Multilayer absorber

As its name suggests, a multilayer absorber is composed of multiple layers of semitransparent metal and dielectric material in such a way that may resemble a sandwich. A multilayer absorber is depicted in Figure 3.8, which has alternating layers of dielectric and metal over a metallic conductive surface. Using a multilayer structural design makes absorption very efficient. A top layer of anti-reflective material can be used in this kind of absorber, and the sputtering method is most commonly used for such a coating. A general example of a multilayer absorber is $Al_2O_3/Mo/Al_2O_3$, as it has been fabricated by the large-scale sputtering method [37].

3.5.5 Thickness sensitive

The paint coating is a process of distributing solid particles, known as 'pigments', over a wide area with uniformity. Pigments are introduced into the paint to carry the phenomenon of color during the absorption and reflection of light [40]. Paint coatings are normally dispersed into resin, which creates a macromolecular thin film that is suspended into an organic solvent and water [41]. Resin is usually made of organic silicone, which has a strong absorption band in the middle of the infrared region. The fabrication techniques are inexpensive to apply for such paint coatings, such as roll coating (also known as coil coating) and spin coating [42]. Morphology and thickness of the surface can be vary according to the application area. The main disadvantage associated with this kind of paint coating technique is a higher thermal emittance as opposed to the techniques used for spray coating thin metal and dielectric compounds [12].

Figure 3.9: A schematic diagram of a Solar transmitting absorber.

3.5.6 Solar transmitting

Solar transmitting absorbers can be fabricated by using a high doped semiconductor over a conductive surface area. The coating must be highly reflective in the infrared region, as well as transparent enough in the solar spectrum. Due to its structure, it is also known as a heat mirror or black substrate. The substrate is often chosen for its long term durability. A top coated SnO_2 over black enamel with a metal substrate can be seen in Figure 3.9 [43].

3.5.7 Metal-Semiconductor

For a high-quality absorber it should be possible to absorb all incoming radiation for wavelengths under 2.5 μm. But to fulfill this criteria, the energy band gap should be analogous to the 0.5 eV, which can be calculated using the following equation:

$$\lambda \leqslant \frac{hc}{E_g} \tag{3.14}$$

The application of a semiconductor material layer with a low band energy gap on top of the highly reflective metallic surface can be used to obtain a spectral selective semiconductor surface, which can be used as metal semiconductor absorber. It is also helpful to utilize a top layer of anti-reflective coating to compensate for the higher refractive index of the semiconductor, which can cause high front reflective losses to afford a passage to low absorptance. A structured diagram of a metal semiconductor absorber can be seen in Figure 3.10. Lead sulfide (Pbs), is promising material with respect to the energy band gap of 0.4 eV. But on the other hand this is a poisonous material, which can harm both humans and environment. So the feasibility of using the material at a commercial level depends on finding the best possible way to dispose of it safely and sustainably [12, 37].

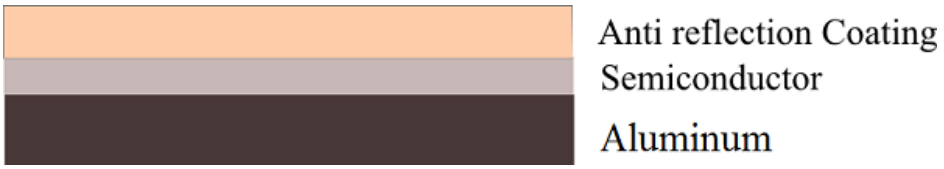

Figure 3.10: A schematic diagram of a Metal semiconductor absorber.

Figure 3.11: A schematic diagram of a Dielectric composite absorber.

3.5.8 Metal: dielectric composite

This type of collector is normally composed of metal within dielectric material in an embedded form, also known as cermet, as can be seen in Figure 3.11. Metal oxide can also be imbedded in nano-sized particles, and the distribution of these particles can be uniform or uneven. It possesses a high degree of flexibility due to its structure, and the solar spectral can be optimized by applying a certain type of particle, particle size, thickness of coating, orientation and concentration. The absorption can also be boosted by choosing a particular substrate and additional anti-reflective coating. Because of all the advantages listed above, it is the most widely used absorber in solar thermal systems. Dielectric composite absorbers can be fabricated by several methods such as electroplating, sputtering, anodization, sol-gel and chemical vapor deposition (CVD) [12].

Chapter 4

Carbon Nano Tubes

Two of the most well known allotropes attributed to carbon are diamonds and graphite, with graphite typically being found as mineral ore. Graphite materials have a layered structure with carbon atoms in each layer, much like a honeycomb lattice. The textures and structures of graphite range from macro to nano. The acoustic, mechanical, thermal and electrical properties of this mineral have a vital potential in science, research and technical applications due to its structural character [44].

In 2004 when the ability to isolate graphene from graphite was discovered, it revealed the existence of 2D materials such as graphene in a flat state on a substrate instead of in a curled shaped. Graphene also has a honeycomb lattice structure similar to graphite, but the structure is made of densely sp^2 bonded carbon atoms. Figure 4.1 demonstrates the hexagonal, honeycomb lattice structure of graphene. Graphene is the original source behind all graphitic materials. It has been actively researched and studied for many years due to its interesting and unique properties. It has amazing strength, thermal and electrical conductivity, a high current density, a high area to volume ratio, a light weight and easy interaction with other materials. Graphene can also be molded into a single carbon atom sheet of two dimensional structure, making it a better choice at a nanoscale level to integrate with other materials due to its easy yield to penetration [45].

The discovery of carbon nanotubes (CNTs) dates back to 1991 [47]. After this discovery [48,49] it was revealed that a certain combination of other elements were able to form CNTs, and this discovery paved the way for in-depth research into nanoscale science. Such advancements helped to break down the synthesis and characterization of materials at a nanostructural level. Due to the application of this new knowledge,, researchers were lead to CNT synthesis. This gave scientists the ability to develop tools and experiments for the characterization of materials at low dimensions [50].

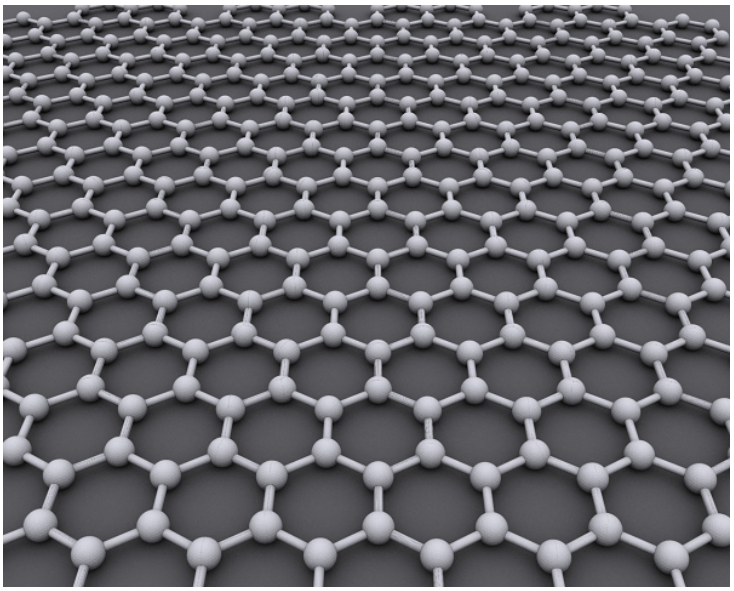

Figure 4.1: Hexagonal, honeycomb lattice structure of graphene made of carbon atoms [46].

CNTs represent an additional kind of carbon allotrope alongside graphite and diamonds, and takes the shape of a cylindrical structure with a very high length to diameter ratio of $132,000,000:1$ [51]. They also belong to the same family as fuller in terms of their structure. The name 'nanotube' has been given to these formations due to their long length and hollow shape. The structure of this shape is determined by the graphene, which is identified by a single atom-thick sheet of carbon atoms. In fact, CNTs can be thought of as rolled sheets of graphene. They have an extensive range of special properties due to their rolled structure with an angle called "Chiral", as demonstrated in Figure 4.2.

The aspect ratio of CNTs is what makes the structure so unique, with a high variation between length and diameter at nanoscale. So when CNTs are used as a reinforcement element, their interfacial surfaces increase, which intensifies adhesion and leads to higher energy absorption as the material expands. This provides better interfacial strength to composite material structures. They are very strong and stiff, and can withstand extreme pressure conditions without taking damage due to their elasticity and bending capacity. They possess many other properties such as kinetic, electrical, optical, thermal, and resistance to shape change. Because of their low density and mechanical strength, CNTs cover a wide range of applications such as electronics, optics, automobiles, energy, medical, electrical circuits, textiles,

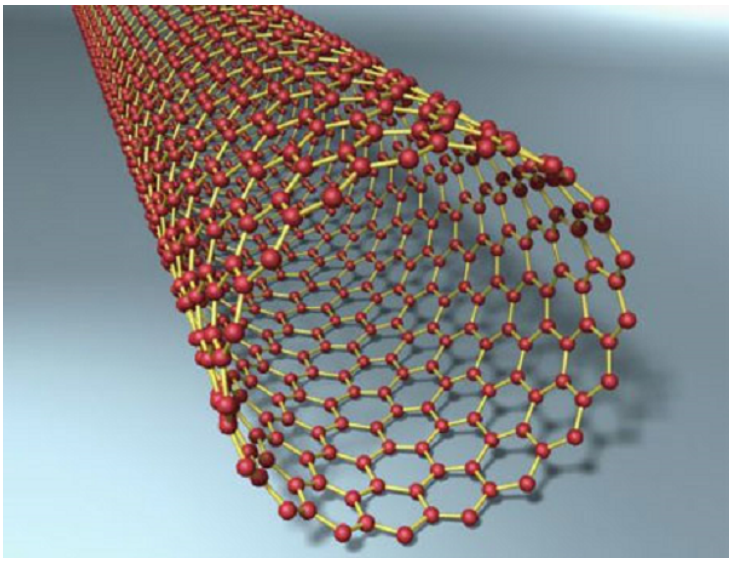

Figure 4.2: A simple view of Carbon Nanotubes with graphene rubes [53].

sound systems and batteries [52].

4.1 Categorization of CNTs

CNTs typically fall into two categories: single walled and multi walled. These are examined further below.

4.1.1 Single walled CNTs

Single-walled carbon nanotubes (SWCNTs) are the simplest and most basic structure of nanotube. The diameter of most SWCNTs is approximately one nanometer, but the length can be many times longer than the diameter. The structure of SWCNTs is a cylindrical shape, resulting from graphene as described in the previous section. They possess extensive electrical properties due to the unusual two-dimensional structure of graphene [54].

4.1.2 Multi walled CNTs

When multiple layers of graphene sheets are rolled concentrically, they formed a multi-walled carbon nanotube (MWCNT). As evident in Figure 4.3, there are three concentric nanotubes forming the MWCNT. The diameter and length of the MWCNTs can range from 5 to 50 nanometers by 10 micrometers, respectively. The electrical conducting capacity of these nanotubes is

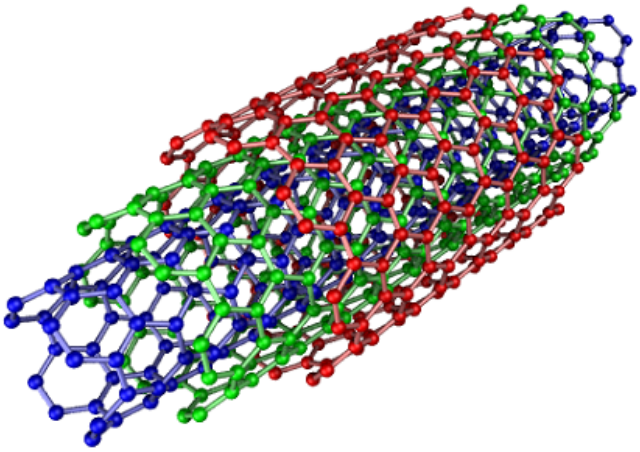

Figure 4.3: Multi wall Carbon Nanotubes as concentrically rolled shaped [57].

extremely high. MWCNTs possesses greater thermal conductivity than a diamond [55]. Double-walled carbon nanotubes (DWCNT) form a special class of nanotubes which have similar morphology and properties as SWCNTs, with a chemical resistance property that is immensely magnified. This can help in the chemical synthesis of the surface, especially where improvements and new characteristic are needed in the CNT [56].

4.2 Synthesis

Synthesis techniques for CNTs have been under research and development for more than 15 years. The driving force behind such long and intense research is the promising electrical and mechanical properties of these nanotubes. There are many synthesis processes that are now available on the market, although they vary in levels of development and compatibility. Figure 4.4 is a depiction of all available synthesis techniques. Each one has its own advantages and disadvantages for synthesizing particular types of CNTs. Most of these techniques take place in either a vacuum or in a processed-gas environment. Some processes can also take place in atmospheric pressure,

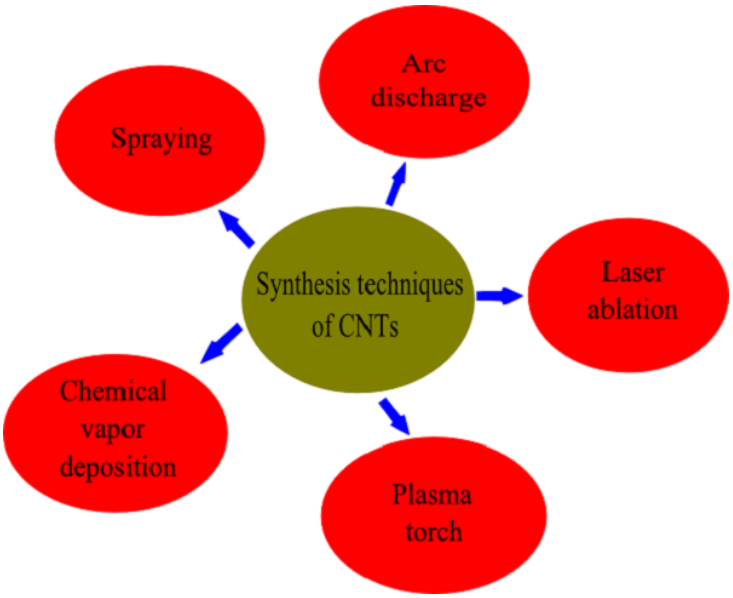

Figure 4.4: Available techniques for CNTs synthesis [58].

due to the advancement in technology and presence of a catalyst. The mass production of CNTs is made possible by utilizing some of these techniques. Gas-processed methods are possible in large volumes, which makes them favorable for composite material requiring a large amount of nanotubes and industrial-level fabrication, making them much more economical to use. But there are also disadvantages to this system, such as the life-span of the catalyst as well as the low percentage in nanotube yield. One common result from each of the synthesis techniques is the impurity of the synthesized CNTs. The type and level of impurity corresponds to the particular method used, but they all may result in the alteration of the CNT's most desired characteristics. This causes a conceptual challenge for the researcher in developing appropriate and realistic methods for CNT purification. The most common available and affordable purification technique currently on the market is an acid based treatment of synthesized [58].

4.2.1 Arc discharge

The first and oldest method of CNT material production is called arc discharge. Japanese physicist Sumio Iijima was the first scientist to observe and produce CNTs utilizing the arc discharge method in 1991. This method is based on the condensation of carbon atoms by involving the evaporation by any solid carbon source. In general the set-up consists of an anode, a

cathode, an AC source, a linear motion actuator and a pump. The arc discharge method is a high-temperature synthesis process utilizing temperatures around 3200 Kelvin between the electrode gap, which makes the arc discharge process quite difficult to control. A high current of around 50 to 120 Amperes is passed along the graphite electrodes separated by a distance of approximately one millimeter. This takes place in a synthesis chamber which causes material to transform from a gaseous state into a solid form, from cathode to anode. Because of high current and temperature prerequisites, this method is uneconomical and energy-demanding. It also generates undesired byproducts such as polyhedron graphite particles [59], with a low yield factor at about 30% of its weight. This method is capable of synthesizing both SWCNTs and MWCNTs. The length of the nanotubes can be up to 50 micrometers long and may include structural impurities and defects [60].

4.2.2 Sputtering

Eroding solid surfaces by the application of particle bombardment is a process known as sputtering. It was recognized for the first time in gas discharge around the middle of the last century, and now it is known all over the world. The erosion rate for sputtering can be identified by the sputtering yield, which is the average number of atoms emitted per incident particle. This makes it easy to define sputtering as a process in which atoms are thrown out forcefully from solid target material with energetic particles by bombardment to the substrate [61]. Sputtering can be done in many ways, such as ion beam, roll coating or DC magnetron sputtering. Different ways of sputtering make it more flexible to deposit a wide variety of materials and maintain the ability to use reactive gases. It is the most common technique used for thin film deposition, which is much cleaner compared to other chemical deposition methods. It is easy to control and accurately produces micro-scale and multilayer coating with higher accuracy. Advance sputtering methods are sufficient on a commercial scale to produce thin film absorber coatings [62].

4.2.3 Laser ablation

Laser ablation is a series of actions in which solid surface materials are expose to radiation by laser application to remove them. A focused beam with both high and low intensity levels is usually used with respect to the particular stage of the process. In the beginning, the laser with the lower intensity is used to provide enough energy to heat the material and change it directly into vapor. It can also be transformed into plasma by applying the high-intensity laser beam instead. A pulse laser is more commonly used than a

high-intensity continuous laser beam, because it is not easy to maintain that high level of intensity in order to evaporate material. For CNT synthesis the pulsed laser deposition process (PLD) is referred, but it relies heavily on several factors: the many physical properties of the reactive gas in the chamber, the structure and chemical composition of the target material, the distance from the substrate to the target, the ambient temperature and several laser properties such as flux intensity, repetition rate and oscillation wavelength. It is considered one of the best synthesis processes to produce high-quality and high-purity SWCNTs. Arc discharge and laser ablation are work with same mechanism rather than laser ablation use a laser source for material removal. A factor that has not been clear until now is the association of the growth of SWCNTs with the excitation wavelength. Research suggests that the ultraviolet (UV) laser may be the solution to finding different types of nanoscale particles to improve the growth mechanisms of SWCNTs, which is more effective for photo thermal ablation This may be done by the application of continuous CO_2 in laser ablation to produce SWCNTs without using any additional heat. It has also been observed that by increasing the laser power during the process, the average diameter of the produced SWCNTs increases [63].

4.2.4 Chemical Vapor Deposition

Chemical vapor deposition (CVD) is a common process used to produce a wide range of solid materials with high purity and high quality. It has a wide and open application area, especially when it comes to thin film deposition in a semiconductor field. The basic principle of this method is to expose the metal substrate to the target material in vapor form, where they react chemically and deposit a thin film. CVD is one of the most frequently used methods for CNT deposition. Catalytic chemical vapor deposition (CCVD) that is enhanced through either heat or plasma is considered a standard process for CNT synthesis. There are many other CVD techniques which can be associated with water, oxygen, hot filaments and radio frequencies. All of these techniques have an economical developing process at a higher stage with better purity as compared to laser ablation. A primary beneficial factor of the process is that it is easy to control the chemical reaction while maintaining a high quality of material. In CVD, the most commonly used substrates are stainless steel, glass, copper(Cu), silicon(Si), and silicon oxide (SiO_2). Graphite also has been tested. A key element of CVD is the catalyst, so choice and preparation can be a critical step in development. The role of the catalyst in the process is to decompose the carbon source to bring together it's new nucleus. The most commonly preferred catalysts are Iron(Fe), Nickel(Ni),

Cobalt(Co) as well as transition metals [63]. The size of the catalyst can play a big role in developing the desired diameter of the CNT. For instance, if the size of the catalyst is small, the CNT will be thinner and the number of wall layers will be fewer. The catalyst can, however, have an adverse effect on the process as a result of weakening of the cohesion to the substrate and due to the difficulty of removing it from the surface as a result of the chemical behavior [52].

4.3 Deposition

4.3.1 Spraying

Spraying is a common coating method which can be achieved by using compression in combination with the desired coating material directly on the surface of the substrate. It's working mechanism makes it more simple, inexpensive and provides it with a wide application for coating. In the solar thermal field, spraying is the most commonly used method to cover a large area with a black paint coating and solar selective surfaces over a wide range of substrates. The flexibility of direct coating on the surface adds a great advantage, as the amount of material used is less and the coating can be applied over any shape [37]. CNTs can also be easily deposited, utilizing this process with a variety of substrates. The biggest drawback of this process is the lack of uniformity of the coating surface. There is often an uneven surface, especially at a micron and sub-micron scale. In the case of CNTs, the coating tends to stick to the top and does not cover the whole surface area, which can lead to clusters of paint in some areas [52].

4.3.2 Spin coating

The basic working principle of the process is to use a centrifugal force to distribute a small amount of material in the center of the flat substrate while it is spinning at a particularly high speed. The apparatus used to apply the coating is called a spin coater. The particular thickness achieved depends upon a couple of factors: the angular speed of spinning and the coating material properties. The angular speed is commonly inversely proportional to the thickness, meaning the higher the angular speed the thinner the deposited file. Secondly, the physical properties of the material used for coating are important, such as the concentration of the solution and the viscosity. Spin coating is the most widely used technique for the development of polymers in the solar industry. It is also the most favorable method for producing a thin

layer of film over any flat substrate. Spin coating has many advantages over other coating processes: the coating interaction between the solution and the substrate is easy to calculate, there is a uniformity of thickness and it uses the least amount of material for coating. It does have some limitations, however, such as not being applicable for large area coating or for substrates aside from those that are flat. These could be critical points to address for the future development of this method [64].

4.3.3 Electrophoretic Deposition

The working principle for Electrophoretic deposition (EPD) is based on the application of an electric field. The electrode and cathode are dipped into the coating material as a colloidal solution, while at the same time an electric field is applied in order to make the metal ions form a thin layer on the target electrode. The deposit thickness in the process can be controlled either by the current or the voltage. Other parameters that also play a factor in the morphology, structure and chemical composition of the coatings are the solution concentration, the solution temperature, the process time, the current and the voltage density. The EPD technique is a quite common process for the formation of thin film, coating bulk shapes and the processing of ceramics. Moreover, it is absolutely effective in film production and the coating of microscopic particles in the colloidal stage. It possesses several advantages over other coating and thin film techniques, such as the high purity of deposit materials, a high deposit rate, a high density of deposition, the easy coating of complex structures, uniformity in deposition and flexibility in controlling material properties. In addition, coating thickness can be feasible to control and a wide variety of materials can be used for coating. Even though it has wide range of application areas and benefits, there is still more research that must be done on this method for CNT deposition. EPD can be considered in the mid-range as compared to the other techniques in working mechanism complexity [52,64]. This will be discussed in more detail along with an experimental set-up in the chapter called 'Sample Preparation.'

4.4 Characterization

The term 'characterization' in general refers to the act of describing different characteristics and essential features of a person or a object. It is a quite useful and exciting tool of material science. The characterization of any material implies the deep study of that material based on several fields and criteria in order to determine existence and feasibility for further application

in all possible sectors. It can be used as an external act of exploring internal complex structures and properties of the material. Due to advancements in technology and scientific research, characterization is a proper tool that is used to gather and analyze detailed information about the material properties of an object. Characterizations can be classified into many categories, but some of the main ones are mechanical, thermal, structural and optical. These will each be examined in the next four subsections.

4.4.1 Mechanical

A mechanical property can be defined as the response of a material under any external and internal force, while the process of characterizing the behavior of that response is known as mechanical characterization. It is quite important to perform all necessary mechanical tests in order to characterize and ascertain the functionality of a material in different application areas and conditions.

CNTs have been under investigation for quite some time, and it is clear that they posses versatile mechanical and physical properties. They are one of the strongest materials found in nature, especially in terms of axial direction. Based on the geometry of CNTs, they posses different properties for radial and axial directions, but the radial direction seem to be softer than the axial. They also have many remarkable properties, such as a very light weight, a highly conductive nature and a high surface area to diameter, providing great opportunities for further deep and nanoscale research. Since CNTs are being utilized in engineering and manufacturing sectors, their basic as well as advanced properties must be explored and studied with great interest. CNTs can be mechanically characterized as a mass of bundles and compounds with polymers [65, 66].

Mechanical tests and characterizations are governed by particular sets of instructions for the specific instruments and equipment used to carry out various experiments. The test specifications can be formed according to the material and desired application field. There are many techniques available to carry out mechanical characterization for several mechanical properties. Some of these are as follows:

- Tensile test: This is defined as the strength of an item to withstand stress without becoming broken or deformed. It is carried out in plane axis to determine the material deformation ability weather it is linear elastic or not, which can be define as linear strain-stress relationship. It can be performed even with variations in the angle to obtain directional strength, as with CNTs. Research suggests that SWCNTs can exhibit

greater tensile strength than all other materials. For SWCNTs, strain at tensile failure forecasts as high as 30%, and the tensile can be at 300 GPa [66].

- Compressive strength test: When a material comes under an applied external force and begins to shrink or reduce in size, this is called compression force. The ability of materials to stand against such force is known as compressive strength. This is a linear or inversely proportional relationship between compression force and change in size, which can be recorded and plotted for observation. Compressive tests can vary in terms of test specifications and local measurement conditions. It is necessary to follow international standards to achieve a proper test result, as that can be a crucial step in designing. Especially in the case of CNTs, the surface area is quite important as a selective surface.

- Fracture toughness test: This is the measure of how well materials containing a crack remain firm against further fracture. It is considered a stress factor, regarding a particular energy which initiates a fine crack on the surface of a material. Materials with less fracture toughness tend to be brittle, and a high fracture toughness makes them ductile. This can be counted as one of the vital properties of a material, especially in the sense of design application.

- Fatigue strength test: This is defined as a application of cyclic stress, or the amount of pressure that a material can withstand without encountering any fatigue failure. This is especially useful for those applications which accommodate frequent force and extreme weather conditions, such as aerospace, sports, solar thermal and photovoltaic.

- Yield strength test: This is a point on a material under stress when it reaches elastic deformation, and the deformation become permanent. Just before reaching the yield point, the material can bounce back to its normal structure after removal of the applied force. After the yield point, however, the deformation is non-reversible. This is a key point or limit that must be defined in the manufacturing and design of any element to the load application. It can also be used as a measure in many synthesis and production processes to assure the prior and ultimate break down of a structure.

4.4.2 Thermal

Thermal properties are those of a material which define how it handles heat variations over a period of time. The process to characterize these properties is called thermal characterization. Thermal characterization is used to gather the thermal response of a material and its constituents under various standard conditions. There are a wide range of thermal properties, such as thermal conductivity, heat flow, heat capacity and thermal expansion, which all have to be understood well enough for the interest of the material. Especially when it comes to CNTs and their areas of application, thermal characterization can become an important factor due to the involvement of CNTs in the solar thermal and photovoltaic fields. There are a number of available tests and techniques available to access deeper information on the thermal properties of materials and composites. Some thermal characterization methods are described below.

- Dielectric Thermal Analysis (DTA): This is a typical test for the determination of dielectric constants, such as permittivity and loss factor. In this test, a specimen must be placed between two electrodes under the application electrical quantity, and in this way the required parameters can be calculated. It plays an important role in hardening polymer, resin and composites.

- Differential Scanning Calorimetry (DSC) and Differential Thermal Analysis (DTA): These are used to measure thermal transition in terms of temperature and heat flow. These are the most widely used techniques for this process. DSC measures the net rate of heat flow with respect to the heat flow for a reference inert sample. The basic difference between these two methods is that DTA is comparative and DSC is analytical. They are both mostly used to monitor glass transitions, phase changes, crystallization and melting. DSC can also be used as a quality control instrument [52].

- Thermo Mechanical Analysis(TMA): This is a basic technique that deals with the changes in material properties with respect to temperature variations. These changes can be measured by a change in the temperature, and are dimensional and mechanical properties of a material. It is use to calculate glass transition and the coefficient of thermal expansion [52].

- Thermal Gravimetric Analysis (TGA): This provides an analysis of thermal measurements within physical and chemical material properties with respect to changes in variable increasing temperatures or time

under specific atmospheric condition. It is used to determine thermal and chemical compositions, phase transitions, vaporization, decomposition and solid gas reactions [67].

4.4.3 Structural

Structural characterization deals with the solar spectral calculation for different wavelength regions. There are techniques available for calculating structural properties. Those can be used to measure reflectance, transmittance, refractive indices and other spectral measurements. In addition, Profilometers are used for surface profile measurements and for judging surface thickness. Structural characterization with applicable tools will be discussed in more detail in the chapter-6.

4.4.4 Optical

Optical characterization is a tool for characterizing morphology and chemical composition at nanoscale by using different kinds of electron microscopy and spectroscopy. As well as ellipsometer or a spectrometer for calculation of optical constants. These are methods that uncover detailed information regarding internal perspectives on different materials by using several optical techniques. Some of the more important optical characterization techniques will be discussed further in the chapter-6.

4.4.5 Other possible characterizations

In addition to the all of the main characterization categories mentioned in earlier subsections, there are many other potential characterizations which can be used to measure other information about CNTs doped with composite material.

- Ultrasonic measurement: This technique is used to investigate the irregularities and defects in certain materials. It is also known as the C-scan method, as the basic principle of the method is based upon scanning the surface of a material. In this method, the surface of a material is scanned with an ultrasound wave and the reflected data is collect with the help of a detector in the $X - Y$ plane coordinate. This can be plotted on a color map to interpret the information about surface structure with different color codes.

- Electrical characterization: This can be used to measure some basic electronic properties, such as resistivity, carrier lifetime, deep level impurities, electron concentration and mobility ions. These properties are all essential for semiconductor devices and their production, especially when it comes to thin film semiconductors, because the effects can be much higher at nanoscale. To exploit the various effects there are many techniques available, such as deep-level transient spectroscopy (DLTS), Hall effects measurement and capacitance voltage profiling.

- Indentation test: This is a technique for measuring the hardness of a material, which establishes the correlation between hardness and tensile strength. It can measure the hardness at micro-scale and nanoscale. Thus, it can be used to give a more precise evaluation of the hardness of deposited CNTs over different surfaces [52].

4.5 Carbon Nano Tubes as solar thermal absorber

The absorber is a key element in a solar thermal system as it drives the performance of the system. Therefore, selection of the material for solar thermal application as an absorber is a critical and important factor. CNTs exhibit many thermal, optical and mechanical properties which can also act as solar thermal absorbers. Below is an evaluation of these characteristics.

- High absorption: To work as an ideal absorber, the absorptance rate of a CNT must be as high as possible. Due to the higher adhesion quality of CNTs, this contributes to higher energy throughout the course of fracture propagation. Higher absorption will lead to higher temperature gains in the solar thermal system. CNTs are importantly also selectively absorbing, they absorb strongly up to 1 μm but are transparent for infrared region.

- Thermal conductivity and thermal isolation: CNTs possesses extremely high thermal properties. For example, Multi Walled Carbon Nanotubes ($MWCNTs$) have much higher thermal conductivity than a diamond. Higher thermal conductivity constitutes better heat flow in the system, which is an essential function of a solar thermal absorber. CNTs are good thermal conductors in the axial direction as well as good thermal isolators in the radial direction [52].

- Strength and stiffness: CNTs are very strong and stiff, which are desirable properties of a good absorber. Toughness of the CNT provides better durability under extreme weather conditions, and stiffness adds more flexibility to be bent without breakdown.

- Higher surface area: The unique property of a CNT is a high diameter to length ratio at nanoscale, which provides a higher interfacial surface during reinforcement. This can improve the adhesion property of CNTs. Moreover, their linear geometry makes them a more conductive medium.

Chapter 5

Optics of thin films

Before addressing the optics of thin film, we should review its history and the technology behind it which makes it a reality today. In addition, the physics of surface science will be discussed in order to have a better understanding of thin films.

A thin film is a microscopic layer of any material which can be coated over any solid or semisolid surface, such as plastic, glass, metal, ceramic and semiconductors. It can range from a few nanometers to up to a few micrometers. Thin film technology is widely applied in the semiconductor and optics fields, but the application area is much wider. It can range from household application such as mirrors to highly advanced industrial field such as lenses, miniature circuits and solar cells. It also contributes to thin film solar cell, thin film batteries and coatings to protect against corrosion and aging of any surface. Thin film technology is much older than semiconductor technology. Ancient people used to turn gold into thin film with just a hammer at a thickness of less than 1 micrometer [68]. Thin film deposition can be done chemically or physically.

The field of science centered around both the physical and chemical transformations and alterations involved in the process of interface between any two phases (such as liquid and gas, solid and liquid, or solid and gas) is known as surface science. This encompasses both surface physics and chemistry. Engineering deals with all surface applications and problems, called surface engineering. Surface science is mostly based on interface science and chemistry. Surface chemistry can be defined as a tool by which we can understand the chemical composition and behavior of an interface. It plays an important role in altering, improving and changing any particular surface property of any element by interfacing with other desired materials. On the other hand, surface physics mainly deals with the physical condition of an interface, such as surface morphology, surface condition, reconstruction

and the nanostructure of a surface. There are many techniques available for physical and chemical analysis. Most of them fall under the umbrella of modern spectroscopy and microscopy, such as X-ray photoelectron spectroscopy, thermal desorption spectroscopy, electron energy loss spectroscopy, scanning-tunneling microscopy and ion scattering spectroscopy. Some optical techniques can also be used for better study of interface structure under different circumstances [69].

Whenever materials or any thin film surfaces are subjected to light, it is interesting to predict and alter it's response. Thus, to understand the mechanisms of optical behavior and optical properties, it is essential to acquire knowledge about optics and their interrelated elements. With the use of optical properties, the intention is to evaluate a response by exposing material to electromagnetic radiation, especially to visible light [70]. That is an essential concept in the design of a proper spectrally selective solar absorber.

5.1 Electromagnetic radiation and absorption

Electromagnetic radiation is a type of electromagnetic wave, which is an energy propagating through either a medium or space. Electromagnetic radiation is composed of electric and magnetic field components, which are perpendicular to one another and also to the direction of the propagation. Radio waves, X-rays, heat and light are all types of electromagnetic radiation [70].

A plane electromagnetic wave propagating in an absorbing medium at a particular time t, assumed linear polarized in x axis direction can be expressed in terms of its electric field component as $E(x;t)$:

$$E(x,t) = E_0 exp[i(kx - \omega t)] \tag{5.1}$$

In this equation, E_0 is the initial amplitude of an electromagnetic wave before it enters the medium with the angular frequency ω, k is a propagation factor. For better comprehension of wave propagation in conductive media, the propagation factor should be expressed in a complex form. Furthermore, it's known that $k = n\omega/c$, then the above equation can be rewritten as:

$$E(x,t) = E_0 exp(-k\omega x/c + i(n\omega x/c - \omega t)) \tag{5.2}$$

In this equation, c is the speed of light in a vacuum and n is a real part of the refractive index. The speed of the light in a medium is characterized by the index of refraction of the refractive index. The complex form of refractive index can be expressed as:

$$N = n + ik \tag{5.3}$$

In this equation, N denotes the complex refractive index. The real part of the refractive index is n, which determines the phase information when a wave enters the media and demonstrates how much it will bend or refract. The other part of the complex refractive index is the imaginary part k, which is known as wave propagation or extinction coefficient. It is related to the absorption loss or damping amplitude of the wave in the propagating direction through the media.

The energy transfer rate of any medium through an electromagnetic wave can be determined by the **Poynting vector**. The time average of the Poynting vector is known as wave intensity I. This provides an important relationship where the intensity is directly proportional to the square of the electric field E. Furthermore, when electromagnetic waves propagate through a medium, the energy is absorbed and experiences exponential decay as explained by the **Beer-Lambert law**. Thus, the change in intensity of a electromagnetic wave in a medium can be expressed as:

$$I = I_0 exp(-\alpha x) \tag{5.4}$$

In this equation, I_0 is the initial intensity before penetration of the medium, and α is the absorption coefficient.

If the wave is traveling in a vacuum, then the wavelength λ_0 can be defined as:

$$\lambda_0 = \frac{2\pi c}{\omega} \tag{5.5}$$

By combining equations 5.2,5.4,5.5 and with the Beer-Lambert law, α can be defined as:

$$\alpha = 4\Pi k \cdot \frac{f}{c} = 4\Pi k \cdot \frac{\frac{v}{\lambda}}{c} = (if : v = c) = \alpha = \frac{4\Pi k}{\lambda} \tag{5.6}$$

Where, f is frequency in Hertz, v is velocity in m/s and k is a wavenumber. The logarithmic state of dependence between light intensities through a thin film medium with a path length d and the absorption coefficient, is explained by the Beer-Lambert law combined with equation 5.6. The result is expressed as:

$$ln\left(\frac{I}{I_0}\right) = -\alpha d = -4\pi\frac{kd}{\lambda} \tag{5.7}$$

The above equation expresses the intensity rate or change in thin solar absorbing film. The variation in the quantity kd/λ will be a determining factor when designing solar selective surfaces. The surface can behave as a transparent layer if $\lambda >> kd$. The transition of absorptance from low to high is determined by the combination of d and k. In composite absorbing surface or cermet the k value can be varied, which can be achieved by changing the size and shape of the embedded metal particles. In this section, all derived equations and their descriptions refer to source [12].

5.2 Optical characterization of a solar selective surface

When solar radiation penetrates through one medium to another, such as thin film and air, there are several optical phenomena that occur. One part of the radiation may be reflected back at the interface, another may be absorbed into the thin film and the rest may be transmitted through it. If the light with intensity I is incident to the thin film surface, then the total incident intensity I must be the summation of the reflected intensity (I_r), absorbed intensity(I_a) and transmitted intensity(I_t) as stated by the energy conservation law. It can be expressed as:

$$I = I_r + I_a + I_t \tag{5.8}$$

The above equation can be rewritten in an alternate form, for a spectral wavelength λ:

$$R(\lambda) + A(\lambda) + T(\lambda) = 1 \tag{5.9}$$

In this equation, R(λ) is reflectance, A(λ) is absorptance and T(λ) is transmittance. The quantity of each corresponds to the radiation wavelength, material properties and interface medium.

As described by **Kirchhoff's law**, in thermodynamics a blackbody in equilibrium absorbs all the radiation that strikes its surface and re-radiates that radiation into its surroundings. In other words, the absorptance and emittance e(λ) of the body should be equal. This can be expressed as:

$$e(\lambda) = A(\lambda) \tag{5.10}$$

By combing Equation 5.10, Equation 5.9 can be modified as:

$$e(\lambda) = A(\lambda) = 1 - R(\lambda) - T(\lambda) \tag{5.11}$$

During the usual practice of coating a solar absorbing surface, an opaque aluminum material substrate is used. In this kind of absorber, one part of the radiation reflects off the surface of the thin film, another part is absorbed by the thin film and the rest is reflected by the aluminum substrate. So, for that reason the transmittance is zero. Thus, Equation 5.12, can be expressed as:

$$e(\lambda) = A(\lambda) = 1 - R(\lambda) \tag{5.12}$$

In most cases, normal solar absorptance α_{sol} can be formalized as a static ratio of absorbed radiation to the incoming solar radiation. The solar spectrum I_{sol}, between $0.3 - 2.5\ \mu m$ is taken from the ISO standard $9845 - 1$, at an air mass of 1.5 [12].

$$\alpha_{sol} = \frac{\int_{0.3}^{2.5} I_{sol}(\lambda)(1 - R(\lambda))d(\lambda)}{\int_{0.3}^{2.5} I_{sol}(\lambda)d(\lambda)} \tag{5.13}$$

Normal thermal emittance $\varepsilon_{thermal}$ can be calculated in the same manner. But in place of absorbed radiation is emitted radiation, and also included is Planck's black body radiation, $B(\lambda, T)$ at 100°C in the region $2.5 - 20\ \mu m$ [12].

$$\varepsilon_{thermal} = \frac{\int_{2.5}^{20} B(\lambda, T)(1 - R(\lambda))d(\lambda)}{\int_{2.5}^{20} B(\lambda, T)d(\lambda)} \tag{5.14}$$

All above expressions have been considered with a normal angle of incident radiation.

5.3 Thin film interference

Interference occurs in thin films when incoming light waves reflect from the outer most edges and from bottom of a surface and intersect with one another at some point. The thickness of the film and index of refraction of the film determines the interference. Thin film has a wide area of application such as the semiconductor field, electronic equipment, solar thermal systems and many optical applications.

The thickness of thin film ranges from nanometers to microns. The process of interference happens when the incident radiation strikes the upper surface of medium, which in this case is a thin film. A fraction of this radiation is reflected and another fraction is transmitted into the thin film. The remainder of the transmitted radiation continues to travel until it finds

the succeeding boundary of the thin film, and may be reflected or transmitted. The reflected radiation from the outermost edge and the bottom of the surface will intersect at some point. To quantify the amount of reflected or transmitted radiation at the point of interaction is calculated by using the Fresnel equation. There are two kind of interferences: destructive and constructive. The course of constructive and destructive interference by the combined effort of the two waves depends upon several factors, which are listed below

- The phase difference between the two reflected lights from upper and lower surfaces.
- The thickness of the thin film layer.
- The index of the refraction of the two medium.
- The incident angle of the incident radiation.
- The source of the incident light. For instance monochromatic light and broadband light.
- An additional 180° phase shift is added at the interface of reflectance, if the incoming light medium has a lower refractive index than the medium it is penetrating. The result of this interference can be a dark stripe or s multiple-colored stripe, and it will rely on the point of origin of the incident light. For example, from air to water. The refractive index of water($n_{water} = 1.33$) is higher than the air($n_{air} = 1$).
- If the light travels from a medium with a higher refractive index to a medium with a lower refractive index, no phase shift is added. For example, from air to oil.The refractive index of oil($n_{oil} => 1.33$) is higher than the air.

The constructive and destructive interferences also contribute to the phenomenon of a color pattern in thin films.

Constructive interference is possible if the reflected waves have a phase difference in integers or in multiples of 2π. In simple terms, when two waves are in same phase and frequency, they multiply their amplitude as one. It is also important for constructive interference that the film thickness must be in the order of the wavelength. Constructive interference is used in optical filters, mirrors, sound amplification and ellipsometry.

Destructive interference is taking place if the reflected waves show a phase difference in a multiple of π. In other words, when two waves are in opposite

phase and frequency, they cancel out their amplitude somewhat or entirely. Destructive interference is used in anti- or non-reflective coating on camera lenses, mirrors, noise cancellation, diffraction grating and spectroscopy.

5.4 Optical absorption and properties of inhomogeneous medium

When incoming radiation falls on a thin film surface, it undergoes many surface reactions, such as reflection and transmission. The amount of energy that is absorbed from the incoming light is just a transformation of that energy from one form into another by photon, which can be done using heat in the case of a thin film solar absorber. A particular category of the material seems to have an inherent property used to convert the incident photon energy into electrical energy. The transformation of energy begins from the surface to the deep interior of the film. The absorbed photons in the thin film, is further interact with an atom to transform its energy to an electron of absorbing film. The passing of energy from one to the other should be done with conservation of energy and momentum in mind. The momentum provided by the zero mass photons is not that quantitative compared to that of the electrons and the holes in the absorbing film. By virtue of the electron to go into a higher state within atom or be set free from the atom, totally conditioned by the amount of energy transfer from photon to electron. The electron that has been released can move inside the absorbing film, until it gains more momentum from other phenomena such as temperature or an applied electric field [71].

An inherent property of inhomogeneous media is the ability to scatter the light that passes through it. There are many inhomogeneous materials used in several different applications. The properties of inhomogeneous material can be formalized, especially the optical properties by application of experimental methods and applicable theory. In this section, this refers to the optical properties of the embedded material particles on a non-absorbing surface. The theories will be applicable based on the size of the particles compared to the impinging wavelength. If the size of the particle is significantly smaller than the striking wavelength, then the effective medium theory can be put into practice. But if the particle size is either equivalent or larger than the incident wavelength, then the Lorenz-Mie Scattering theory will be applicable. Especially when it comes to absorption, scattering has a great importance. But a limitation of the Lorentz theory is that it must deal with a single scattering at a time, so a multiple scattering model

should be developed in order to deal with the such effects [62]..

5.5 Lorentz Mie Scattering Theory

The Lorentz-Mie theory is applicable for the scattering of light in a particular direction by an inhomogeneous medium. If a single particle is exposed to incoming electromagnetic radiation, a part of it is absorbed and rest is scattered away. This theory involves many parameters, such as the refraction index, particle size, wavelength of incident radiation and the medium index of refraction in terms of the spherical Bessel equation. Using boundary condition of the electric and magnetic fields of a scattering amplitude, the scattering condition $S(0)$, can be characterize in the propagating direction:

$$S(0) = \frac{1}{2}\sum_{n=1}^{\infty}(2n+1)(b_n + c_n) \tag{5.15}$$

In this equation, b_n and c_n are scattering coefficients holding Bessel functions and their derivatives.

For a spherical particle with the size of a, complex refractive index N_1, the refractive index of the enclosing medium is N_2, then the scattering size parameter x is given by:

$$x = k \cdot a \tag{5.16}$$

In this equation, k is wavenumber in the enclosing medium: $k = 2\Pi/\lambda = 2\Pi N_2/\lambda_0$, and λ and λ_0 are the wavelengths in the enclosing medium and vacuum.

By using an optical theorem, which describes the relationship between the extinction cross section C_{ext} and the scattering amplitude $S(0)$ real part. This relationship can be expressed as:

$$C_{ext} = 4\Pi \cdot Re\left\{S(0)/k^2\right\} \tag{5.17}$$

By application of series expansion the full description of the extinction C_{ext}, scattering $C_{scatter}$ and absorption C_{absor} cross section can be achieved, as follows:

$$C_{ext} = \frac{2\Pi}{x^2}\sum_{n=1}^{\infty}(2n+1) \cdot Re\left\{(b_n + c_n)\right\} \tag{5.18}$$

$$C_{scatter} = \frac{2\Pi}{x^2}\sum_{n=1}^{\infty}(2n+1) \cdot \left\{|b_n|^2 + |c_n|^2\right\} \tag{5.19}$$

$$C_{absor} = C_{ext} - C_{scatter} \tag{5.20}$$

In a case where the size of the particle is immensely smaller than the incident wavelength, then C_{absor} is directly proportional to the volume of the particle and inversely proportional to the wavelength. On the other hand, $C_{scatter}$ is proportional to the square of the volume and inversely proportional to the fourth power of the wavelength. C_{absor} and $C_{scatter}$ can reach to the geometry of the cross section, if the size of the particle is significantly greater compared to the wavelength. In this section, all derived equations and their descriptions referred to source [62].

5.6 Effective Medium theory

The basic requirement of the Effective Medium Theory (EMT) is that the embedded particles in the inhomogeneous materials are significantly smaller than the wavelength of incident radiation. The most commonly derived effective theories are Bruggeman(BG) and Maxwell Garnett(MG). Both theories make their own assumptions, thus the simplification of the random unit cell (RUC) is used. It approaches to the two different random structures, and these bedded structures in an effective medium should not be evident by incident radiation. The two different theories require separate unit cells. If the EMT theory is taken into account, that means the RUC should be invisible for a given incident electromagnetic wavelength, then the forward scattering amplitude $S(0)$ should be equal to zero according to the Lorentz-Mie theory.

$$S(0) = 0 \tag{5.21}$$

To derive the theory for BG, we should begin with forward scattering amplitude by considering a coated sphere (CS), then the $S^{cs}(0)$ can be expressed in expansion form:

$$S^{cs}(0) = \frac{2\Pi}{x^2} \sum_{n=1}^{\infty} (2n+1) \cdot \{(b_n + c_n)\} \tag{5.22}$$

In this equation, b_n and c_n are scattering coefficients holding Bessel functions and their derivatives. We also know about the filling factor:

$$f = \left(\frac{a}{b}\right)^3 \tag{5.23}$$

In this equation, a and b are the inner and outer sphere of the RUC. The series in Equation 5.22 can be expanded more and set to zero to satisfy the

effective medium condition in a simple manner. It can lead to obtaining the effective MG dielectric function ε^{-MG}, which can be expressed as:

$$\varepsilon^{-MG} = \varepsilon_B \left(\frac{\varepsilon_A + 2\varepsilon_B + 2f(\varepsilon_A - \varepsilon_B)}{\varepsilon_A + 2\varepsilon_B - f(\varepsilon_A - \varepsilon_B)} \right) \tag{5.24}$$

In this equation, ε_A and ε_B are the dielectric constant.

To drive the Bruggeman theory, we should again begin with forward scattering amplitude by considering a sphere with a small sphere limit. It can lead to obtaining the Bruggeman effective dielectric permeability approximation, ε^{-BR}, that can be expressed as:

$$f \left(\frac{\varepsilon_A - \varepsilon^{-BR}}{\varepsilon_A + 2\varepsilon^{-BR}} \right) + (1 - f) \left(\frac{\varepsilon_B - \varepsilon^{-BR}}{\varepsilon_B + 2\varepsilon^{-BR}} \right) \tag{5.25}$$

In this equation, f and $1-f$ are the filling factor of the material A and B respectively; meaning the metal and dielectric components. In this section, all derived equations and their descriptions referred to sources [12, 62, 72].

5.7 Absorber performance enhancement

The performance of the solar absorber has had a major impact on all solar thermal systems. By enhancing the performance of the absorber, they become more feasible and efficient. There are some techniques available to improve performance, which are listed below.

- Anti Reflection (AR) coatings: This is a thin coating or layer of optical material (usually dielectric oxide) on the surface of the absorber used to reduce the effects of reflection. By reducing the amount of reflection, it improves the energy gain of the absorber.

  The index of refraction is a key element in light interaction with a surface, which describes the speed of light in the medium as well as the interference of the wave. With the proper selection of refractive index in the AR coating, the reflectance can be nullified by producing destructive interference on the absorber surface. It can also improve the transmission of the wave by constructive interference. Both types of interference rely on the incident angle, wavelength and refractive index of the anti reflectance material and the underlying material.

  There is one more optical equation that conveys the concept of enhancement in the AR coating. It states that the AR coating will have an optimal effect if the square root value of the refractive index of the

anti reflection material is equal to the refractive index of its underlying material. That can be expressed as:

$$n_R = \sqrt{n} \tag{5.26}$$

In this equation, n_R and n are the refractive index of the AR coating and the material, respectively. But this formula is limited by only being applicable for non-absorbing materials. Absorbers coated with AR have an increase in solar absorptance and providing the AR layer is ($< 100nm$), it does not account for additional thermal emittance. The concept as mentioned above about the refractive index has adopted for AR coating in this project. There are many material available for AR coating, such as Silica (SiO_2), Titania (TiO_2) and Aluminum Oxide (Al_2O_3). Sol-gel fabricated Amorphous silica and Titania have a refractive index of 1.4 and $2.0 - 2.2$ respectively [12].

- Graded index: In a graded index, the indexing of refraction is used for better absorptance. The design of the graded index is done in such a way that the refractive index is altered, step by step, from the top to the bottom of the structure. This method provides the best performance if the surface of the coating contains no metal, and the solar absorbing layer has its highest concentration of particles at the cermet interface [12]. The index profile can imitate several mathematical models, such as linear, quintic and cubic. A significantly lower reflection can be achieved over a broad spectral range of the incident angle. The limitation selection of material for the index profile is associated with its restriction from practical application. The fabrication of a graded surface by application of oblique-angle physical vapor deposition has a refractive index from 1.0 to 2.0 [73].

Chapter 6

Methodology

Methodology is a combination of the practices, procedures and principles which have been emphasized throughout the research. It is a theoretical or qualitative analysis tool which corresponds with the stream of basic knowledge behind the techniques and methods used in research.

6.1 Characterization tools

For optical characterization, certain techniques have been chosen to determine the structural and chemical composition of the absorbing layer and the anti reflection coating of a material. Scanning Electron Microscopy and Energy Dispersive X-ray spectroscopy have been carried out to discover the nano structural properties, morphology and chemical composition of these elements. Addition to this a spectrophotometer and an ellipsometer were used to determine the physical properties of absorbing layer.

6.1.1 Scanning Electron Microscopy(SEM)

Scanning electron microscopy (SEM) is based on an electron gun that is able to eject a focused beam of electrons containing a very high energy, which is utilized to produce a different range of useful signals from the surface of the sample. SEM uses a well focused electron beam which is moved over the surface of the sample, and the interaction of the electrons to the sample surface remits signals, as backscattered and secondary electrons, which can be collected by using appropriate detectors to reveal the desired information. The secondary and backscattered electrons are of much interest, because they change as the surface topography changes. The data in most applications is gathered by using a particular detector for a selected surface area on the

sample, which is focused on a screen by using a Cathode Ray Tub (CRT) to produce a 2 dimensional image. The sample scanning in SEM is performed in a vacuum chamber, and conductive samples are usually used. SEM is a quite efficient and widely-used technique for surface investigation [52, 62].

A Zeiss Merlin Compact VP with high resolution up to $0,8\ nm$ has been used to evaluate the surface morphology and uniformity of the CNT-coated aluminum substrate.

6.1.2 Energy Dispersive X-ray(EDX) spectroscopy

SEM combined with an energy dispersive x-ray (EDX) detector is currently the most common combination of techniques used to perform a chemical analysis. EDX is also commonly known as chemical characterization technique. EDX uses the same mechanism as SEM, but it uses an X-ray to interact with the sample. The working principle of EDX relies on the concept that each material has a different atomic structure, and when a material interacts with a focused beam of electrons, they produce peaks in its X-ray spectrum. These can be detected with the EDX detector. EDX is used to more clearly examine the crystalline structure and orientation of a material by means of Electron Backscatter Diffraction (EBSD) [52].

A Scanning Electron Microscope with EDX (with an X-max SDD detector with 80 mm^2 diameter sensor), manufactured by Zeiss Merlin Compact VP, was used in this experiment. AZtec 2.2 Software was integrated with the EDX detector to analyze the chemical composition of the material, as well as perform element mapping. EDX was performed to evaluate the element constituents, particle sizes and various material content of the CNT-coated aluminum substrate. The atomic percentage of Carbon (C), Aluminum (Al), Oxygen (O) and Sulfur (S)have also been recorded.

6.1.3 Spectrophotometer

A reflectance measurement was performed using a spectrophotometer in order to determine the value of absorptance and the emittance of the absorber. These measurements have not been carried out by myself. The normal reflectance measurement was performed for prepared absorber samples in the wavelength range of 0.3 to 20 μm. A Perkin-Elmer Lambda 900 spectrophotometer (furnished with an integrating sphere with a diameter of 150 mm, the diameter of circular beam entrance and sample ports of 19 and 25 mm, respectively) was employed in the range of 0.3 to 20 μm. A Bomen Michelson 110 and a Bruker Tensor27 FTIR spectrophotometer were used for the measurement of infrared wavelength intervals of 2.5 to 20 μm. As a reference, a

mirror a sample of a spectralon and an evaporated gold mirror were used to carry out the measurement for the visible and infrared spectrophotometer, respectively. Furthermore, the measurements were merged to form a single spectrum, and normal α_{sol} and $\varepsilon_{thermal}$ values were determined by deploying equations 5.13 and 5.14, respectively [12].

6.1.4 Ellipsometry

An ellipsometer was used to try determine the refractive index values of the CNT-coated aluminum substrate. Ellipsometry is an optical-based practical method, which is employed to determine the dielectric properties of a thin film material. The instrument used to perform ellipsometry is known as an ellipsometer. The basic principle of ellipsometry is to measure the changes in polarization after a light is reflected or transmitted from the sample. The basic components of an ellipsometer are a light source, a polarization generator, a sample, a polarization analyzer and a detector. The greatest interest of ellipsometry is to evaluate the change in p and s components during light interaction with the sample. A light with a known polarization passes through a polarizer generator. The polarizer is set between the p and s axis in such a manner that both reach the sample surface. The linearly polarized light reflects from the sample surface and travels further through the rotating polarizer. The amount of light that will pass through depends on the polarized orientation related to the incoming electric field from the sample. The light will be detected and converted into an electrical signal used to evaluate the reflected polarization. To determine the cause of polarization-changes in the light by the sample reflection, the detected signal is compared to the known polarization. It can be expressed in terms of amplitude ratio and phase difference. The changes in polarization can vary with the changes in optical properties and the thickness of each sample. An ellipsometer is limited in that the collected information should be modeled using a proper model to drive the desired parameters. It is most commonly used to determine complex refractive index, thin film thickness and surface roughness [74].

An ellipsometer manufactured by Wollam was used in this experiment. It was used to measure the refractive index and to measure the film thickness of the CNT-coated aluminum substrate absorber. The proper model, gain setting, and light dispersion were the main issues of the project. This experiment took place at NORUT located in Narvik. But the measurement was unsuccessful.

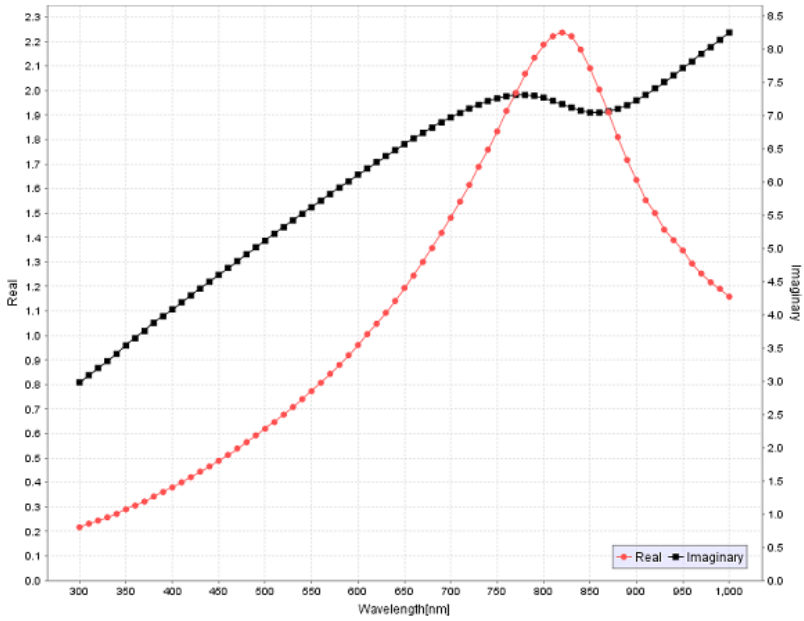

Figure 6.1: Real(n) and imaginary(k) parts of the complex refractive index of aluminum as a function of wavelength [75].

6.2 Simulation of spectrally selective absorbers

This simulation was performed to gain theoretical and experimental data on spectrally selective absorbers. The complex refractive index of the selected materials were simulated to determine the reflectance values for the wavelength range, from 0.3 to 20 μm.

6.2.1 Material Used

The simulation was focused on carbonaceous material due to its optical and physical properties at nanostructural level. Therefore, seven different forms of carbon materials plus aluminum were chosen as substrates. Furthermore, for the anti reflection coating, three different oxide materials were used. These are explained in detail below. It is also important to note that the refractive index (n) and extinction coefficient (k) values for each section were taken either from the material database of the simulation software called Setfos or using the literature's, and are available along with their corresponding wavelengths in the associated Table. In addition, to achieve a more thorough understanding of the n and k values in each section, especially the variation of both values against the wavelength, refer to the associated Figure.

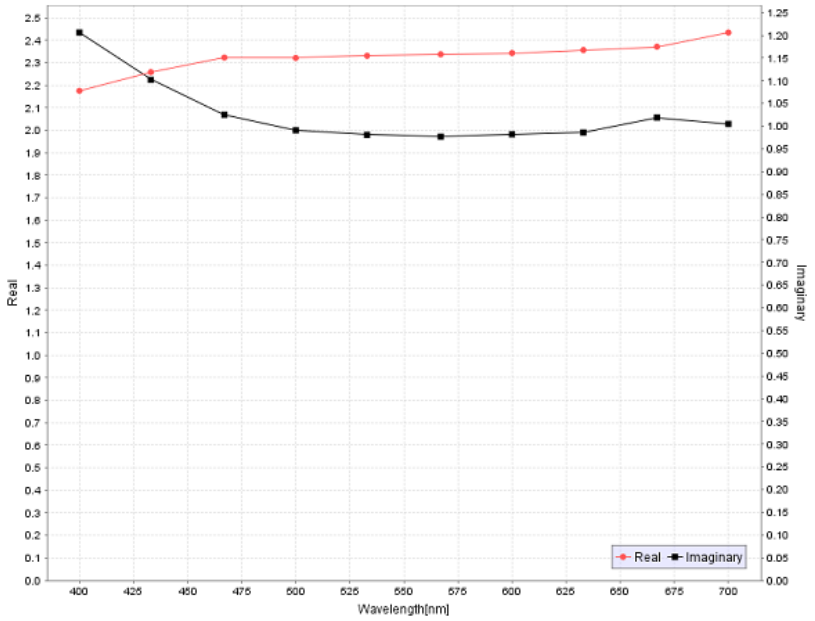

Figure 6.2: Real(n) and imaginary(k) parts of the complex refractive index of amorphous carbon as a function of wavelength at 25°C [76].

- Aluminum (Al): Aluminum was used as a substrate because of its ease of availability, as well as its physical and optical properties. Al is a material which exists in really large quantities on the Earth's surface, making it cheap to produce for application. It has a wide range of physical properties: low density (making it light weight), durability, ductility and lack of magnetism (making it difficult to ignite). It also holds a chemical property which allows a thin layer of oxide to form when it comes into contact with air, preventing corrosion. Al also possesses optical property such high reflectance in infrared wavelengths. Its thermal and electrical conductivity is also quite efficient in comparison to other elements such as copper. All of the aforementioned properties make it one of the most favorable materials to act as a solar absorber substrate. The complex refractive index values were taken from the Setfos material database but, the end source is [75]. The wavelength range in this experiment spans from 300 to 1000 nm. For further details, refer to Table 9.1 and Figure 6.1.

- Amorphous Carbon (AC): AC now can be fabricated in a pure form due to the advancements in nanotechnology, especially those related to CVD. It does not consist of a crystalline structure, and the bonds are much more flexible that other carbonaceous materials. It is consist of

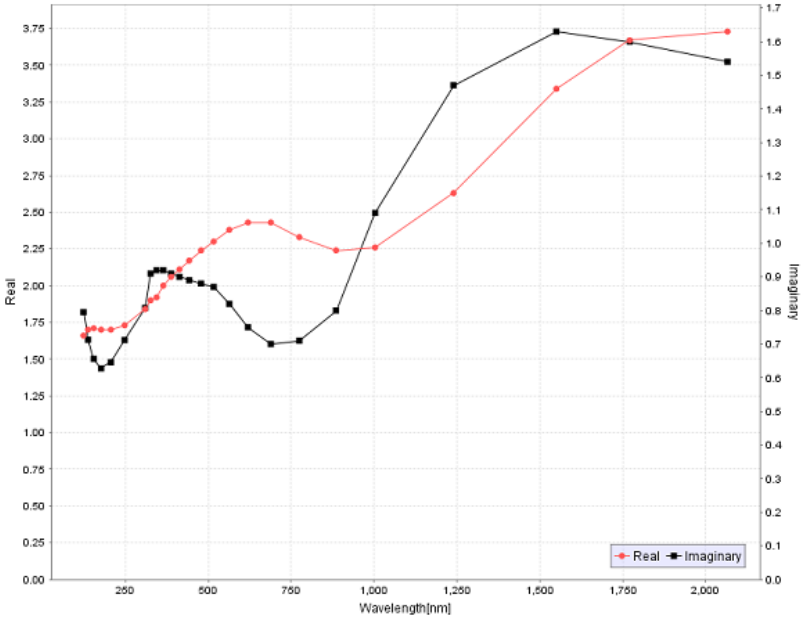

Figure 6.3: Real(n) and imaginary(k) parts of the complex refractive index of arc evaporated carbon as a function of wavelength [77].

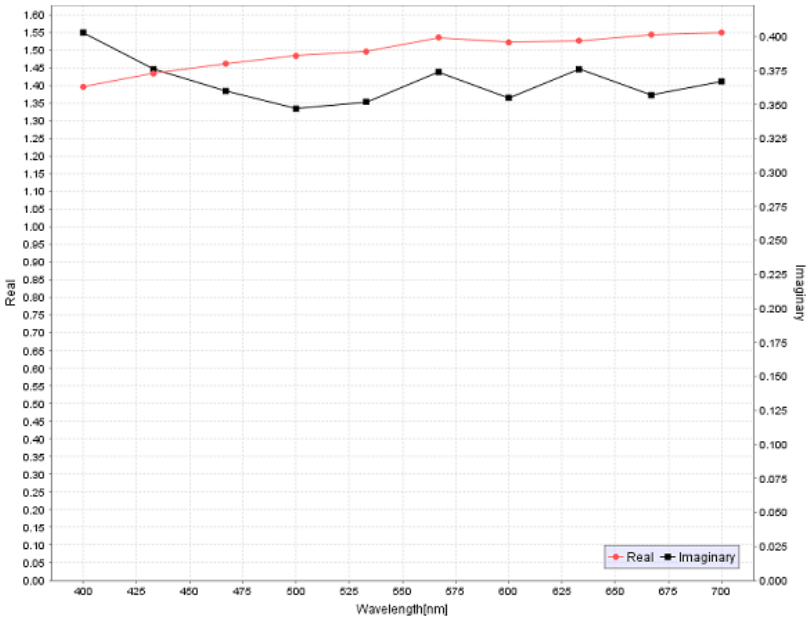

Figure 6.4: Real(n) and imaginary(k) parts of the complex refractive index of amorphous carbon as a function of wavelength at 25°C [76].

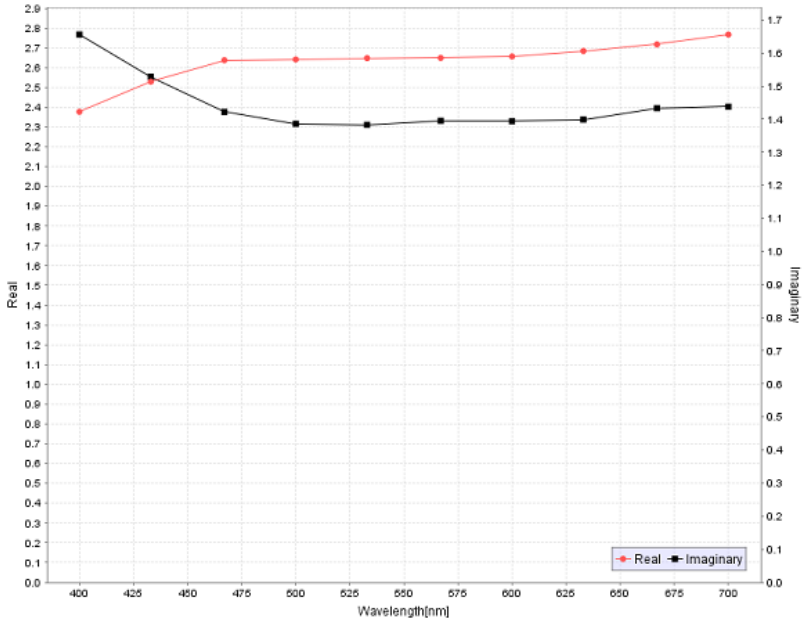

Figure 6.5: Real(n) and imaginary(k) parts of the complex refractive index of graphite as a function of wavelength at 25°C [76].

dangling bonds in majority that result in inter atomic space, which can be perfect for the reinforcement of any desired material. The refractive index (n) and extinction coefficient (k) values used here have been taken from the literature [76], and the values can be found in Table 2 at 25°C. Also found in the literature, AC is a sample with dimensions of 2.5 X 2.5 X 0.6 cm with a concentration of impurities as high as 700 ppm [76]. The wavelength range in this experiment spans from 400 to 700 nm, and the n and k values were taken at 25°C. For further details, see Table 9.5 and Figure 6.2.

- Arc evaporated carbon(AEC): AEC is usually produced by the evaporation of a carbon rod in a vacuum evaporator. It can be produced with high mechanical stability and as an extremely thin homogenous film. AEC can be used as a coating due to its anti-oxidizing properties under normal atmospheric conditions, which also allows it to be used as a protective covering for metal. This type of carbon lacks the distinct crystalline structure than other forms of carbon contain, making it unique in this way [78]. The refractive index n and extinction coefficient k values were taken directly from the literature [77], and these values can be found in Table-VII. For further details, see Table 9.9 and Figure 6.3.

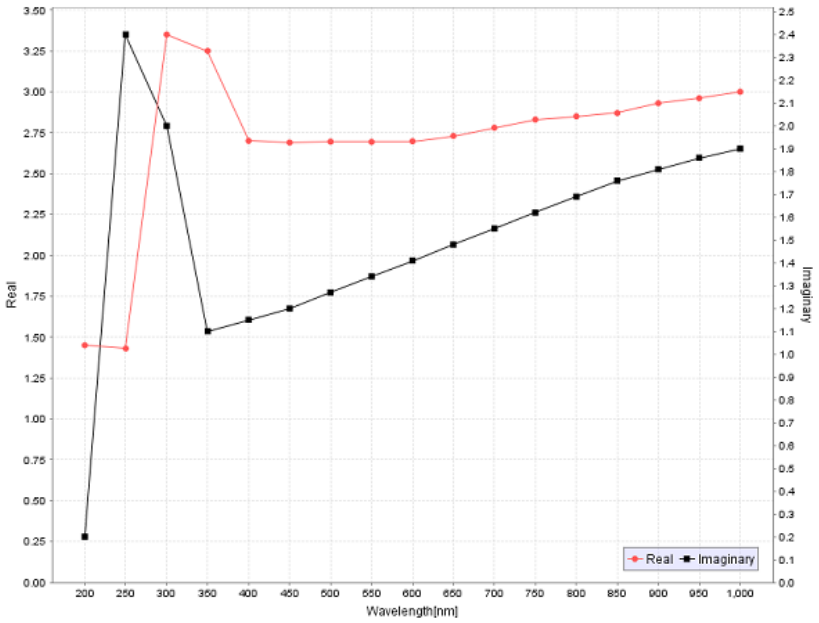

Figure 6.6: Real(n) and imaginary(k) parts of the complex refractive index of graphene as a function of wavelength [79].

- Soot: Soot is a result of the incomplete combustion of hydrocarbons, which exists in the form of impure carbon particles. There are many different ways to produce soot: through the burning of coal, house fires, internal combustion engines and many more. The complex refractive index has been referred from literature [76], which can be found in Table 3 of the literature. The article states that the soot was collected from a premixed propane-oxygen flame on a stabilizing ceramic honeycomb, which was placed 30 cm over the surface of the burner [76]. The wavelength range in this experiment spans from 400 to 700 nm, and the n and k values were taken at 25°C. For further details, see Table 9.7 and Figure 6.4.

- Graphite: Graphite is an allotrope of carbon, and is a much better thermal and electrical conductor than a diamond. It is one of the most stable forms of carbon, which is typically used in thermochemistry as the standard. Due to its honeycomb lattice structure, it is referred to as carbon fiber-reinforced polymer. The refractive index values for n and k are adopted from the literature [76], and can be found in Table 1 of the article. Pyrolytic graphite has been used in the experiment outlined in the article, which is very similar to the properties of natural graphite. The graphite is in the shape of a disc with a diameter of 2.54

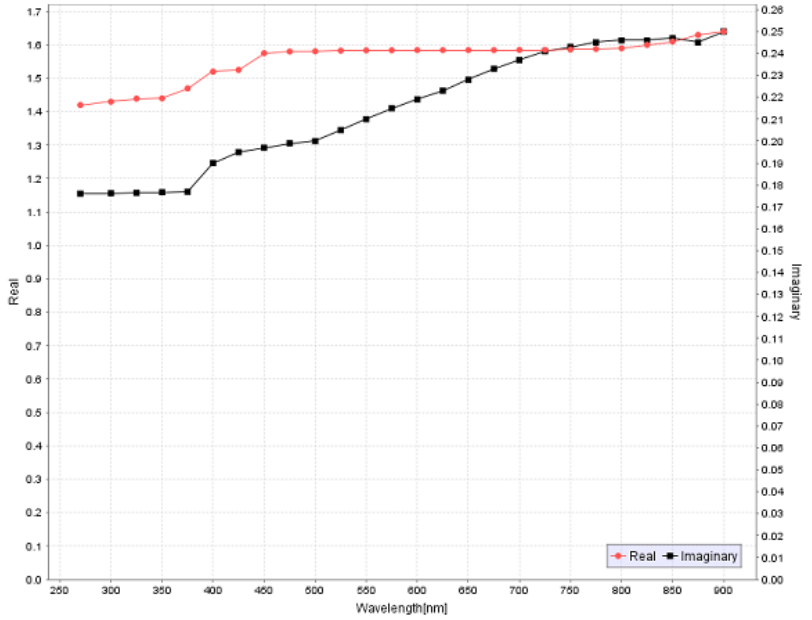

Figure 6.7: Real(n) and imaginary(k) parts of the complex refractive index of SWCNT(High) as a function of wavelength [80].

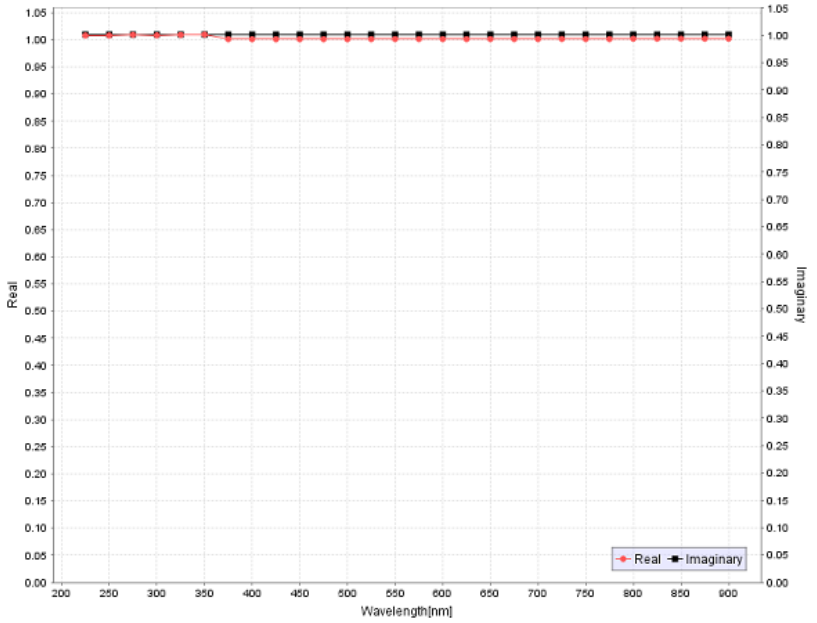

Figure 6.8: Real(n) and imaginary(k) parts of the complex refractive index of SWCNT(Low) as a function of wavelength [80].

cm and a thickness of 0.6 cm. It was bought from the Pfizer Chemical Corporation of Easton, Pennsylvania in the U.S.A. The number of impurities in the sample were less than 15 ppm. An ellipsometer has been used to measure the complex refractive index in the literature [76]. The wavelength range in this experiment spans from 400 to 700 nm, and the n and k values were taken at 25°C. For further details, see Table 9.8 and Figure 6.5.

- Graphene: Graphene is also an allotrope, which is a pure form of carbon, and can be referred to as a single-atom sheet of carbon. It appears as an extremely thin layer with a honeycomb lattice structure, making it very low in weight with exceptional strength. It possesses extraordinary conductive properties, therefore is highly efficient in conducting electricity and heat. It is also contains various thermal and optical properties. The complex refractive index values were taken from Figure 2 of literature [79]. The graphene is used in the literature as a mechanically exfoliated graphene flake of 150X380 m^2 over a silicon substrate with a of thickness of 98 nm, as well as an anti reflection coating of silicon oxide (SiO_2), 300 nm thick. The thickness and complex refractive index were calculated using ellipsometry [79]. The wavelength range in this experiment spans from 200 to 1000 nm. For further details, see Table 9.6 and Figure 6.6.

- Single walled carbon nano tube (SWCNT): The SWCNT has emerged as the best material for electrical, mechanical and electronic application. It is considered to be a single layer of graphene sheet rolled into a nano diameter cylinder. SWCNTs posses extraordinary electrical and thermal properties, due to their unique atomic two-dimensional structure obtained from the graphene. They also contain properties somewhere between a metal and a semiconductor, which makes their application of use even wider [84]. The complex refractive index n and k values for $SWCNT(High)$ and $SWCNT(Low)$ were taken from Figure 6 (B and C respectively) in the literature [80]. The sample structure used in the article is a 1 mm thick bulk silicon as a substrate, SWCNTs coating with a thickness of 15 to 40 nm (which has been approximated by effective medium approximation) as well as a layer of silica at 3 nm thick. Two different types of n and k values were used, due to the mean square error (MSE) used to find the base optical model. So the same optical model is used with different MSE values of 5.03 and 7.54 for $Si/SiO_2/CNT_{High}$ and $Si/SiO_2/CNT_{Low}$, respectively. One main difference is the fraction of void space in $Si/SiO_2/CNT_{High}$ was found

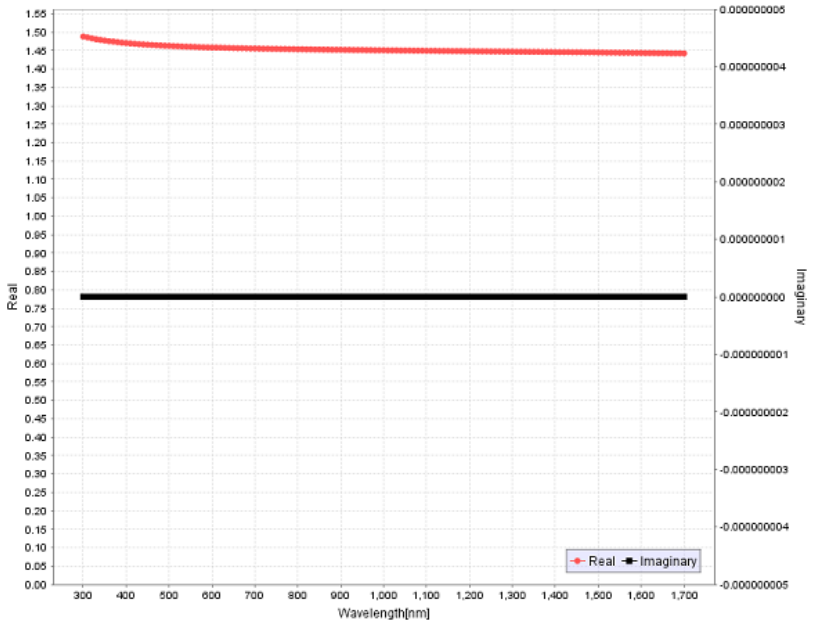

Figure 6.9: Real(n) and imaginary(k) parts of the complex refractive index of S_iO_2 as a function of wavelength [81].

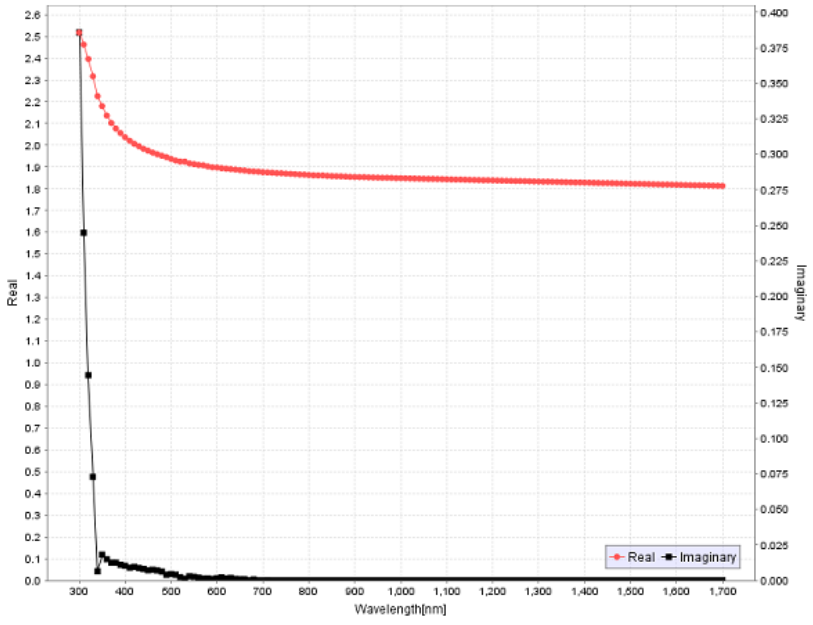

Figure 6.10: Real(n) and imaginary(k) parts of the complex refractive index of T_iO_2 as a function of wavelength [82].

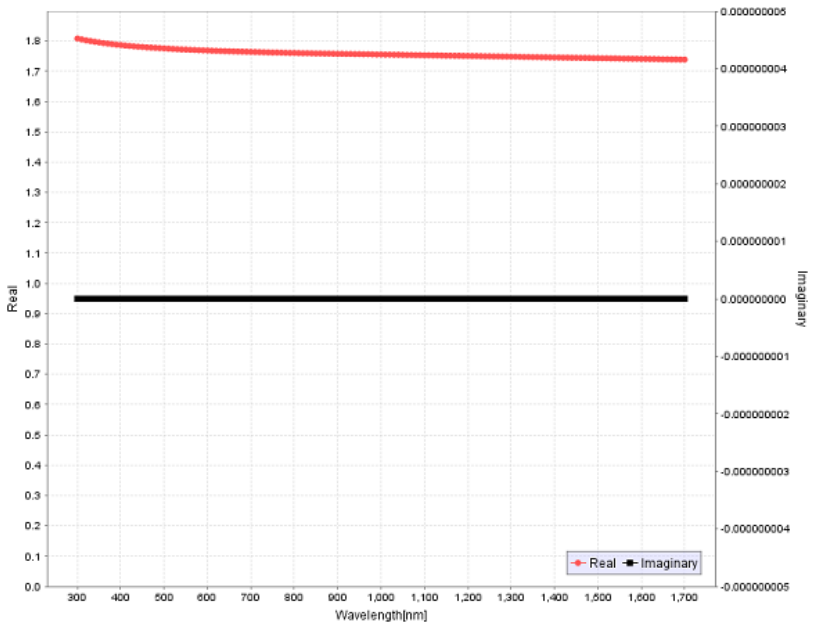

Figure 6.11: Real(n) and imaginary(k) parts of the complex refractive index of Al_2O_3 as a function of wavelength [83].

at 30%, and $Si/SiO_2/CNT_{Low}$ was found at 98% only. The wavelength range in this experiment spans from 270 to 900nm. Further details can be found in Tables 9.10 and 9.11, as well as Figures 6.7 and 6.8.

- Anti reflection material: To achieve the best and most optimum anti reflection coating, the relative index Equation 5.26 was also taken into account. The refractive index values for SiO_2, TiO_2 and Al_2O_3 have been taken from the Setfos simulation software material database but the end source are [81–83], respectively. The wavelength range in this experiment spans from 300 to 1700 nm. Further details can be found in Tables 9.2, 9.3 and 9.4 and as well as Figures 6.9, 6.10, 6.11.

6.2.2 Simulation software

The Semiconducting Thin Film Optics Simulation Software (Setfos), version 3.4 is a Windows-based software that was chosen for several reasons. These include its simple graphical user interface, easy and quick steps for editing solar absorbing layers and its price.

Setfos is a easy to use and powerful software system for numerical simulation for further development in optoelectronic thin film based technology. It has been used to obtain a better understanding of the internal physics of

solar selective absorber layers, by evaluating the physical parameters that affect the electrical and optical properties of a material. In addition, it also aids in understanding and optimizing the design as well as the performance parameters of the solar selective absorber [85].

Setfos has provided three different system modules: an **Absorption module** for the optical design of solar cells and optical coatings, a **Drift-diffusion module** for charge transport in organic semiconductor devices such as organic light emitting diodes ($OLEDs$) as well as organic solar cells (OPV) and an **Emission module** for the optical design of emissive multi-layer structures such as OLEDs and LEDs. It also consists of four different modes: toggle passive optics, toggle absorption, select sweep mode and select optimize mode. The modes can be utilized for any of the three modules. The Graphical user interface (GUI) consists of four main tabs. These are described below, along with some other features of Setfos.

- Graphical input tab: The graphical input screen consists of all the necessary toolbars for operation, layer and physical module settings to create and run simulations, as well as a graphical representation of the layer structure, which can be visualized on the same screen. It also contains the side tabs, which facilitate the switch from one screen to another. This is considered to be the main screen, with all the aforementioned modes, layer setting and the physical parameters (such as thickness, refractive index, wavelength intervals and many more). The diagrams representing energy levels are in the tab next to the layer structure setting. In addition, the validation of the graphical user input rectifies the basic fundamental errors before execution, and provides an easier way to start a simulation from the very beginning. The validation text states: 'validation status is okay', 'simulation can run' or 'validation error,' with the respective reason in the bottom of the graphical input tab.

- Script editor tab: This tab offers a much more efficient way to editing the existing script or text file of the simulation. The editor can also be used to edit general text. The new version 3.4 allows the conversion of the script to GUI. It also possesses an optical material as well as an electrical material editor. These can be used to analyze the data by plotting it on a graph. For instance, the material editor was used for plotting the complex refractive index as a function of wavelengths. The plotting can also be edited.

- Output console tab: This provides all the information on the simulation while it is running by displaying a progress bar, which can be used to

abort the simulation if necessary. The screen has all of the important information produced by both GUI and kernel while the simulation is in progress, along with warnings and errors to the console. Therefore, it is always important to keep an eye on this tab after each simulation in order to make sure that the simulate output is error free.

- Result tab: This is the final tab that appears after completion of a successful simulation, with all of the results presented in an organized manner. The final results are arranged on the left side of the screen, containing additional information and a spectral section organized in a categorized manner by box. The additional information box usually consists of a warning regarding the simulation results, if there are any regarding the key optical figures. The spectral box also contains all of the diagrams. In addition, the results tab serves the purpose of data importation and exportation, and also functions as a diagram editing tool. The data and diagrams can be exported and saved by just clicking the plot and choosing the particular option. Of special value is a plot enrichment tool on the right side of the screen, used for plot editing. This tool has many functions which affect the plots, such as changing color, changing width and shape, setting the x and y axis as logarithmic form.

The description and information are in above subsection refer to source [85].

6.2.3 Simulated parameters

This section will discuss the data used for the simulation, as well as the parameters derived from the simulation. As mentioned in section titled 'Materials Used,' the wavelength range for the collected n and k values is 270 to 1700 nm. This data has been collected from the given tables and figures in the referred literature, and the complex refractive index for some materials were directly taken from the Setfos material database.

The simulation began by structuring the absorber selective layers on the main graphical input screen. The mode used was toggle passive optics, which is symbolized as an eye on the top of the input screen that evaluates the absorption, reflection and transmission parameters of the material. The screen has an interactive layer-setting panel, which can be used to define the layers name, thickness in nm, thickness in μm, and refractive index. An aluminum substrate of 100 μm was used throughout the simulation. The thickness of the absorbing material layer varied from 20 to 480 nm in an attempt to achieve

optimal $\alpha_{sol}$and $\varepsilon_{thermal}$ values. The anti reflection coating is about 100 nm for all selected materials. The refractive index values can be chosen as a constant or as a file with three column wavelengths, n and k values respectively. For air, the refractive index used is 1 as a standard, otherwise for substrate, solar absorbing layers and anti reflection coating a file with multiple n and k values as a function was used. Once the necessary information was entered into the layer setting panel, the layer structure simultaneously formed on the right side of the screen, with a different color, name of layers and thickness for each material. The wavelength range used for the simulation is 300 to 20000 nm with a step value of 15 nm. The simulation 'quick run' button in the top tab of the screen was used to start the simulation. The screen switched to an output console screen containing all of the information regarding the simulation progress. After the simulation was finished, it again switched to the results tab with final additional information and relative spectral plots. The simulated parameters were then saved, exported and re-edited in the results tab. From the simulated parameters, only the reflectance data has been used. For further calculations of the absorptance and emittance values, the simulated reflectance data is combined with the matlab program. The matlab program was adopted from the Uppsala University, Sweden and further edited it to suit the Setfos data.

Extrapolation of refractive index: As previously mentioned, the simulation wavelength range extended from 0.3 to 20 μm, although the collected refractive index data typically fell under a wavelength of 1 μm. When the values do fall out of the typical wavelength range, the simulation software treats them as a constant and extrapolates the dataset constantly [85]. The simulation has been carried out in the project with this information in mind.

Chapter 7

Sample preparation

The samples that have been used in this project were prepared by PhD student Chen Zhonghua at the laboratory of Renewable Energy (PV) at Norut Northern Research Institute AS, which has locations in both the towns of Narvik and Tromsø in Norway. In order to identify optical and structural characterizations as a part of this project, SEM and EDX have been utilized. A brief description regarding sample preparation is included in this chapter.

7.1 Aluminum substrate

A smooth aluminum surface with a protective Al_2O_3 layer on the top has been used in this experiment. The protective layer is there to prevent any unwanted damage as well as to minimize contamination of the surface and have to be removed before the coating process. The aluminum substrate used has a dimension of 30X30 mm and a thickness of about 300 μm. This particular size has been chosen to prevent the changes in structure due to the edge effect and in order to fit inside of the furnace. Due to the natural oxidation phenomenon a about 10 nm, a thin layer can be seen on the surface of the aluminum in transmission electron images. The thin layer is usually composed of alumina that instantly manifests itself when the aluminum surface is exposed to air [12].

7.2 CNT solution

A CNT dispersion solution mixed with water has been used in the experiment, which was bought from an n-tech company and can be seen in Figure 7.1. The concentration of CNT in the dispersion solution is one gram per liter, and is stabilized with Sodium Dodecyl Sulfate (SDS). SDS is most

Figure 7.1: CNT dispersion solution in water.

commonly used for its fine solvent and stabilization qualities, which allow CNTs to disperse in water. The CNT dispersion solution is stirred in a simulator for many hours in order to facilitate better dispersion and stabilization of the CNTs, as a better CNT stabilization provides a more uniform coating.

7.3 EPD for CNT deposition

EPD techniques have been used for the deposition of CNT on the aluminum substrate. These techniques have been chosen due to low cost, a higher quality coating and better homogeneous deposition. In addition, the conductivity of CNTs is very efficient, which is helpful to the working principle of EPD.

A photo of the experimental setup can be seen in Figure 7.2, which has been used for CNT deposition in the laboratory. The setup for EPD is very simple: it is composed of a *DC* power supply, a holding structure with two aluminum electrodes and a pot filled with the CNT solution. The electrodes

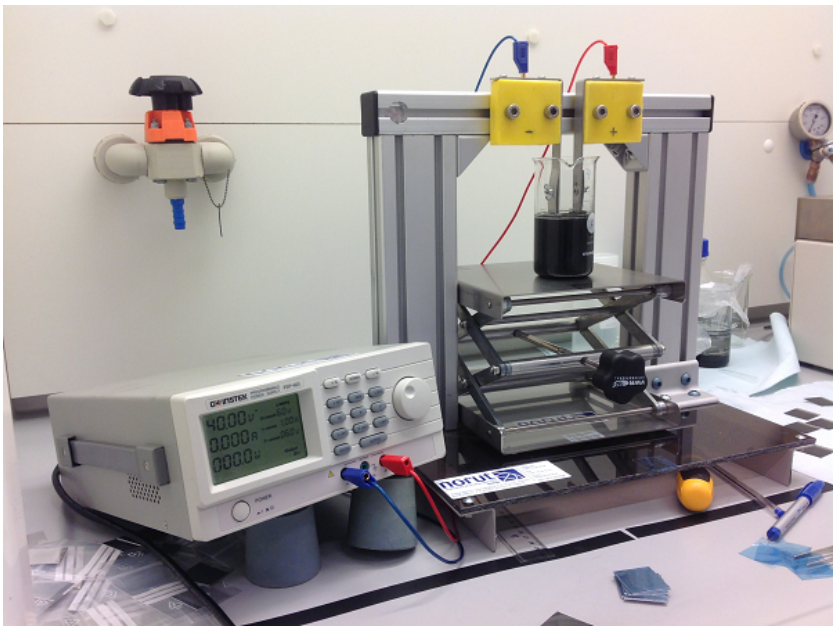

Figure 7.2: EPD experimental set up, the right side electrode in the figure used as anode or counter elctrode for CNTs deposition.

were etched and dried with compressed air before they were inserted into the CNT suspension, where they were arranged parallel to one another. The best control parameters to achieve the desired CNT deposition for the EPD method were found after several trials. The working principle of EPD is based on the influence of electric field on suspended particles to move towards electrode in the solution. The electrodes were submerged into the CNT dispersion solution with a measured distance between the two, and a voltage was then applied to each electrode. Due to the natural flow of the electric field, the CNT suspended particles began to move towards the anode and accumulated on its surface, where the aluminum substrate had been fixed. An electrical charge was applied for a calculated amount of time until the deposition was completed, then the electrodes were removed from the CNT dispersion solution and left to dry at room temperature. A smooth aluminum was used as a substrate. The CNT dispersion solution were mixed with water(as a solvent) as well as Sodium Dodecyl Sulfate (SDS) (as a stabilizer) in order to prepare the samples. The selected prepared samples were S60, S61, and S72 and each one had a different deposition time and thickness. After many trails the optimum common parameters for the EPD process were: a voltage of 50 V, a starting current of 251 mA and ending current of 240 mA, a distance between the electrodes of 30 mm. The deposition times

were 3, 1 and 5 seconds as well as the thicknesses of the CNT deposition have been estimated were 700, 400 and 900 nm, for S60, S61, and S72, respectively.

7.4 Anti reflection solution

Both a silica and a hybrid-silica solution were used in the Anti Reflection (AR) coating. To start the preparation, Tetraethoxysilane (TEOS) and methyltrietoxysilane (MTES) were used as the primary materials. Although the use of TEOS alone makes a film of 100% silica, the combination of TEOS and MTES will produce a hybrid-silica solution. To achieve a coating with higher flexibility, the proportion of MTES should be higher than the proportion of TEOS in the solution. In the very first step, TEOS was blended together with ethanol, followed by blending in a mixture of H_2O containing 0.06 $wt\%$ HCL. The blended solution was stirred for about one hour at room temperature to better hydrolyze the TEOS. A suitable amount of MTES was mixed in with the solution, and the solution was again stirred for the next 24 hours in an enclosed container. This ensures the complete hydrolysis of the solution, which is necessary for coating. The proportion of ethanol and H_2O to the total alcoxide (TEOS + MTES) was 5 and 4, respectively. The blended solution remained stable for more than one week [12].

7.5 Anti reflection coating by Spin coating

There are many methods available for the coating of a surface with a liquid medium, but the most suitable and commonly used method for a laboratory exercise is spin coating. In this spin coating technique, an enclosed chamber manufactured by Specialty Coating System (SCS) and a 6800 series spin coater have been used, as depicted in Figure 7.3. Approximately $0,35$ ml of AR coating solution was ejected on the top and-center of the substrate, using a syringe. In about a fraction of a second, the coating solution covered the full substrate and achieved a fully homogeneous and uniform film. By allowing the solution to evaporate over 30 seconds by a continuation of the spinning process, this results in a more stable coating over the substrate. The thickness of the coating applied by the spin coater depends on several factors, such as the rotational speed of the coater itself as well as the amount of time allowed to spin. Three different rotation speeds (3000, 5000 and 6000 rpm) have been used for coating, resulting in a thinner coating at higher speeds. The total concentration of metal ions in the coating solution is also a crucial factor in the coating thickness. The higher the total concentration of metal

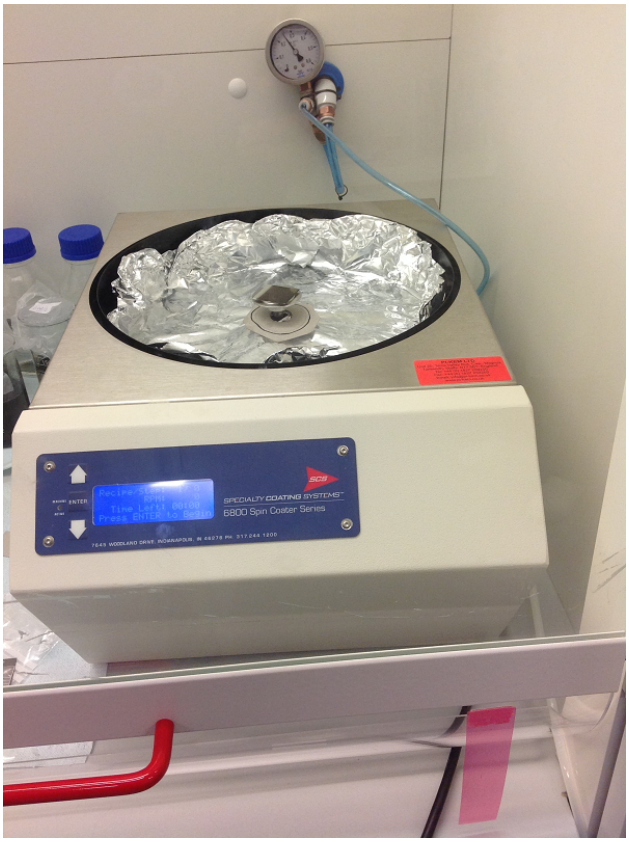

Figure 7.3: Spin coater used for anti reflection coating with 6800rpm.

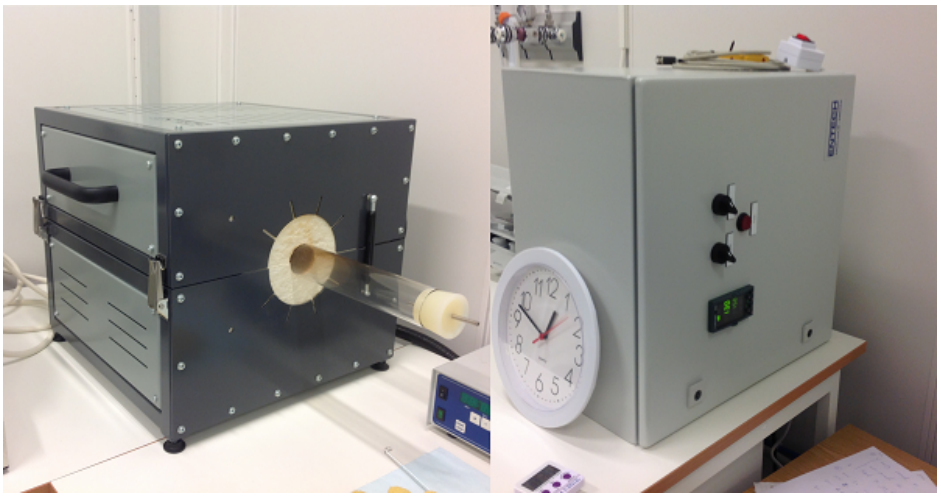

Figure 7.4: Furnace for heat treatment: on the left side of figure furnace with a glass tube and right side a temperature controller.

ions, the thicker the coating on the substrate. Distinct types of structural and physical properties of the substrate can also affect the thickness of the coating [12].

7.6 Heat treatment

After the substrate was removed from the spin coater, it was heated inside the $ESTF\ 50/14 - S$ split-able furnace manufactured by ENTECH. A example of this furnace can be found in Figure 7.4. The coated substrate was heated inside of the furnace, within a glass tube that was 66 mm in diameter. Two parameters were varied throughout the heat treatment process: the incremental temperature levels (*temperature rate*) as well as the end temperature. The starting temperature should be sufficient, otherwise the organic compounds would not be fully removed and the quality of coating on the substrate would be poor. The standard heat treatment for an absorber with an anti-reflection coating was carried out in the following manner: it began at room temperature and increased until reaching the final temperature at 450°C [12].

Chapter 8

Result and Discussion

This chapter is meant to convey the results regarding the simulation of spectrally selective solar absorbers with a single absorbing layer, with and without anti reflection(AR) coating. It will also show SEM, EDX analyses and spectrophotometer of experimentally prepared samples and measured reflectance study, as well as an evaluation of the reliability of the refractive index used for simulation.

8.1 Simulation of reflectance of carbonaceous material

The simulation section compares several single solar selective absorbing layers of varying thicknesses as a function of wavelength, and also examines the best curve for each absorbing layer for optimum absorption and emittance values. This also includes an evaluation of the most favorable thickness of the single layer of anti reflection coating, for enhanced absorptance and lowest emittance values.

8.1.1 Simulation of Reflectance of absorbing layer

The simulation to measure reflectance has been conducted on seven different carbonaceous solar selective absorbing materials at various thicknesses levels in order to examine the variations on reflectance in visible and higher wavelength regions, as well as the varying levels of absorptance and emittance. The optical properties of these materials differ due to inherent absorption and optical interference. Hence, the variation in thickness drives the change in optical properties and causes each curve to differ from others. A change in

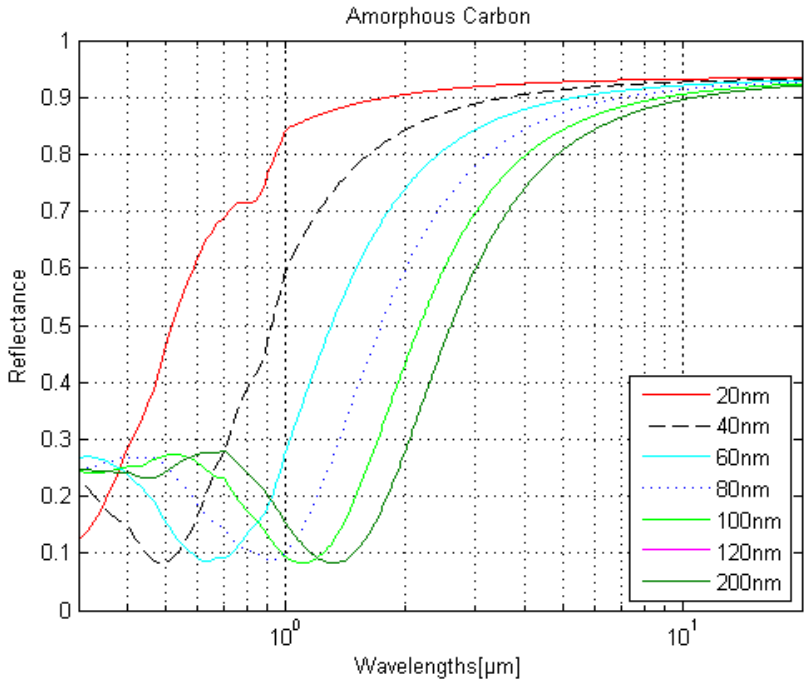

Figure 8.1: The comparison of reflectance at different thicknesses of amorphous carbon form 20 to 200 nm.

the refractive index causes a variation in absorption and reflection of a wavelength. The absorptance(α_{sol}) and emittance($\varepsilon_{thermal}$) of the tested materials were determined using the calculated reflectance values.

- Amorphous carbon(AC): Figure 8.1 demonstrates reflectance curves as a function of wavelength at varying thicknesses levels of amorphous carbon. The destructive interference dip showed a linear shift towards the infrared region with respect to the change of thickness.

  The values of α_{sol} and $\varepsilon_{thermal}$ are listed according to thickness and in relation to absorptance and emittance, as represented in Table 8.1. The α_{sol} increased by increments in thickness until it reached 80 nm, where it became constant at larger values. The selected optimum thickness is 80 nm, with a corresponding value of α_{sol} at 0.78 and $\varepsilon_{thermal}$ at 0.11.

- Arc evaporated carbon(AEC): Figure 8.2 displays the reflectance curves as a function of wavelength at varying thickness levels of AEC. In the infrared region, reflectance decrease as wavelength and thickness also increased. There was no noticeable constructive and destructive interferences up to a thickness level of 20 nm, but from 40 nm and up

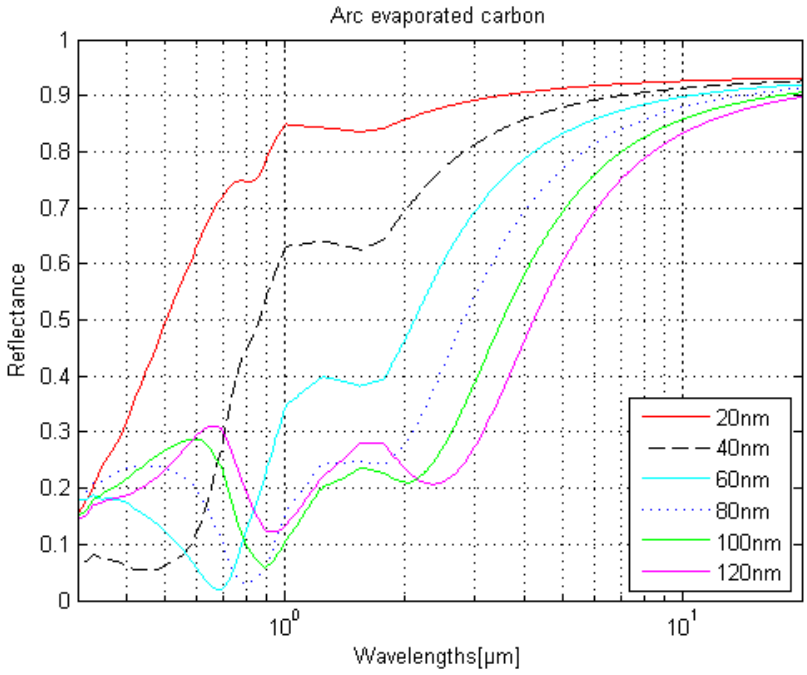

Figure 8.2: The comparison of reflectance at different thicknesses of arc evaporated carbon from 20 to 120 nm.

Table 8.1: Absorptance and emittance values for amorphous carbon.

Thickness(nm)	Absorptance	Emittance at 100°C
20	0.32	0.09
40	0.60	0.09
60	0.74	0.10
80	**0.78**	**0.11**
100	0.78	0.12
120	0.78	0.13
200	0.77	0.11

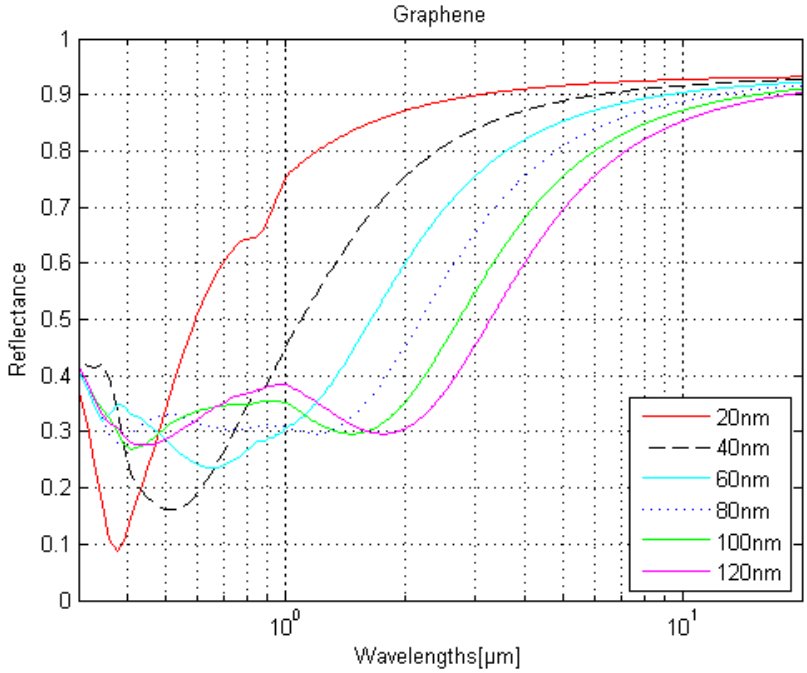

Figure 8.3: The comparison of reflectance at different thickness of graphene from 20 to 120nm.

they occurred with an increasing amplitude towards the infrared region. The contribution of destructive interference to the improvement of absorptance in the solar region reduced as the curve moved towards the infrared region.

The relationships between the α_{sol} and $\varepsilon_{thermal}$ values, and the corresponding thicknesses of the AEC are depicted in Table 8.2. The α_{sol} value increased along with thickness up to a level of 80 nm, but decreased for thicker samples. The selected optimum thickness is 80 nm, with corresponding values of α_{sol} at 0.82 and $\varepsilon_{thermal}$ at 0.15. The $\varepsilon_{thermal}$ value is slightly higher for AEC as compared to AC.

- Graphene: Figure 8.3 displays the reflectance curves as a function of wavelength at varying thickness levels of graphene. The reflectance decreased as wavelength and thickness increased in the infrared region. The destructive interference at 20 and 40 nm thickness had a much higher amplitude compared to the other levels of thickness towards the infrared region. The amplitude of destructive interference dip decreased as the thickness of the graphene increased.

Table 8.2: Absorptance and emittance values for arc evaporated carbon.

Thickness(nm)	Absorptance	Emittance at 100°C
20	0.31	0.09
40	0.63	0.11
60	0.79	0.12
80	**0.82**	**0.15**
100	0.80	0.17
120	0.78	0.20

Table 8.3: Absorptance and emittance values for graphene.

Thickness(nm)	Absorptance	Emittance at 100°C
20	0.41	0.09
40	0.63	0.10
60	**0.68**	**0.12**
80	0.68	0.13
100	0.67	0.15
120	0.67	0.18

The α_{sol} increased with thickness until 60 nm, with minimal changes at further values are depicted in Table 8.3. The selected optimum thickness is 60 nm, and the corresponding value of α_{sol} is at 0.68, with $\varepsilon_{thermal}$ at 0.12.

- Graphite: Figure 8.4 depicts the reflectance curves as a function of wavelength at varying thickness levels of graphite. Within the solar region, destructive interference is evident as displayed in Figure 8.4, moving from 0.3 μm for the 20 nm sample to 1.5 μm for the 120 nm sample. The destructive interference with constant amplitude was seen throughout the solar region, and moved towards the infrared region with incremental increases in thickness. It can be inferred from the curve that destructive interference constantly contributed to absorptance, irrespective of an increase in thickness.

  The relationship between the α_{sol} and $\varepsilon_{thermal}$ values, with the corresponding thickness levels of graphite, are illustrated in Table 8.4. The selected optimum thickness is 80 nm, and the corresponding value ofα_{sol} is at 0.71 with the $\varepsilon_{thermal}$ at 0.12. The value of α_{sol} is slightly higher for graphite compared to graphene, but the $\varepsilon_{thermal}$ value remains the same.

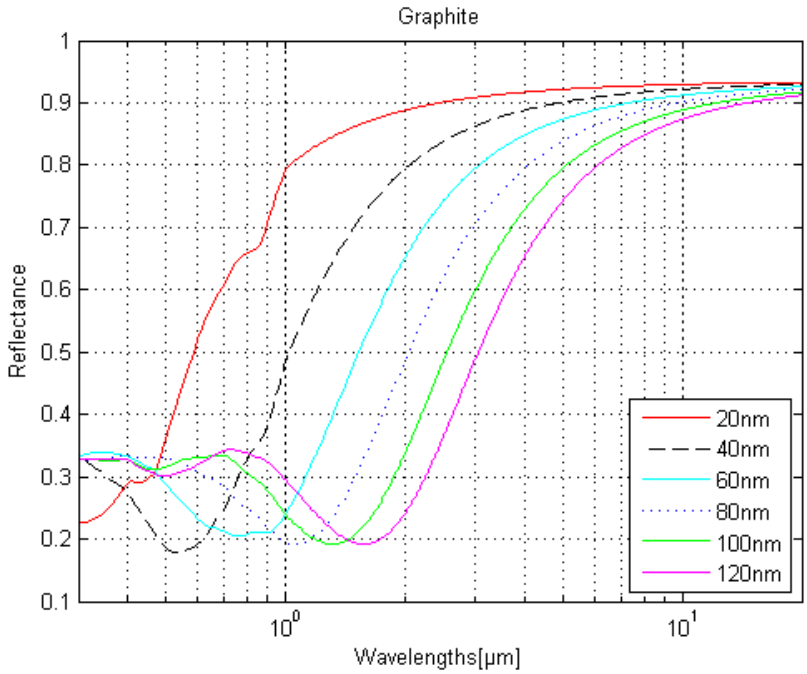

Figure 8.4: The comparison of reflectance at different thicknesses of graphite for 20 to 120nm.

Table 8.4: Absorptance and emittance values for graphite.

Thickness(nm)	Absorptance	Emittance at 100°C
20	0.38	0.09
40	0.62	0.10
60	0.70	0.11
80	**0.71**	**0.12**
100	0.71	0.14
120	0.70	0.15

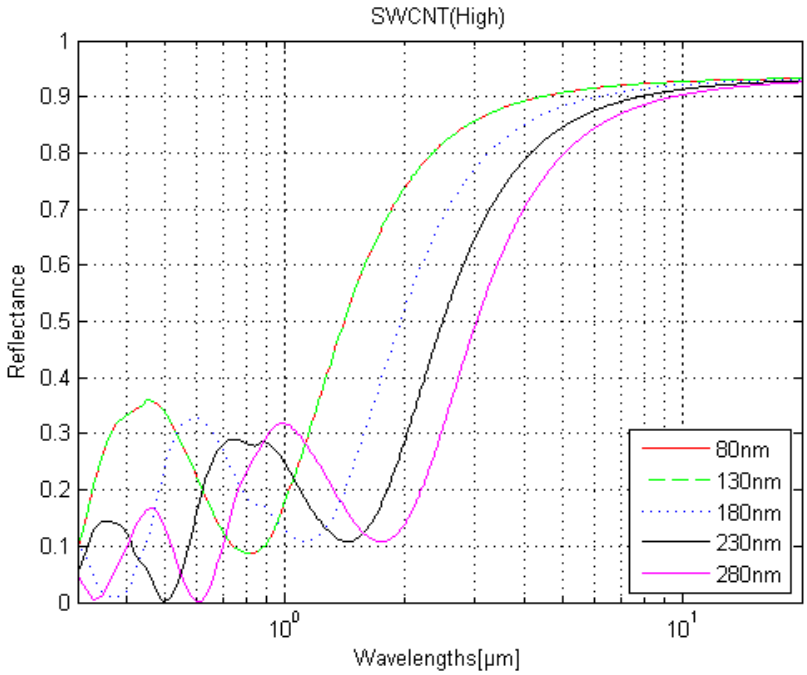

Figure 8.5: The comparison of reflectance at different thickness of SWCNT(High) from 80 to 280 nm.

- Single walled carbon nano tube(SWCNT)(High): Figure 8.5 illustrates reflectance curves as a function of wavelength at varying thickness levels of SWCNT (High). The phenomenon of optical thin film interference is easily observed in SWCNT (High). For example, the 280 nm sample exhibited 3 destructive interference minima at 0.35, 0.6 and 1.8 μm as well as 2 constructive interference maxima at 0.46 and 1.0 μm.

  As derived from the Table 8.5, as the thickness of the material increased, so did both the α_{sol} and the $\varepsilon_{thermal}$ values. The selected optimum thickness is 230 nm, and the corresponding value of α_{sol} is at 0.81 and $\varepsilon_{thermal}$ is at 0.11.

- Single walled carbon nano tube(SWCNT)(Low): Figure 8.6 depicts the reflectance curves as a function of wavelength at varying thickness levels of SWCNT (Low). The results reveal a linear shift from low to high reflectance.

  Table 8.6 shows that both the α_{sol} and $\varepsilon_{thermal}$ values increased as thickness increased throughout the experiment. The selected optimum thickness is 230 nm, and the corresponding value of α_{sol} is at 0.78with

Table 8.5: Absorptance and emittance values for SWCNT(High).

Thickness(nm)	Absorptance	Emittance at 100°C
80	0.72	0.09
130	0.72	0.09
180	0.77	0.10
230	**0.81**	**0.11**
280	0.83	0.13

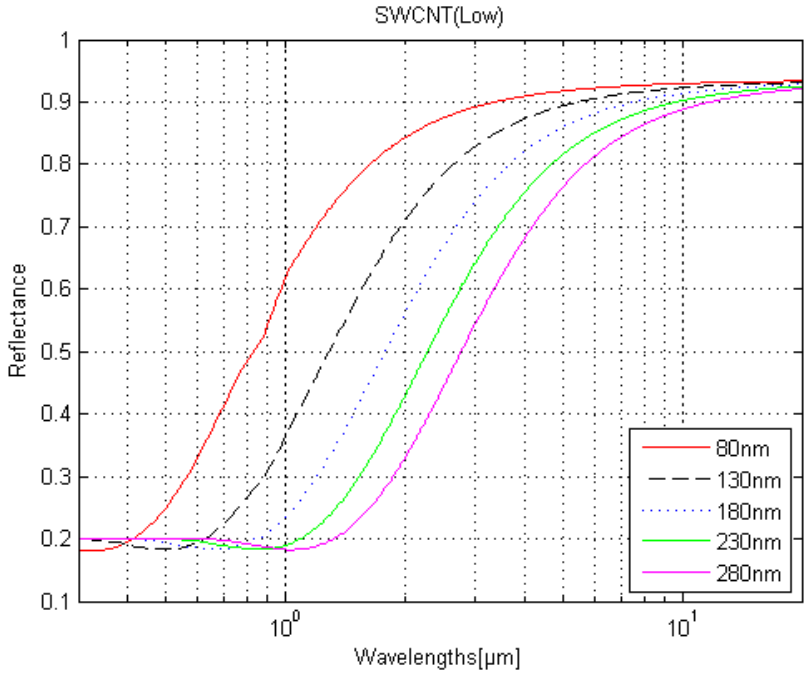

Figure 8.6: The comparison of reflectance at different thickness of SWCNT(low) from 80 to 280 nm.

Table 8.6: Absorptance and emittance values for SWCNT(Low).

Thickness(nm)	Absorptance	Emittance at 100°C
80	0.52	0.09
130	0.68	0.10
180	0.75	0.11
230	**0.78**	**0.12**
280	0.79	0.14

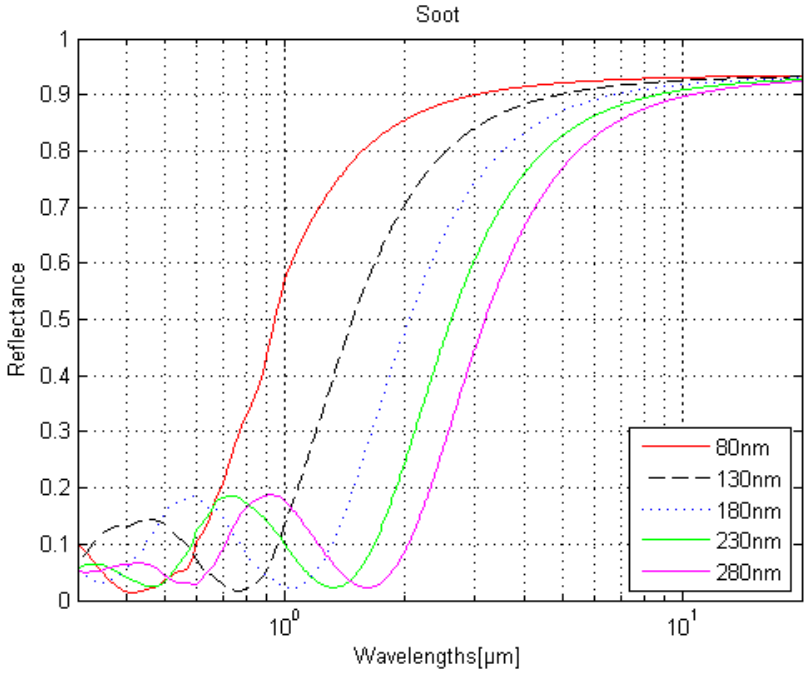

Figure 8.7: The comparison of reflectance at different thickness of soot from 80 to 280 nm.

a $\varepsilon_{thermal}$ value at 0.12.

Soot: Figure 8.7 demonstrates the reflectance curves as a function of wavelength at varying thickness levels of soot. The behavior of soot is similar to that of graphite, but with lower destructive interference minima in terms of reflectance. Hence, soot has higher absorption values than graphite.

As represented in the Table 8.7, incremental increases in value were observed in α_{sol} as well as the $\varepsilon_{thermal}$ throughout successive levels of soot thickness. The selected optimum thickness is 230 nm, and the corresponding value of α_{sol} is at 0.88, with a $\varepsilon_{thermal}$ value at 0.12.

Table 8.7: Absorptance and emittance values for Soot.

Thickness(nm)	Absorptance	Emittance at 100°C
80	0.66	0.09
130	0.82	0.10
180	0.8	0.10
230	**0.88**	**0.12**
280	0.89	0.14

It has been determined that all carbon materials studied in this section exhibit the same trend as thickness is increased. The transformation from low to high reflectance shifted towards longer wavelengths. Destructive interference in the visible region is a main contributor to the absorptance value, though SWCNT(Low) featured only flat patterns instead of any interference. One common occurrence in all selected absorbing materials was for the reflectance to decrease as the wavelength and thickness increased in the infrared region. The average minimum and maximum values for reflectance were 0.09 and 0.9 in visible and infrared regions, respectively. The optimal thickness for the higher α_{sol} and corresponding $\varepsilon_{thermal}$ ranged between 60 and 80 nm for AC, AEC, graphene and graphite, and hovered around 230 nm for SWCNT(high), SWCNT(Low) and soot. The highest value of α_{sol} was 0.88 coupled with a minimal $\varepsilon_{thermal}$ of 0.12, at 230 nm thickness of soot.

8.1.2 Optimal design with a single layer anti reflection coating

This subsection describes the optimum thickness of each spectrally selective solar absorbing layer, as well as the corresponding anti reflection coating and the related absorptance (α_{sol}) and emittance ($\varepsilon_{thermal}$) values. Optimal thickness was chosen on the basis of the best possible combination of α_{sol} and $\varepsilon_{thermal}$ values, and consequently the transition of reflectance from low to high should be around 2.5 μm.

The selection of the AR coating is evaluated by using the equation 5.26, at 0.55 μm. Because the spectrum of terrestrial solar radiation is found between 0.3 to 2.5 μm, this accounted for 98.5% of the total incoming solar radiation, and maximum solar intensity can be found around 0.55 μm. Therefore, it is necessary for any selective absorbing layer and AR coating to maximize absorptance in the solar region, as well as minimize emittance in higher wavelength regions [12]. Silica (SiO_2) and alumina (Al_2O_3) are two different types of AR material coatings that were used to enhance the α_{sol} value. For SWCNT(Low), no AR coating was chosen because its refractive index value does not match any available AR material. Table 8.8 shows how closely the two refractive indexes matched, with approximately 0.55 μm of absorbing layer and AR coating.

It must be kept in the mind that the increase in α_{sol} value is twice as important as that of the incremental increase in $\varepsilon_{thermal}$ when selecting the optimum thickness for the absorbing layer and AR coating.

- Amorphous carbon(AC): The optimum thickness of AC was chosen with corresponding α_{sol} and $\varepsilon_{thermal}$ values at 0.78 and 0.11, respec-

Table 8.8: Comparison of refractive index between absorbing layers and anti reflection coating.

Absorbing layer	Square root refractive index	AR coating with refractive index
AC	1.53	Silica(1.46)
AEC	1.54	Silica(1.46)
Graphite	1.62	Alumina(1.77)
Graphene	1.64	Alumina(1.77)
SWCNT(High)	1.26	Silica(1.46)
SWCNT(Low)	1	None
Soot	1.24	Silica(1.46)

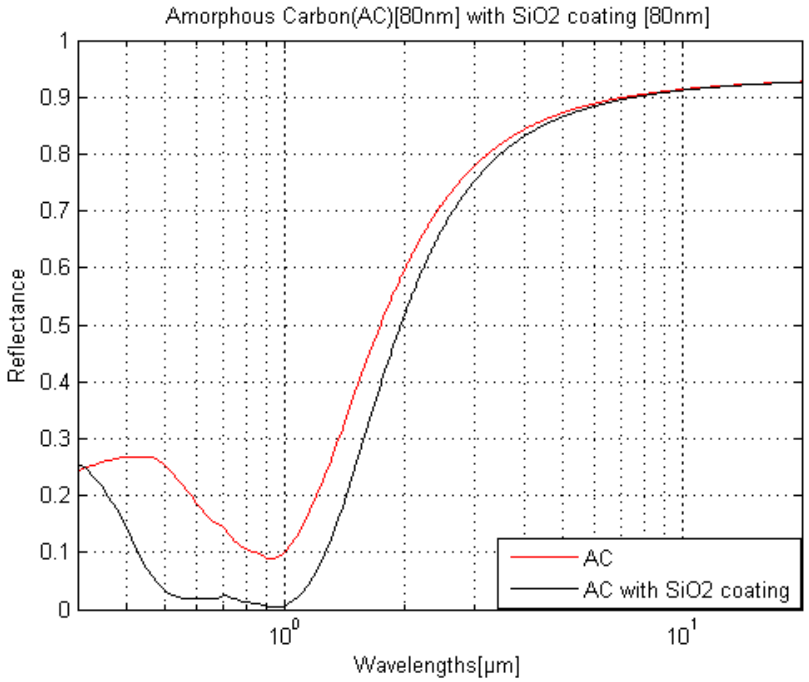

Figure 8.8: Comparison of amorphous carbon before and after with a silica anti reflection coating.

Table 8.9: Absorptance and emittance values for amorphous carbon[80nm] with different thickness of silica coating.

Thickness(nm)	Absorptance	Emittance at 100°C
20	0.81	0.11
40	0.85	0.11
60	0.89	0.11
80	**0.91**	**0.11**
100	0.91	0.11
120	0.88	0.11

tively, as listed in Table 8.1. After the application of the AR coating, the reflectance value increased nearly to that of an ideal selective absorber. There are now 2 interference minima seen in Figure 8.8, which contributed to the more efficient absorptance of the incident light for the shorter wavelength.

The relationship between the α_{sol} and $\varepsilon_{thermal}$ values with the corresponding thickness of SiO_2 are presented in Table 8.9. The optimum values of α_{sol} and $\varepsilon_{thermal}$ are 0.91 and 0.11, with an 80 nm thick SiO_2 coating, respectively. The value of α_{sol} increased by 0.13, and the $\varepsilon_{thermal}$ value is constant after the AR coating.

- Arc evaporated carbon(AEC): Figure 8.9 illustrates the reflectance curve as a function of wavelength for AEC with and without a silica coating. The optimum thickness of AEC was chosen with values of α_{sol} and $\varepsilon_{thermal}$ at 0.82 and 0.15, respectively, as reflected in Table 8.2. The constructive interference peaks became smaller as the destructive interference peaks became larger in the visible spectrum, as demonstrated in Figure 8.9.

  The improved values of α_{sol} and $\varepsilon_{thermal}$ were 0.93 and 0.15, respectively, with an 80 nm thick SiO_2 coating, as listed in Table 8.10. The improvement in the α_{sol} value was 0.11, and the $\varepsilon_{thermal}$ value remained constant as a result of the AR coating.

- Graphene: The optimum thickness in this case took into account the best possible values of α_{sol} and $\varepsilon_{thermal}$, which were 0.68 and 0.12 respectively, as seen in Table 8.3. The reflectance curve after an alumina coating was similar to Figure 8.8, while the silica coating transitioned in reflectance from low to high, but the interference amplitude and frequency were much higher. The reflectance value in the visible region was reduced by around 0.25, as represented in Figure 8.10.

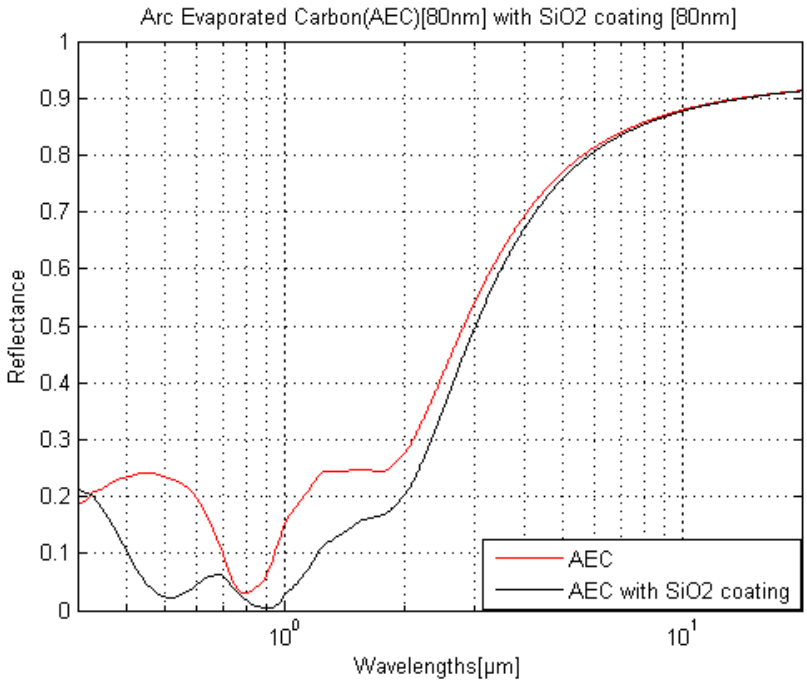

Figure 8.9: Comparison of arc evaporated carbon before and after with a silica anti reflection coating.

Table 8.10: Absorptance and emittance values for arc evaporated carbon[80nm] with different thickness of silica coating.

Thickness(nm)	Absorptance	Emittance at 100°C
20	0.85	0.15
40	0.88	0.15
60	0.91	0.15
80	**0.93**	**0.15**
100	0.93	0.15
120	0.91	0.15

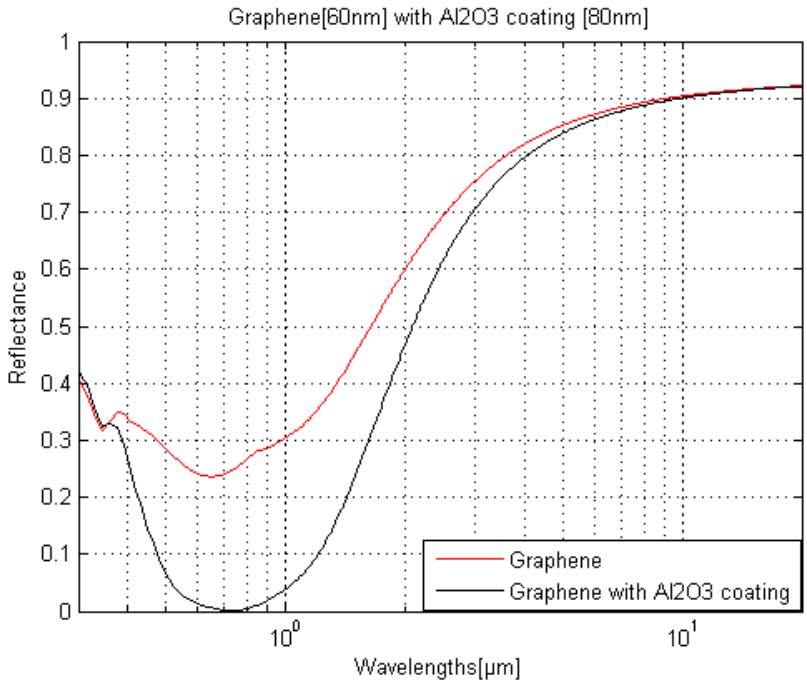

Figure 8.10: Comparison of graphene before and after with a alumina anti reflection coating.

Table 8.11: Absorptance and emittance values for graphene[60nm] with different thickness of alumina coating.

Thickness(nm)	Absorptance	Emittance at 100°C
20	0.74	0.12
40	0.83	0.12
60	0.89	0.12
80	**0.90**	**0.12**
100	0.87	0.12

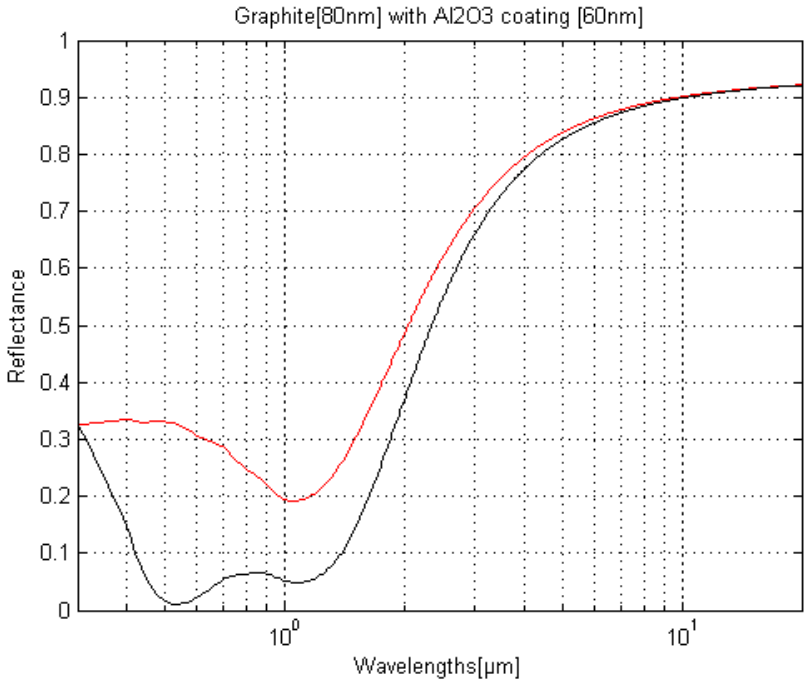

Figure 8.11: Comparison of graphite before and after with a alumina anti reflection coating.

The best values of α_{sol} and $\varepsilon_{thermal}$ were 0.90 and 0.12, respectively, after an Al_2O_3 coating of 80 nm, as reflected in Table 8.11. The value of α_{sol} improved by about 0.22 in the visible region, but the value of $\varepsilon_{thermal}$ remained unchanged.

- Graphite: The reflectance curve as a function of wavelength for graphite, both before and after a silica coating, can be seen in Figure 8.11. The best thickness levels to achieve the most ideal values of α_{sol} and $\varepsilon_{thermal}$ are 0.71 and 0.12, respectively, as listed in Table 8.4. An AR coating with a thickness of 60 nm was chosen because of it's minima at 0.55 μm. After application of the AR coating, 2 interference minima can be seen in Figure 8.11. The reflectance value in the visible region was reduced by about the same amount as in the graphene.

  The association between the α_{sol} and $\varepsilon_{thermal}$ values, with respect to the thickness of Al_2O_3, are listed in Table 8.12. The optimum values for α_{sol} and $\varepsilon_{thermal}$ are 0.91 and 0.13, respectively, with Al_2O_3 coating of 60 nm. The improvement in the value of α_{sol} is increased by 0.20, but the value of $\varepsilon_{thermal}$ is increased by 0.01.

Table 8.12: Absorptance and emittance values for graphite[80nm] with different thickness of alumina coating.

Thickness(nm)	Absorptance	Emittance at 100°C
20	0.77	0.12
40	0.86	0.12
60	0.91	0.13
80	**0.91**	**0.13**
100	0.88	0.13

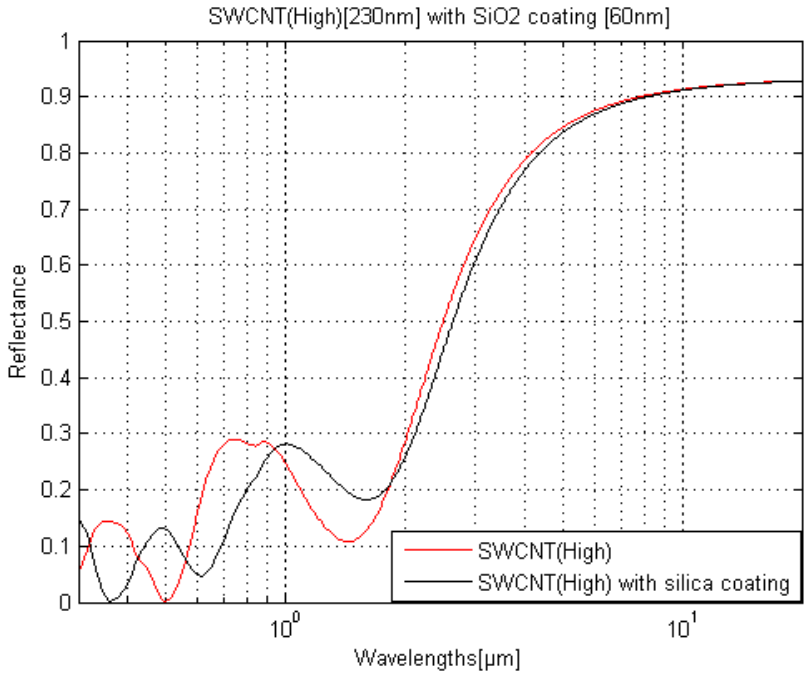

Figure 8.12: Comparison of SWCNT(High) before and after with a silica anti reflection coating.

Table 8.13: Absorptance and emittance values for SWCNT(High)[230nm] with different thickness of silica coating.

Thickness(nm)	Absorptance	Emittance at 100°C
20	0.82	0.11
40	0.82	0.11
60	**0.83**	**0.11**
80	0.83	0.12
100	0.83	0.13

- SWCNT(High): The effect on the reflectance curve as a function of wavelength for SWCNT (High) after a silica coating can be seen in Figure 8.12. The optimum thickness to achieve the most effective values of α_{sol} and $\varepsilon_{thermal}$ are 0.81 and 0.11, respectively, as depicted in Table 8.5. The transition of the reflectance is slightly shifted to the higher wavelength region, after an application of silica coating. The reflectance in the solar region is reduced by the presence of 2 destructive interferences, as seen in Figure 8.12, and 2 peaks are produced after the coating of SiO_2.

  The α_{sol} value after the SiO_2 AR coating improved by only 0.02 in the visible region, but $\varepsilon_{thermal}$ value remained constant in the infrared region, as depicted in Table 8.13. The reason for the poor improvement is likely the bad refractive index matching see Table 8.8.The optimum values of α_{sol} and $\varepsilon_{thermal}$ after a silica coating of 60 nm were 0.83 and 0.11, respectively.

- Soot: The optimum thickness required to facilitate the most effective α_{sol} and $\varepsilon_{thermal}$ values were 0.88and 0.12, respectively, as can be seen in Table 8.7. The SiO_2 coating of 40 nm thickness was chosen due to its corresponding troughs at about 0.55 μm, which accounted for the maximum solar intensity of the incoming light. The reflectance peak became smaller in the visible region as a result of the silica AR coating, which can be seen in Figure 8.13. The reflectance was reduced by about 10% in short wavelength after the application of the silica coating.

  The optimum values of for α_{sol} and $\varepsilon_{thermal}$ were 0.91 and 0.12, respectively, with a SiO_2 coating of 40 nm, as presented in Table 8.14. The improvement in the value of α_{sol} was 0.03 in the visible region, and the $\varepsilon_{thermal}$ value remained constant for higher wavelength intervals.

It is interesting to note that the shift from a lower to higher reflectance improved in nearly all of the absorbing layers after a coating of AR, with

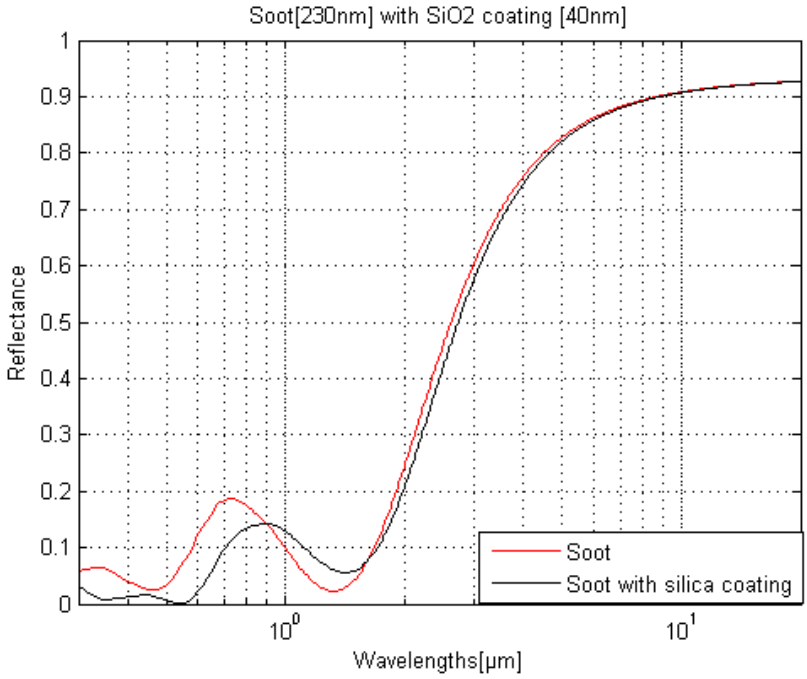

Figure 8.13: Comparison of soot before and after with a silica anti reflection coating.

Table 8.14: Absorptance and emittance values for soot[230nm] with different thickness of silica coating.

Thickness(nm)	Absorptance	Emittance at 100°C
20	0.90	0.12
40	**0.91**	**0.12**
60	0.91	0.12
80	0.91	0.12
100	0.90	0.12

the exception of soot and SWCNT(High) due to a poor matching of the AR refractive index. The best improved absorptance of 22% was achieved for graphene with an alumina coating. The least improved absorptance was for soot and SWCNT(High) at 3% and 2%, respectively, with a silica coating. The value of thermal emittance was almost constant in the infrared region across experiments after the AR coating since the thin silica and alumina films did not absorb infrared light.

8.2 Measured reflectance for prepared samples

The samples prepared by the PhD student Zhonghua Chen were labeled S60, S61 and S72. Each had absorbing layers of multi walled carbon nanotubes (MWCNTs), and were measured in one UV-VIS-NIR and IR spectrophotometer in order to obtain the reflectance values for the wavelength range of 0.3 to 20 μm. The aluminum substrate was used without any treatment prior to the application of an absorbing layer. A CNT dispersion solution were mixed with water(as a solvent) as well as Sodium Dodecyl Sulfate (SDS) (as a stabilizer) in order to prepare the samples. Each one had a different deposition time and thickness. A tape test for adhesion was performed, and indicated a solid adhesion between the CNT coating and substrate after a heat treatment. The $\varepsilon_{thermal}$ values were calculated at 100°C, via a matlab program that used imported reflectance data.

- S60: Two destructive interference valleys can be seen in Figure 8.14, each having contributed to a lower reflectance in the solar spectrum region. The calculated values of α_{sol} and $\varepsilon_{thermal}$ were 0.83 and 0.18, respectively. The thickness of the absorbing layer was approximately 700 nm. The constructive interference peak of 1 μm could be reduced by the application of an AR coating with an appropriate refractive index value.

- S61: The small flat portion of the reflectance curve of S61 is illustrated in Figure 8.15. This was a good addition to the absorptance value until about 0.8 μm, but then it began to follow the sudden steady incremental increase of the reflectance value in the solar region. The transition from low to higher reflectance in this sample does occur at shorter wavelengths compared to S60. This is why the calculated value of α_{sol} was 0.63, which is low compared to the 0.83 recorded for S60. On the other hand, the $\varepsilon_{thermal}$ value of S61 was 0.06, which was three times less than the $\varepsilon_{thermal}$ value of S60. An additional difference between the two samples was the level of thickness of the respective absorbing

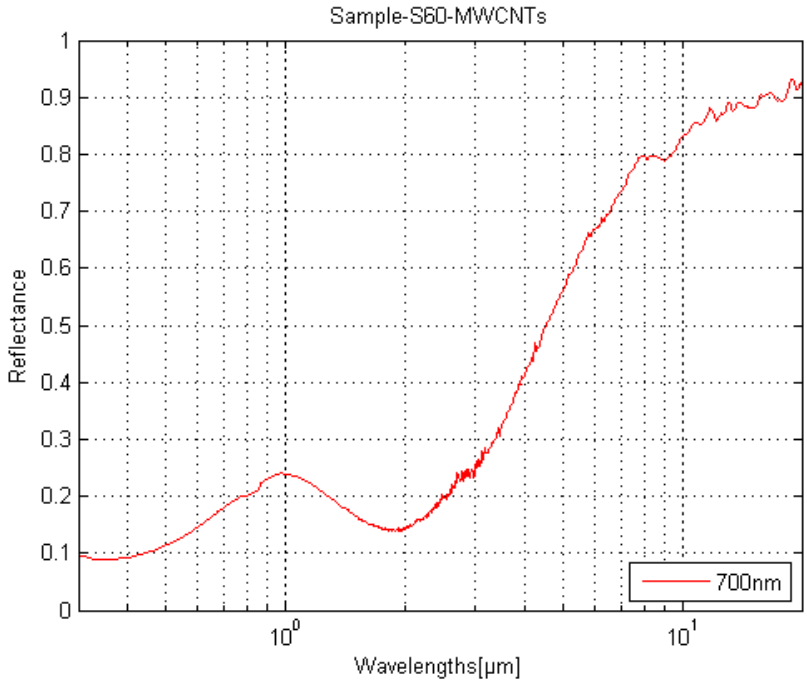

Figure 8.14: The reflectance of sample-S60.

layers: 400 nm for S61, which was 1.75 times less than the thickness of S60.

- S72: The reflectance curve of S72 followed the reflectance curve pattern of S60, with a shift from low to high reflectance in the infrared region, as demonstrated in Figure 8.16. The phase shift in the reflectance curve contributed to better absorptance, as well as lower emittance, by having shifted constructive interference to the end of the solar region and destructive interference to the infrared region. The measured values of α_{sol} and $\varepsilon_{thermal}$ were 0.85 and 0.22, respectively. Those were the highest values among all three samples, and the thickness of the absorbing layer at 900 $nm$was the highest as well. A small trough was noticed in the same wavelength as in S60. The introduction of destructive and constructive interference respectively, by using the AR coating of a suitable refractive index could reduce the thermal emittance and improve the absorptance of the material.

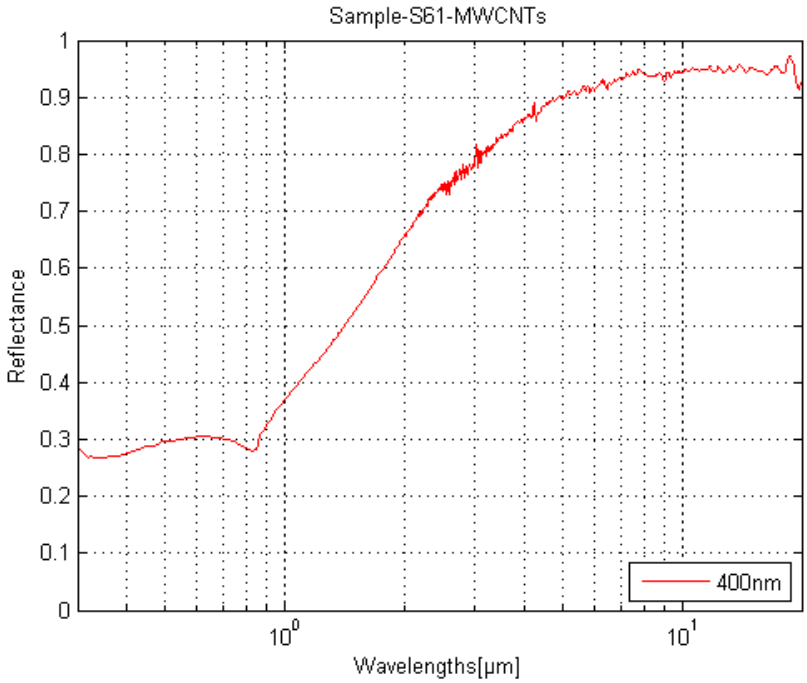

Figure 8.15: The reflectance of sample-S61.

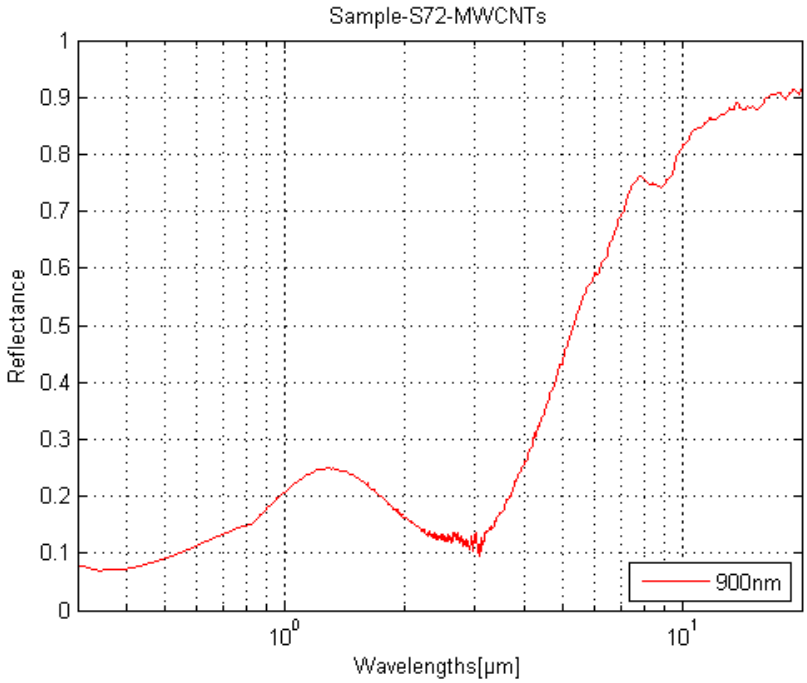

Figure 8.16: The reflectance of sample-S72.

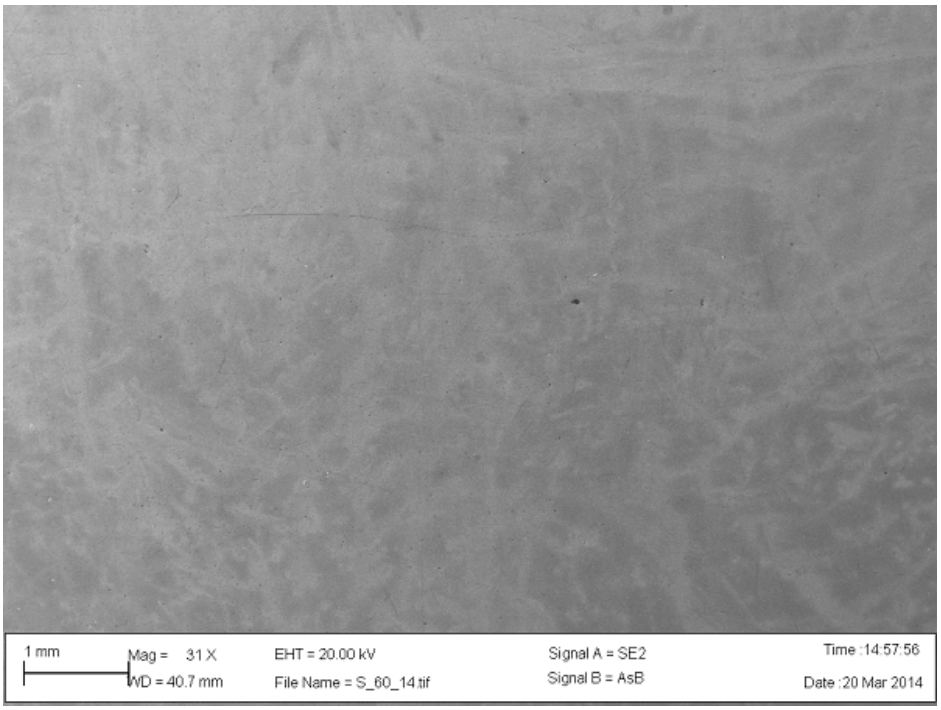

Figure 8.17: SEM image of sample S60, 31X magnification.

8.3 Surface morphology

A surface morphology analysis has been conducted by scanning electron microscopy to investigate the properties of the absorbing surface in each sample, such as uniformity, porosity, CNT alignment and homogeneity. The MWCNTs were deposited by the EPD technique, with no AR coating. The EPD process times differed for each sample, as did the thickness of the associated material. The deposition times were 1, 3 and 5 seconds, and the absorbing layer thickness levels were at 400, 700 and 900 nm for samples S61, S60 and S72, respectively. For each sample, two SEM images were chosen with millimeter and nanometer features in mind.

8.3.1 Sample-S60, 3 seconds deposition time

Figure 8.17 illustrates the surface morphology of S60 at a magnification of 31 times. As the magnification level used was quite low, it was possible to see most of the visible features in this figure with bare eyes. The regions with two different colors were the most obvious to differentiate, possibly being varying levels of thickness in the deposited layer. This magnification

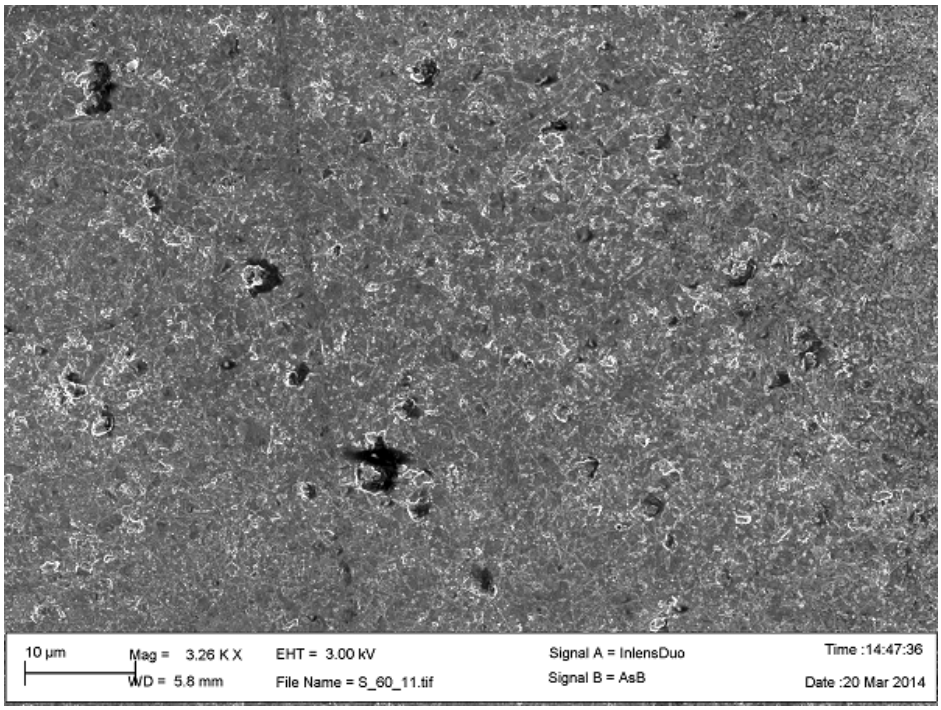

Figure 8.18: SEM image of sample S60, $3.26KX$ magnification.

revealed micro-pores, which could not be seen with the bare eyes. Increasing the magnification by 1000 times displayed the uneven surface structure at micrometer scale, as seen in Figure 8.18. There were no cracks in the material, but holes of nanometers to micrometers in size could be observed on the surface, although without depth information. Polymer protuberances stood out against the deposited surface (and the variation in size were quite noticeable,) leading to a pronounced surface roughness. For this particular sample, the deposition of CNTs was not aligned in any particular direction. A visible line of about 0.1 μm in diameter on the sample surface could have been the track of a dust particle left in the slide during the rolling of the aluminum sheets.

8.3.2 Sample-S61, 1 second deposition time

Figure 8.19 looks similar to Figure 8.17 at low magnification, without any particular difference. Significantly less polymer was seen at a magnification of 1000 times, as depicted in Figure 8.20. The deposited CNTs were not aligned, and the aluminum substrate was clearly visible. In this sample the partial clustering of CNTs is visible. The observation of millimeter to micrometer

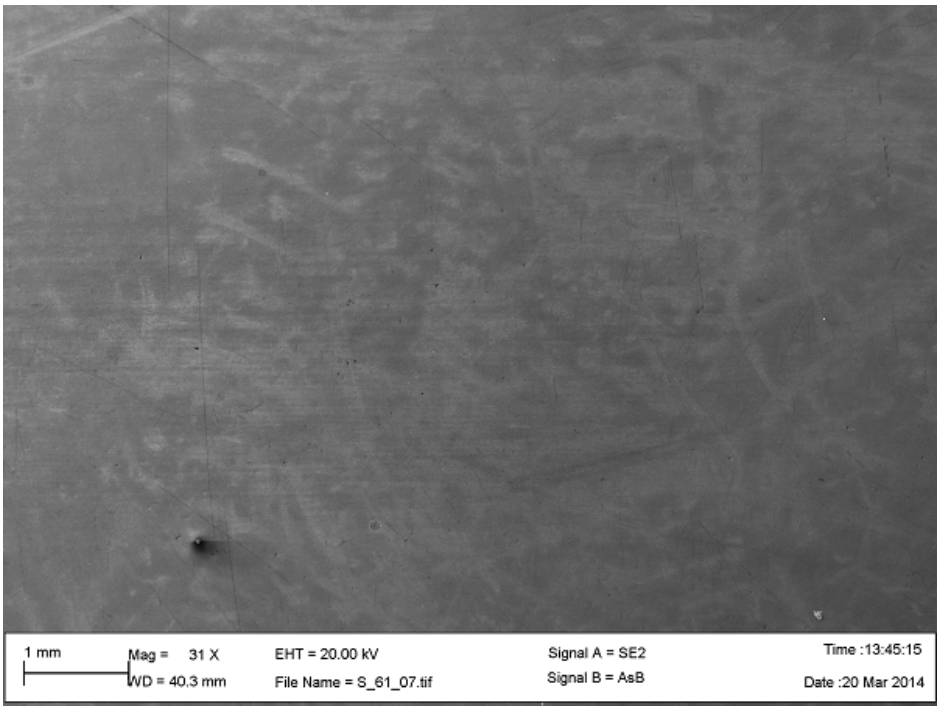

Figure 8.19: SEM image of sample S61, 31X magnification.

also differs.

8.3.3 Sample-S72, 5 seconds deposition time

In Figure 8.21, the brighter looking regions can be related to mechanical stress(scratches). The porosity of the surface at micro to nano scale can be seen at higher magnification in Figure 8.22. In this sample there were also no visible cracks on the surface. S72 was also fully covered with the deposited layer and the aluminum substrate was not visible, as in case of S61. Compared to S60, there appears to be less polymer on the surface than expected for the longer deposition time. In general, a higher porosity and lower surface roughness can be made out. This might lead to a higher light absorption through to the multi reflection of the trapped light into pores.

Summarizing, SEM was used as a tool to investigate the alignment, surface roughness and CNT to polymer ratio of the sample. No aligned CNTs could be observed. The 1 *second* EPD process displayed an inhomogeneous surface. Surface parameters such as porosity and surface roughness seemed to increase, respectively reduce as the EPD time and the thickness of the CNT deposition were increased.

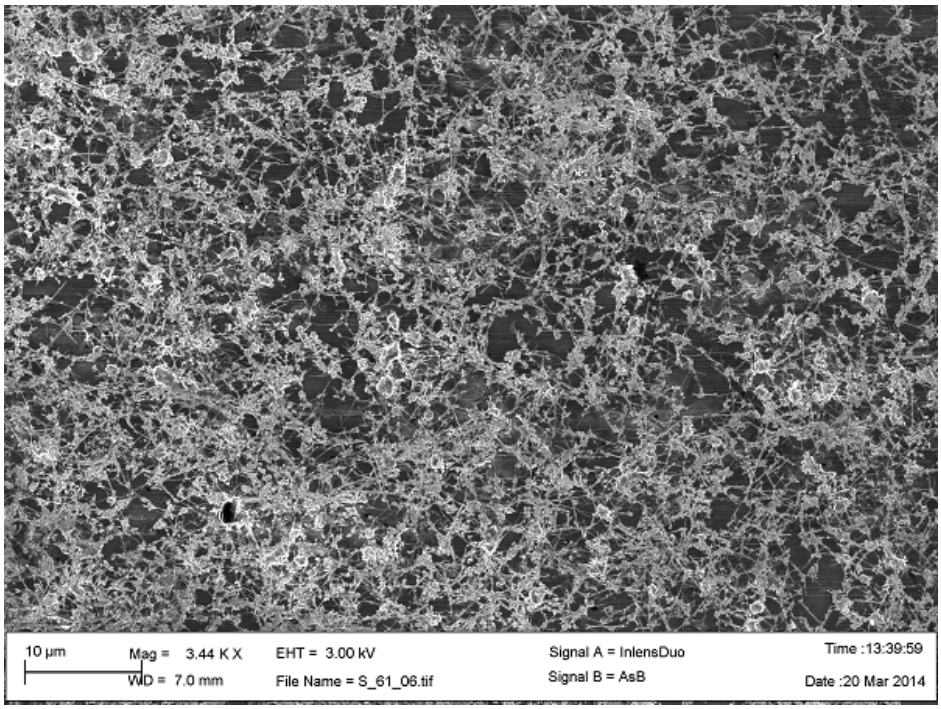

Figure 8.20: SEM image of sample S61, $3.44KX$ magnification.

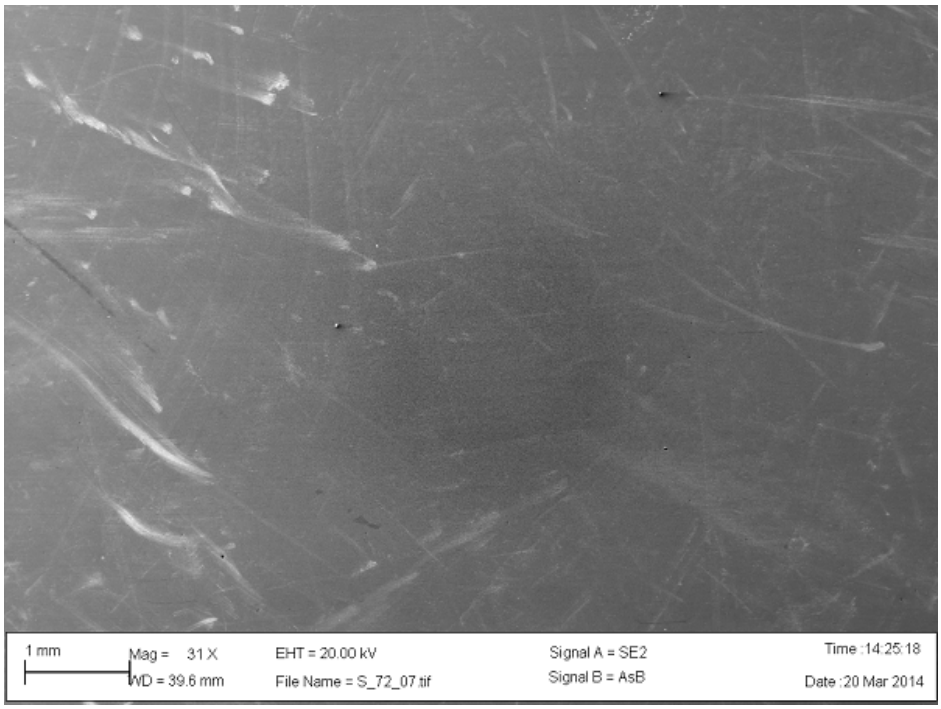

Figure 8.21: SEM image of sample S72, $31X$ magnification.

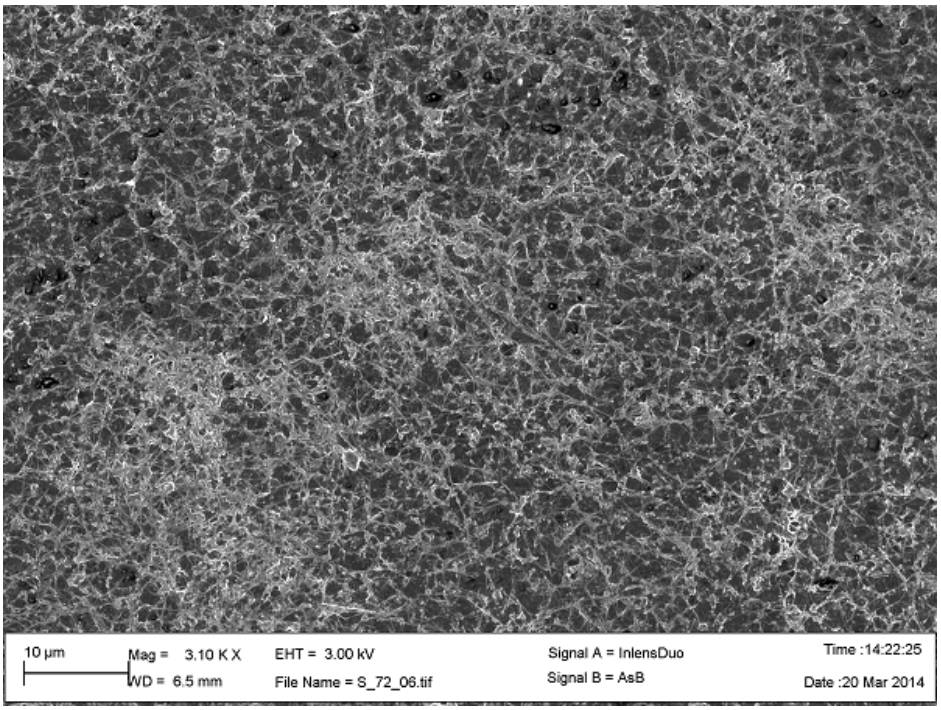

Figure 8.22: SEM image of sample S72, $3.10KX$ magnification.

8.3.4 Structural properties of CNT

Figures 8.23 and 8.24 are SEM images taken from an old sample, allowing to study the structural properties of the CNTs utilized in the framework of this thesis. Figure 8.23 illustrates deep cracks over the surface of the material at microscopic scale. Cracks are usually formed in the drying process of the sample. The ratio of polymer to CNTs seemed balanced. Most of the CNTs were not aligned in any particular direction, but a few were aligned in a parallel manner, which can be attributed to the crack. Such cracks in a sample increase the interfacial surface of the CNTs, which can result in a better absorptance of light. Figure 8.24 presents a better overview of the CNTs at nanoscale. The figure shows that the CNTs varied in length, diameter, shape and especially aspect ratio. The relationship between diameter and length typically seems to be inversely proportional, but here they appeared to be random.

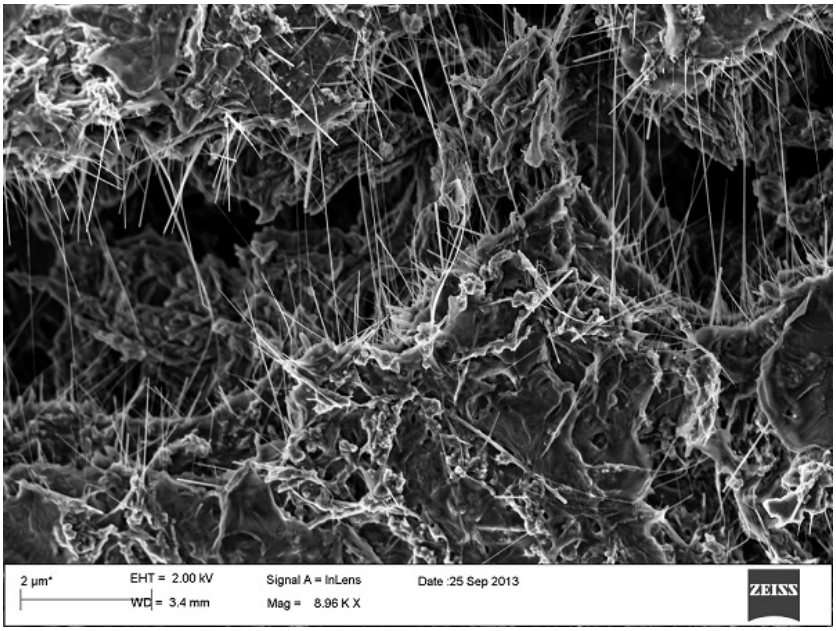

Figure 8.23: SEM image of a CNT-polymer layer deposited on aluminum substrate shows the cracks at micro scale.

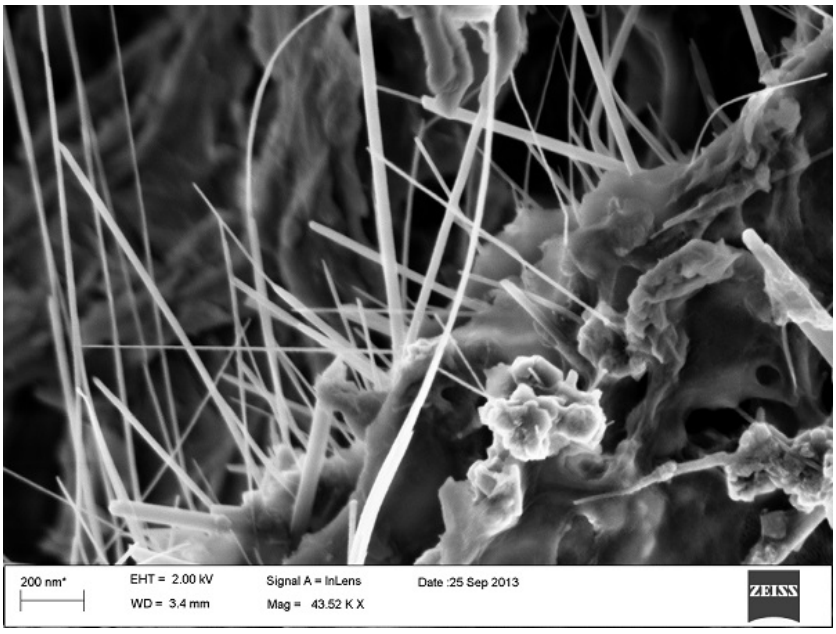

Figure 8.24: SEM image of a CNT sample deposited on aluminum substrate shows the cracks at micro scale.

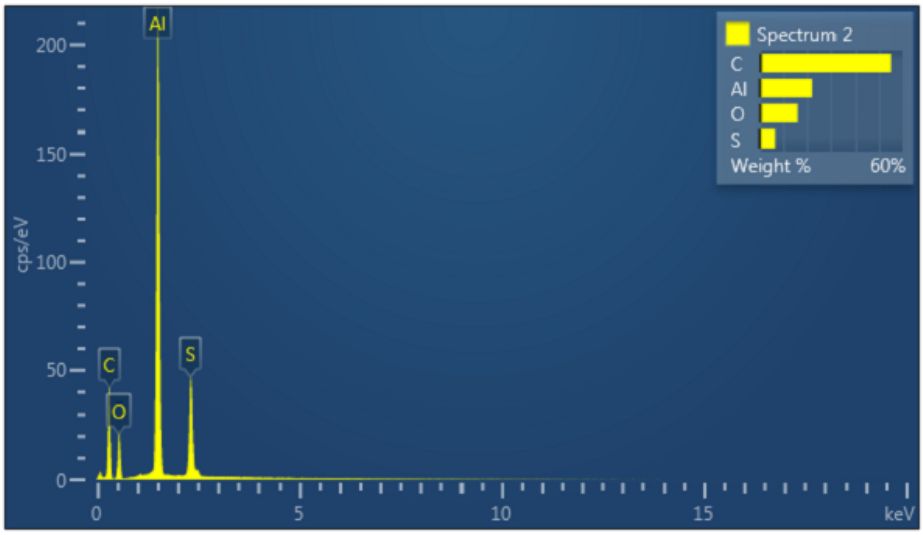

Figure 8.25: EDX analysis, which illustrates peaks for carbon, oxygen, aluminum and sulfur.

8.4 Element characterization

EDX analysis was performed for different CNT samples. The EPD parameters were a voltage of 15 V, a start and end current of 120 and 22 A (respectively), a distance between the electrodes of 9 cm and a deposition time of 60 seconds.

For the EDX analysis, different regions (the measurement of a region composed of an average of $5-6$ spots) were selected for each sample. Figure 8.25 illustrates an EDX spectrum of the sample S1 with peaks of Carbon(C), Oxygen(O), Aluminum(Al) and Sulfur(S). Table 8.15 gives the values in atomic percentage obtained for a region. the aluminum peak comes from the substrate, probably visible because of the relatively thin and inhomogeneous coating layer. The CNT suspension was deposited in a matrix of sodium dodecyl sulfate (SDS, atomic composition: $C_{12}H_5O_4S$). This led to the carbon values in the EDX results to be composed of the CNT and SDS concentrations. In order to analyze variations in the polymer to CNT ratio, the amount of sulfur was compared between different regions of different samples. However, no significant differences could be observed(values for S between 2 and 4 at 4 % and 5 %).

Table 8.15: Typical element composition in atomic percentage.

Spot number	**C**	**O**	**Al**	**S**
1	73	17	7	3
2	71	19	7	3
3	73	13	10	4
4	69	13	13	5
5	70	14	14	3

8.5 Validation of refractive index

As featured in Chapter 6, the refractive index data was normally limited up to 1 μm. But, the simulation was carried out for a wavelength range of 0.3 to 20 μm, which is a much higher wavelength range than the collected refractive index. In addition, the extrapolation of data was done in a constant manner by the simulation software called Setfos, and if the given refractive index value ended up out of simulation range. Refer to the subsection entitled "Simulated parameters" in Chapter 6 for clarity. If the extinction coefficient (k) of the material is either constant or diminishing in the end of the data sets, the extrapolated data should be considered reliable, and therefore also the simulation. This is supported by Equation 8.1 of absorption coefficient, which is directly proportional to the k and inversely proportional to the wavelength(λ), then the absorption coefficient(α) is expressed as:

$$\alpha = \frac{4\pi k}{\lambda} \tag{8.1}$$

The α and the wavelength of incident light are the factors that determine the absorption of light in a material. If λ is increasing and k is constant or diminishing, then α is also diminishing, and hence the absorption of the material will lead to zero. Thus, the k value should be diminishing or constant in the infrared region to keep the reflectance as high as possible and thermal emittance as low as possible. Therefore, the refractive index of the material has been validated for its reliability in higher wavelengths on the basis of k and the absorption coefficient values. To calculate the α_{sol} value can always be trusted but the validity of the $\varepsilon_{thermal}$ value is depending on the k value trend in the respective dataset.

- Graphite: The k values for graphite as a function of wavelength can be seen in Figure 6.5. In the given wavelength range, the k values successively decreased approaching longer wavelengths, and towards the end the K values became nearly constant. Hence, α will decrease

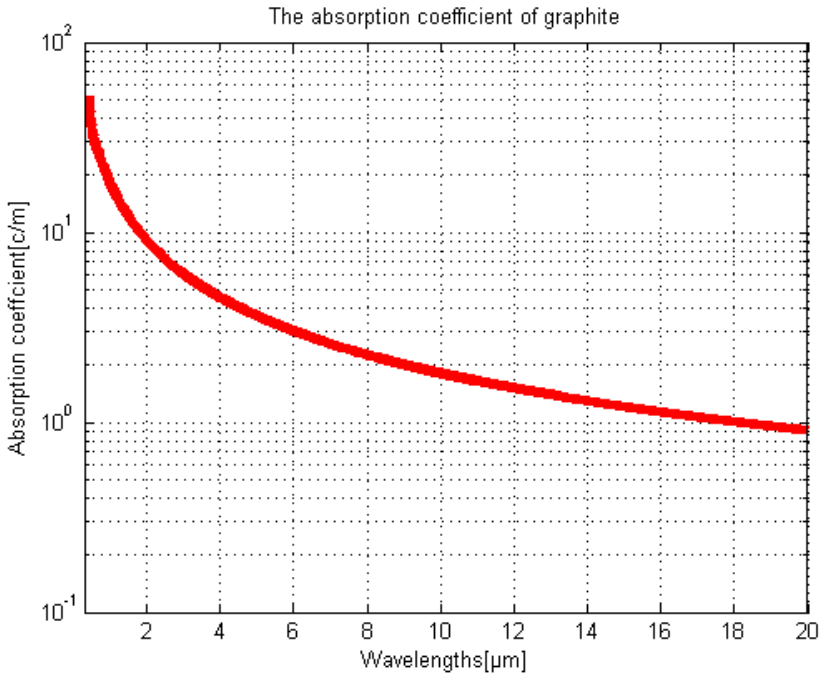

Figure 8.26: The absorption coefficient α, of graphite as a function of wavelength of light

.

or come close to zero with increasing wavelengths. Therefore, graphite is as an example of how the α changes if the refractive index values are constant and equal to n and k at the largest wavelength in the missing infrared region, as demonstrated in Figure 6.5. In Figure 8.26, α values feature an exponentially decaying relationship with wavelength, which means that the refractive index data of graphite should be fairly reliable for the higher wavelength intervals.

- Amorphous Carbon(AC): The refractive index against wavelength can be seen in Figure 6.2 for AC. The k values were nearly constant in most of the wavelength range, especially at the end of the dataset as it began to diminish. Logically, this is desirable for the AC and absorption coefficient. So it can be assumed that the refractive index values should be trusted for higher wavelength simulations.

- Arc evaporated carbon (AEC): The behavior of the refractive index corresponds to its wavelength, which is depicted in Figure 6.3. The k values held a peak and couple of troughs with an increasing trend for

part of the wavelength, but in the end the values faced a sharp fall, which a good sign for data reliability. The value of α should diminish when approaching higher wavelength regions

- Graphene: The relationship between the refractive index of graphene and its wavelength is reflected in Figure 6.6. The k values began with a really high peak followed by a sharp downfall, then steadily increased for the rest of the wavelength period. This demonstrated higher α values for graphene as its refractive index approached a higher wavelength region. Therefore the simulation, in this case, cannot be fully trusted at higher wavelengths.

- SWCNT(High): Figure 6.7 shows the relationship between the refractive index and wavelengths for SWCNT(High). Throughout the wavelength period the k values were fairly constant, without any sudden peaks or drops. Thus, the refractive index behavior should be considered reliable for longer wavelengths.

- SWCNT(Low): The connection between the refractive index of SWCNT (Low) and its corresponding wavelength is depicted in Figure 6.8. There were no signs of variation in the k values over the whole wavelength range, which could lead to diminished α values in the higher wavelength periods. Therefore, the refractive index values should be reliable for the higher wavelength range

- Soot: Figure 6.4 illustrates the connection between the refractive index of soot and wavelength. The k values began with a slight downfall and showed slight variations in a portion of the short wavelength period, but the values at the end were quite close to the constant, which will result in lower α values in the longer wavelengths.

- Substrate: It is commonly known that metals do not absorb in the infrared region, and this applies to the used substrate Aluminum(Al).

- Silica and Alumina: Figures 6.9 and 6.11 show the association between the refractive indexes of silica and alumina as a function of wavelength, respectively. The k values for both were constant over the complete wavelength range. So it is simple to identify that the α decreases as wavelength increases. Hence, the refractive index should be reliable for longer wavelengths

Chapter 9

Conclusion and Future work

9.1 Conclusion

This thesis presents simulations of seven different single layered carbonaceous spectrally selective solar absorbers, with and without an additional layer of anti reflection coating. The simulation was carried out for different single solar selective absorbing layers in order to calculate their reflectance as a function of wavelength according to several predetermined levels of thickness. The best absorbing layer was found to be soot at 230 nm optimum thickness, with the highest value of absorptance at 0.88 coupled with a minimal thermal emittance of 0.12.

After adding an anti reflection coating, the best absorbing layer turned out to be soot. A silica layer was 40 nm thick with the best absorptance value was 0.91, coupled with a minimal thermal emittance of 0.12. Also found that the graphite after a silica anti reflection coating was 80 nm thick with the same absorptance value as soot but, the value of emittance is 0.01 greater. The arc evaporated carbon with Silica anti-reflection coating exhibited an absorptance value of 0.93, higher than soot and graphite. However, its emittance value was higher than soot by 0.03 units. As mentioned earlier that the increase in absorptance value is twice as important as that of the incremental increase in emittance when selected the optimum thickness for the absorbing layer and AR coating. The refractive index of the carbonaceous materials were collected from different sources, which did not include values in infrared region. Thus, the simulation may not be reliable when it comes to longer wavelengths and the emittance value.

The surface morphology was carried out by scanning electron microscopy for prepared MWCNTs using EPD techniques. There was no significant difference in alignment for any of the CNTs. Surface parameters such as

porosity and surface roughness were reduced as the EPD time and thickness of the CNT deposition increased. Energy dispersive spectroscopy does not lead to any clear results regarding chemical characterization of the materials.

9.2 Further research

For further development on the subject, many improvements can be applied to the current research. This could include a focus on:

- The reverse simulation of reflectance in order to calculate desired refractive index levels.
- The collection of data for the development of a database containing refractive index levels in higher wavelength ranges, and thereby setting better quality infrared region simulation.
- The successful measurement of both thickness and refractive index levels for prepared samples using an ellipsometer.
- Cross sectional morphology using transmission electron microscopy.

References

[1] B. Sørensen, "A history of renewable energy technology," *Energy Policy*, vol. 19, no. 1, pp. 8–12, 1991, 0301-4215/911010008-05. [Online]. Available: http://www.sciencedirect.com/science/article/pii/030142159190072V

[2] R. Pode and B. Diouf, "Why clean energy?" in *Solar Lighting*, ser. Green Energy and Technology. Springer London, 2011, pp. 1–18. [Online]. Available: http://dx.doi.org/10.1007/978-1-4471-2134-3_1

[3] V. Quaschning, *Understanding Renewable Energy Systems*. Earthscan, USA-2005, vol. second.

[4] G. Stapleton, Z. Li, and S. Garrett, "Quality renewable energy training in developing countries," in *Proceedings of ISES World Congress 2007 (Vol. I - Vol. V)*, D. Y. Goswami and Y. Zhao, Eds. Springer Berlin Heidelberg, 2009, pp. 3029–3034. [Online]. Available: http://dx.doi.org/10.1007/978-3-540-75997-3_611

[5] E. Serrano, G. Rus, and J. GarcÃŋa-MartÃŋnez, "Nanotechnology for sustainable energy," *Renewable and Sustainable Energy Reviews*, vol. 13, no. 9, pp. 2373 – 2384, 2009. [Online]. Available: http://www.sciencedirect.com/science/article/pii/S1364032109001087

[6] A. and M. Meinel, "Applied solar energy," Addison-Wesley, Reading, UK, 1976. [Online]. Available: A.andM.Meinel,AppliedSolarEnergy, Addison-Wesley,Reading,UK,1976

[7] M. Cassin and B. Zolin, "Can wind energy make a real contribution to improve the quality of life of rural/remote areas? the european union and india compared," *Transition Studies Review*, vol. 16, pp. 735–754, 2009, 10.1007/s11300-009-0105-y. [Online]. Available: http://dx.doi.org/10.1007/s11300-009-0105-y

[8] N. Armaroli and V. Balzani, "The future of energy supply: Challenges and opportunities," *Angewandte Chemie International Edition*, vol. 46, no. 1-2, pp. 52–66, 2007. [Online]. Available: http://dx.doi.org/10.1002/anie.200602373

[9] NASA and G. P. Measurement, "Global energy budget," internet website, 11 2013. [Online]. Available: http://pmm.nasa.gov/education/lesson-plans/global-energy-budget

[10] D. J. Mackay, *Sustainable energy: without the hot air.* UIT Cambridge Ltd, 2009, iSBN 978-0-9544529-3-3.

[11] G. Boyle, *Renewable energy : Power for a sustainable future.* Oxford University Press, 2004, vol. Second edition.

[12] T. Bostrom, "Solution-chemically derived spectrally selective solar absorbers," *Digital Comprehensive Summaries of Uppsala Dissertations from the Faculty off Science and Technology*, vol. 225, 2006.

[13] C. Gearhart, "Black-body radiation," in *Compendium of Quantum Physics*, D. Greenberger, K. Hentschel, and F. Weinert, Eds. Springer Berlin Heidelberg, 2009, pp. 39–42. [Online]. Available: http://dx.doi.org/10.1007/978-3-540-70626-7_14

[14] P. Murdin, Ed., *Black-Body Radiation.* Bristol: Institute of Physics Publishing, Nov. 2000. [Online]. Available: http://eaa.crcpress.com/default.asp?action=summary&articleId=4598

[15] R. A. Rohde., "Solar radiation spectrum," Global Warming Art, 9th, June 2007. [Online]. Available: http://www.globalwarmingart.com/wiki/File:Solar_Spectrum_png

[16] S. Marcel, T. Huld, E. Dunlop, and J. Hofierka, "Solar resource modelling for energy applications," in *Digital Terrain Modelling*, ser. Lecture Notes in Geoinformation and Cartography, R. J. Peckham and G. Jordan, Eds. Springer Berlin Heidelberg, 2007, pp. 259–273, 10.1007/978-3-540-36731-4_11. [Online]. Available: http://dx.doi.org/10.1007/978-3-540-36731-4_11

[17] A. V. D. Rosa, *Fundamental of Renewable Energy Process.* Elsevier Academic press, August 3 2005.

[18] N. Munier, *Chapter5-Energy Sustainability.* Springer Netherlands, 2005, 10.1007/1-4020-3558-6_5.

[19] K. Jordan-Korte, "International markets for renewable energy technologies and export promotion policies," in *Government Promotion of Renewable Energy Technologies*. Gabler, 2011, pp. 139–200. [Online]. Available: http://dx.doi.org/10.1007/978-3-8349-6587-5_5

[20] P. Pourang, M. Masnavi, M. Bavili, A. Damanei, and M. Golmohammadi, "Designing the renewable energy parks in order to reduce the environmental crisis in the framework of ecological design, case of renewable energy park of manjil-iran," in *Design for Innovative Value Towards a Sustainable Society*, M. Matsumoto, Y. Umeda, K. Masui, and S. Fukushige, Eds. Springer Netherlands, 2012, pp. 44–49. [Online]. Available: http://dx.doi.org/10.1007/978-94-007-3010-6_10

[21] Z. Azen, "Atmospheric environment and renewable energy," in *Solar Energy Fundamentals and Modeling Techniques*. Springer London, 2008, pp. 21–45, 10.1007/978-1-84800-134-3_2. [Online]. Available: http://dx.doi.org/10.1007/978-1-84800-134-3_2

[22] W. D. METZ, "Solar thermal energy: Bringing the pieces together," *Science*, vol. 197, no. 4304, pp. 650–651, 1977. [Online]. Available: http://www.sciencemag.org/content/197/4304/650.short

[23] F. Dominguez-Munoz, B. Anderson, J. M. Cejudo-Lopez, and A. Carrillo-Andres, "Uncertainty in the thermal conductivity of insulation materials," *Energy and Buildings*, vol. 42, no. 11, pp. 2159 – 2168, 2010. [Online]. Available: http://www.sciencedirect.com/science/article/pii/S0378778810002227

[24] NCAT, "Solar water-heating system components," National Center for Appropriate Technology, PA Weatherization Providers Task Force, January 2013. [Online]. Available: http://www.pasolar.ncat.org/lesson02.php

[25] D. Close, "Solar air heaters for low and moderate temperature applications," *Solar Energy*, vol. 7, no. 3, pp. 117 – 124, 1963. [Online]. Available: http://www.sciencedirect.com/science/article/pii/0038092X63900379

[26] A. Saxena, N. Agarwal, and G. Srivastava, "Design and performance of a solar air heater with long term heat storage," *International Journal of Heat and Mass Transfer*, vol. 60, no. 0, pp. 8 – 16, 2013. [Online]. Available: http://www.sciencedirect.com/science/article/pii/S0017931012010009

[27] U. D. of Energy, "Solar swimming pool heaters," U.S. Department of Energy, May 29 2012. [Online]. Available: http://energy.gov/energysaver/articles/solar-swimming-pool-heaters

[28] E. Kruger, E. Suzuki, and A. Matoski, "Evaluation of a trombe wall system in a subtropical location," *Energy and Buildings*, vol. 66, no. 0, pp. 364 – 372, 2013. [Online]. Available: http://www.sciencedirect.com/science/article/pii/S0378778813004234

[29] S. U. Enterprises, "Trombe wall," Surya Urza Enterprises, 2012. [Online]. Available: http://suryaurza.com/trombe-wall/

[30] A. McCrea and J. Leggett, *Renewable Energy: A User's Guide*, ser. Environment collection. Crowood Press, Limited, 2008. [Online]. Available: http://books.google.no/books?id=CU2jPAAACAAJ

[31] S. A. Kalogirou, "Solar thermal collectors and applications," *Progress in Energy and Combustion Science*, vol. 30, no. 3, pp. 231 – 295, 2004. [Online]. Available: http://www.sciencedirect.com/science/article/pii/S0360128504000103

[32] F. Struckmann, "Analysis of a flat-plate solar collector," *Heat and Mass Transport, Project Report, 2008MVK160*, 2008.

[33] ASHRAE, *ASHRAE Standard 93:1986 (RA 91), Methods of testing to determine the thermal performance of solar collectors*, ASHRAE Std., 9 September 1991, iSSN 1041-2336. [Online]. Available: http://www.techstreet.com/products/14278

[34] ——, *ASHRAE Standard 93-2010 (RA 2014), Methods of Testing to Determine the Thermal Performance of Solar Collectors*, ASHRAE Std., 7 January 2014, iSSN 1041-2336. [Online]. Available: www.techstreet.com/products/preview/1873286

[35] S. Wijewardane and D. Goswami, "A review on surface control of thermal radiation by paints and coatings for new energy applications," *Renewable and Sustainable Energy Reviews*, vol. 16, no. 4, pp. 1863 – 1873, 2012. [Online]. Available: http://www.sciencedirect.com/science/article/pii/S1364032112000470

[36] J. Twidell and T. Weir, *Renewable Energy Resources*, 2nd ed., Taylor and F. Ltd, Eds. British Library, 2006, 0 419 25320 3.

[37] N. Tile, "Fabrication of high efficacy selective solar absorbers," Ph.D. dissertation, University Of Kwazulu Natal, Durban, Westville, 2012.

[38] G. Pellegrini, "Experimental methods for the preparation of selectively absorbing textured surfaces for photothermal solar conversion," *Solar Energy Materials*, vol. 3, no. 3, pp. 391–404, 1980.

[39] H. G. Craighead, R. E. Howard, and D. M. Tennant, "Textured thin film si solar selective absorbers using reactive ion etching," *Applied Physics Letters*, vol. 37, no. 7, pp. 653–655, 1980. [Online]. Available: http://scitation.aip.org/content/aip/journal/apl/37/7/10.1063/1.92015

[40] M. K. Gunde, Z. C. Orel, and M. G. Hutchins, "The influence of paint dispersion parameters on the spectral selectivity of black-pigmented coatings," *Solar Energy Materials and Solar Cells*, vol. 80, no. 2, pp. 239 – 245, 2003. [Online]. Available: http://www.sciencedirect.com/science/article/pii/S0927024803001685

[41] T. Bullett and J. Prosser, "Paint: a surface modifier," *Physics in Technology*, vol. 14, no. 3, p. 119, 1983.

[42] Z. C. Orel, "Characterisation of high-temperature-resistant spectrally selective paints for solar absorbers," *Solar Energy Materials and Solar Cells*, vol. 57, no. 3, pp. 291 – 301, 1999. [Online]. Available: http://www.sciencedirect.com/science/article/pii/S0927024898001810

[43] F. Simonis, M. van der Leij, and C. Hoogendoorn, "Physics of doped tin dioxide films for spectral-selective surfaces," *Solar Energy Materials*, vol. 1, no. 3âĂŞ4, pp. 221 – 231, 1979. [Online]. Available: http://www.sciencedirect.com/science/article/pii/0165163379900406

[44] J. A. Jaszczak, G. W. Robinson, S. Dimovski, and Y. Gogotsi, "Naturally occurring graphite cones," *Carbon*, vol. 41, no. 11, pp. 2085 – 2092, 2003. [Online]. Available: http://www.sciencedirect.com/science/article/pii/S0008622303002148

[45] R. Murali and J. D. Meindl, "What is graphene?" *SIGDA Newsl.*, vol. 39, no. 8, pp. 1–1, Aug. 2009. [Online]. Available: http://doi.acm.org/10.1145/1862906.1862907

[46] AlexanderAlUS, "Graphene," http://en.wikipedia.org, 26th' August 2010. [Online]. Available: http://commons.wikimedia.org/wiki/File:Graphen.jpg

[47] S. Iijima, "Helical microtubules of graphitic carbon," *nature*, vol. 354, no. 6348, pp. 56–58, 1991.

[48] N. G. Chopra, R. Luyken, K. Cherrey, V. H. Crespi, M. L. Cohen, S. G. Louie, and A. Zettl, "Boron nitride nanotubes," *Science*, vol. 269, no. 5226, pp. 966–967, 1995.

[49] R. Tenne, L. Margulis, M. Genut, and G. Hodes, "Polyhedral and cylindrical structures of tungsten disulphide," *Nature*, vol. 360, no. 6403, pp. 444–446, 1992.

[50] A. Zettl, "Chapter 1 nanotubes: an experimental overview," in *Carbon Nanotubes: Quantum Cylinders of Graphene*, ser. Contemporary Concepts of Condensed Matter Science, S. Saito and A. Zettl, Eds. Elsevier, 2008, vol. 3, pp. 1 – 27. [Online]. Available: http://www.sciencedirect.com/science/article/pii/S1572093408000012

[51] X. Wang, Q. Li, J. Xie, Z. Jin, J. Wang, Y. Li, K. Jiang, and S. Fan, "Fabrication of ultralong and electrically uniform single-walled carbon nanotubes on clean substrates," *Nano Letters*, vol. 9, no. 9, pp. 3137–3141, 2009.

[52] A. G. O. Ozgultekin, "Characterization of cnt doped carbon fiber polymer composites," Master's thesis, Lulea University of Technology, Department of Engineering Sciences and Mathematics, Sweden, May, 2012. [Online]. Available: http://pure.ltu.se/portal/files/37029356/LTU-EX-2012-36998244.pdf

[53] G. Templeton, "Scientists build the first carbon nanotube computer, change computing world forever," ExtremeTech, September 26 2013. [Online]. Available: http://www.extremetech.com/wp-content/uploads/2013/09/nanotube.article.jpg

[54] P. McEuen, M. S. Fuhrer, and H. Park, "Single-walled carbon nanotube electronics," *Nanotechnology, IEEE Transactions on*, vol. 1, no. 1, pp. 78–85, 2002.

[55] B. J. C. Thomas, A. R. Boccaccini, and M. S. P. Shaffer, "Multi-walled carbon nanotube coatings using electrophoretic deposition (epd)," *Journal of the American Ceramic Society*, vol. 88, no. 4, pp. 980–982, 2005. [Online]. Available: http://dx.doi.org/10.1111/j.1551-2916.2005.00155.x

[56] E. Flahaut, R. Bacsa, A. Peigney, and C. Laurent, "Gram-scale ccvd synthesis of double-walled carbon nanotubes," *Chem. Commun.*, pp. 1442–1443, 2003. [Online]. Available: http://dx.doi.org/10.1039/B301514A

[57] E. Wieser, "Multi-walled carbon nanotube," http://en.wikipedia.org, 27 December 2010. [Online]. Available: http://en.wikipedia.org/wiki/File:Multi-walled_Carbon_Nanotube.png

[58] J. Prasek, J. Drbohlavova, J. Chomoucka, J. Hubalek, O. Jasek, V. Adam, and R. Kizek, "Methods for carbon nanotubes synthesis-review," *J. Mater. Chem.*, vol. 21, pp. 15 872–15 884, 2011. [Online]. Available: http://dx.doi.org/10.1039/C1JM12254A

[59] J. P. Gore and A. Sane, "Flame synthesis of carbon nanotubes," in *Carbon Nanotubes - Synthesis, Characterization, Applications*. July'20, 2011, n1 16801. [Online]. Available: http://www.intechopen.com/books/carbon-nanotubes-synthesis-characterization-applications/flame-synthesis-of-carbon-nanotubes

[60] P. G. Collins and P. Avouris, "Nanotubes for electronics," *Scientific American*, vol. 283, no. 6, pp. 62–69, 2000.

[61] P. Sigmund, "Sputtering by ion bombardment theoretical concepts," in *Sputtering by Particle Bombardment I*, ser. Topics in Applied Physics, R. Behrisch, Ed. Springer Berlin Heidelberg, 1981, vol. 47, pp. 9–71. [Online]. Available: http://dx.doi.org/10.1007/3540105212_7

[62] T. Tesfamichael, "Characterization of selective solar absorbers: Experimental and theoretical modeling," *ACTA University Uppsala,*, 2000.

[63] J. Prasek, J. Drbohlavova, J. Chomoucka, J. Hubalek, O. Jasek, V. Adam, and R. Kizek, "Methods for carbon nanotubes synthesis-review," *J. Mater. Chem.*, vol. 21, pp. 15 872–15 884, 2011. [Online]. Available: http://dx.doi.org/10.1039/C1JM12254A

[64] K. Wu, "Advanced materials and fabrication methods for organic solar cells," *Lulea University Of Technology*, 2010.

[65] A. Hartman, "Mechanical measurement of individual carbon nanotubes using mems and the s100 nanomanipulator," Zyvex Corporation, Tech. Rep., 2006, 9706. [Online]. Available: http://www.zyvex.com/Documents/9706.PDF

[66] M.-F. Yu, O. Lourie, M. J. Dyer, K. Moloni, T. F. Kelly, and R. S. Ruoff, "Strength and breaking mechanism of multiwalled carbon nanotubes under tensile load," *Science*, vol. 287, no. 5453, pp. 637–640, 2000. [Online]. Available: http://www.sciencemag.org/content/287/5453/637.abstract

[67] A. W. Coats and J. P. Redfern, "Thermogravimetric analysis. a review," *Analyst*, vol. 88, pp. 906–924, 1963. [Online]. Available: http://dx.doi.org/10.1039/AN9638800906

[68] P. D. H. Foll, "Semiconductor technology," University of Kiel, Faculty of Engineering, Denmark, October 2011. [Online]. Available: http://www.tf.uni-kiel.de/matwis/amat/semitech_en/kap_3/backbone/r3_1_1.pdf

[69] R. Casten, "Algebraic approaches to nuclear structure. interacting boson and fermion models," 1994. [Online]. Available: http://www.tandfonline.com/doi/abs/10.1080/00107519408222096#.UtLNZ7QdCAY

[70] H. Hsiao, "Chapter 21 optical properties," Online:Tunghai University, 30'March 2009. [Online]. Available: http://phys.thu.edu.tw/~hlhsiao/mse-web_ch21.pdf

[71] R. A. Messenger and J. Ventre, *Photovoltaic systems engineering*, 3rd ed. CRC press, 2010.

[72] G. A. Niklasson, C. G. Granqvist, and O. Hunderi, "Effective medium models for the optical properties of inhomogeneous materials," *Appl. Opt.*, vol. 20, no. 1, pp. 26–30, Jan 1981. [Online]. Available: http://ao.osa.org/abstract.cfm?URI=ao-20-1-26

[73] L. Chen, H. Yang, M. Tao, and W. Zhou, "Microstructured anti-reflection surface design for the omni-directional solar cells," *Proc. SPIE*, vol. 7046, pp. 704 608–704 608–11, 2008. [Online]. Available: http://dx.doi.org/10.1117/12.794071

[74] J. W. Company, "Ellipsometry measurements," http://www.jawoollam.com, April 27 2014. [Online]. Available: http://www.jawoollam.com/tutorial_4.html

[75] ——, "Dielectric function," J.A. Woollam Company-tutorial, May 12 2014. [Online]. Available: http://www.jawoollam.com/dielectric_function.html

[76] B. Stagg and T. Charalampopoulos, "Refractive indices of pyrolytic graphite, amorphous carbon, and flame soot in the temperature range 25Âř to 600Âřc," *Combustion and Flame*, vol. 94, no. 4, pp. 381 – 396, 1993. [Online]. Available: http://www.sciencedirect.com/science/article/pii/001021809390121I

[77] S. A. Alterovitz, *Amorphous hydrogenated "Diamond Like" carbon films and are evaporated carbon films(Handbook of optical constant of solid-II)*. Academic press, 1991, iSBN 0 12 544422 2.

[78] E. T. Arakawa, S. M. Dolfini, J. C. Ashley, and M. W. Williams, "Arc-evaporated carbon films: Optical properties and electron mean free paths," *Phys. Rev. B*, vol. 31, pp. 8097–8101, Jun 1985. [Online]. Available: http://link.aps.org/doi/10.1103/PhysRevB.31.8097

[79] J. W. Weber, V. E. Calado, and M. C. M. Van de Sanden, "Optical constants of graphene measured by spectroscopic ellipsometry," *Applied Physics Letters*, vol. 97, no. 9, pp. 091 904–091 904–3, Aug 2010.

[80] H. Soetedjo, M. F. Mora, and C. D. Garcia, "Optical properties of single-wall carbon nanotube films deposited on si/sio2 wafers," *Thin Solid Films*, vol. 518, no. 14, pp. 3954 – 3959, 2010. [Online]. Available: http://www.sciencedirect.com/science/article/pii/S0040609010002191

[81] E. D. Palik, *Handbook of optical constants of solids*. Academic press, 1998, vol. 3.

[82] J. W. Company, "Optical constants," J.A. Woollam Company-tutorial, May 12 2014. [Online]. Available: http://www.jawoollam.com/tutorial_7.html

[83] T. Lichtenstein and T. Lichtenstein, *Handbook of thin film materials*. College of Engineering and Applied Science, University of Rochester, 1979.

[84] P. L. McEuen, M. S. Fuhrer, and H. Park, "Single-walled carbon nanotube electronics," *IEEE transactions on nanotechnology*, vol. 1, no. 1, pp. 78–85, 2002.

[85] Fluxim, *Semiconducting Thin Film Optics Simulation Software (setfos)*, 3rd ed., Fluxim AG, 2014. [Online]. Available: http://www.oledw.com/uploads/soft/pdf/setfos_manual_3.pdf

Appendix

Table 9.1: Refractive index of aluminum [75].

Wavelength(nm)	**n**	**k**
300	0.2169982	2.982331
310	0.2314807	3.092004
320	0.2441945	3.198823
330	0.2575465	3.305539
340	0.2716037	3.412406
350	0.2900822	3.54058
360	0.3053637	3.648751
370	0.3218582	3.757369
380	0.3424799	3.88058
390	0.3608463	3.979542
400	0.3796473	4.082876
410	0.4002459	4.188316
420	0.4214116	4.292106
430	0.4440565	4.396783
440	0.4654078	4.500599
450	0.4879282	4.604027
460	0.5122834	4.706527
470	0.538407	4.810853
480	0.5644833	4.914279
490	0.5922493	5.018071
500	0.6191595	5.118837
510	0.6459123	5.220763
520	0.6766292	5.321967
530	0.7073957	5.423059
540	0.7398599	5.523573
550	0.7725671	5.622132

Continued on next page

Table 9.1 – *Continued from previous page*

Wavelength(nm)	**n**	**k**
560	0.8068635	5.721302
570	0.8431525	5.820921
580	0.8797123	5.917523
590	0.919714	6.012587
600	0.9609698	6.113433
610	1.005489	6.205347
620	1.047717	6.300925
630	1.092922	6.392527
640	1.141207	6.482915
650	1.193956	6.572276
660	1.244376	6.659096
670	1.300197	6.741486
680	1.357039	6.822009
690	1.418723	6.901422
700	1.480797	6.97521
710	1.546586	7.041971
720	1.614953	7.109311
730	1.688431	7.166531
740	1.758443	7.221682
750	1.833182	7.262954
760	1.916784	7.294995
770	1.990925	7.315523
780	2.06884	7.314221
790	2.134087	7.302088
800	2.187829	7.272347
810	2.221816	7.225925
820	2.237131	7.17582
830	2.221914	7.12382
840	2.167254	7.078475
850	2.09148	7.049016
860	2.004554	7.048155
870	1.911496	7.067503
880	1.809762	7.104741
890	1.716822	7.15927
900	1.635215	7.232685
910	1.552198	7.316956
920	1.499707	7.414795
930	1.432331	7.508859

Continued on next page

Table 9.1 – *Continued from previous page*

Wavelength(nm)	**n**	**k**
940	1.389026	7.610199
950	1.347538	7.721204
960	1.293588	7.816066
970	1.253106	7.934302
980	1.217073	8.034137
990	1.19072	8.143808
1000	1.158706	8.254839

Table 9.2: Refractive index of silica (SiO_2) [81].

Wavelength(nm)	**n**	**k**
300	1.48788	0
310	1.485344	0
320	1.482975	0
330	1.480601	0
340	1.478828	0
350	1.477072	0
360	1.475314	0
370	1.473997	0
380	1.472734	0
390	1.47147	0
400	1.470205	0
410	1.469113	0
420	1.468174	0
430	1.467235	0
440	1.466375	0
450	1.465625	0
460	1.464875	0
470	1.46416	0
480	1.463567	0
490	1.462974	0
500	1.46238	0
510	1.461803	0
520	1.461326	0
530	1.460849	0
540	1.460371	0
550	1.459925	0
560	1.459527	0
570	1.459129	0
580	1.458743	0
590	1.458388	0
600	1.458076	0
610	1.457765	0
620	1.457453	0
630	1.457141	0
640	1.456829	0
650	1.456547	0

Continued on next page

Table 9.2 – *Continued from previous page*

Wavelength(nm)	**n**	**k**
660	1.456285	0
670	1.456027	0
680	1.455787	0
690	1.455547	0
700	1.455306	0
710	1.455086	0
720	1.454903	0
730	1.454719	0
740	1.454536	0
750	1.454353	0
760	1.454169	0
770	1.453986	0
780	1.453803	0
790	1.453619	0
800	1.453436	0
810	1.453252	0
820	1.453069	0
830	1.452886	0
840	1.452702	0
850	1.452519	0
860	1.452362	0
870	1.452213	0
880	1.452065	0
890	1.451916	0
900	1.451775	0
910	1.451641	0
920	1.451508	0
930	1.451374	0
940	1.45124	0
950	1.451106	0
960	1.450973	0
970	1.450839	0
980	1.450705	0
990	1.450571	0
1000	1.450437	0
1010	1.450304	0
1020	1.450178	0
1030	1.450059	0

Continued on next page

Table 9.2 – *Continued from previous page*

Wavelength(nm)	**n**	**k**
1040	1.449939	0
1050	1.44982	0
1060	1.4497	0
1070	1.449581	0
1080	1.449461	0
1090	1.449342	0
1100	1.449222	0
1110	1.449102	0
1120	1.448983	0
1130	1.448864	0
1140	1.44875	0
1150	1.448636	0
1160	1.448521	0
1170	1.448407	0
1180	1.448293	0
1190	1.448179	0
1200	1.448064	0
1210	1.44795	0
1220	1.447836	0
1230	1.447722	0
1240	1.447607	0
1250	1.447493	0
1260	1.447379	0
1270	1.447264	0
1280	1.44715	0
1290	1.447036	0
1300	1.446921	0
1310	1.446807	0
1320	1.446693	0
1330	1.446578	0
1340	1.446464	0
1350	1.44635	0
1360	1.446235	0
1370	1.44612	0
1380	1.446004	0
1390	1.445889	0
1400	1.445773	0
1410	1.445658	0

Continued on next page

Table 9.2 – *Continued from previous page*

Wavelength(nm)	**n**	**k**
1420	1.445542	0
1430	1.445427	0
1440	1.445311	0
1450	1.445195	0
1460	1.44508	0
1470	1.444964	0
1480	1.444844	0
1490	1.444723	0
1500	1.444603	0
1510	1.444483	0
1520	1.444363	0
1530	1.444242	0
1540	1.444122	0
1550	1.444002	0
1560	1.443881	0
1570	1.443761	0
1580	1.443641	0
1590	1.44352	0
1600	1.4434	0
1610	1.443279	0
1620	1.443159	0
1630	1.443039	0
1640	1.442918	0
1650	1.442798	0
1660	1.442677	0
1670	1.44255	0
1680	1.442422	0
1690	1.442294	0
1700	1.442166	0

Table 9.3: Refractive index of titania (TiO_2) [82].

Wavelength(nm)	**n**	**k**
300	2.5177	0.3858
310	2.4624	0.24473
320	2.3963	0.14452
330	2.3168	0.072944
340	2.2253	0.0064205
350	2.1795	0.018143
360	2.1359	0.014927
370	2.1022	0.012507
380	2.0763	0.012523
390	2.0554	0.010946
400	2.0363	0.010342
410	2.0203	0.0089487
420	2.0065	0.0095484
430	1.9953	0.0086407
440	1.9833	0.008016301
450	1.9747	0.0071324
460	1.9658	0.0075171
470	1.9581	0.0070122
480	1.9515	0.0062255
490	1.9453	0.0040506
500	1.9369	0.0044365
510	1.9294	0.0040372
520	1.9246	0.0024101
530	1.9241	0.0011548
540	1.9162	0.0028028
550	1.9131	0.0025893
560	1.9091	0.0019554
570	1.9073	0.0013169
580	1.9023	0.001394
590	1.8988	0.0010177
600	1.8973	0.0015459
610	1.8942	0.0021222
620	1.8921	0.0013289
630	1.8904	0.0017003
640	1.8878	0.0010397
650	1.8854	0.00086698

Continued on next page

Table 9.3 – *Continued from previous page*

Wavelength(nm)	**n**	**k**
660	1.8835	0.00085122
670	1.8808	0
680	1.8795	0.00063565
690	1.8782	0
700	1.8762	2.7786e-005
710	1.8746	8.2508e-005
720	1.8735	0
730	1.8717	0
740	1.8713	0
750	1.8693	0
760	1.8684	0
770	1.8667	0
780	1.8654	0
790	1.8645	0
800	1.8625	0
810	1.8616	0
820	1.8609	0
830	1.8608	0
840	1.8594	0
850	1.8582	0
860	1.8577	0
870	1.8569	0
880	1.8558	0
890	1.8547	0
900	1.854	0
910	1.8535	0
920	1.8533	0
930	1.8523	0
940	1.8517	0
950	1.851	0
960	1.8505	0
970	1.85	0
980	1.8497	0
990	1.8487	0
1000	1.8482	0
1010	1.8477	0
1020	1.847199	0
1030	1.846699	0

Continued on next page

Table 9.3 – *Continued from previous page*

Wavelength(nm)	**n**	**k**
1040	1.846198	0
1050	1.845697	0
1060	1.845196	0
1070	1.844695	0
1080	1.844194	0
1090	1.843693	0
1100	1.843191	0
1110	1.84269	0
1120	1.842188	0
1130	1.841686	0
1140	1.841184	0
1150	1.840682	0
1160	1.840179	0
1170	1.839677	0
1180	1.839174	0
1190	1.838672	0
1200	1.838169	0
1210	1.837666	0
1220	1.837163	0
1230	1.836659	0
1240	1.836156	0
1250	1.835652	0
1260	1.835149	0
1270	1.834645	0
1280	1.834141	0
1290	1.833637	0
1300	1.833133	0
1310	1.832628	0
1320	1.832124	0
1330	1.831619	0
1340	1.831114	0
1350	1.830609	0
1360	1.830104	0
1370	1.829599	0
1380	1.829094	0
1390	1.828588	0
1400	1.828082	0
1410	1.827577	0

Continued on next page

Table 9.3 – *Continued from previous page*

Wavelength(nm)	**n**	**k**
1420	1.827071	0
1430	1.826565	0
1440	1.826059	0
1450	1.825552	0
1460	1.825046	0
1470	1.824539	0
1480	1.824032	0
1490	1.823525	0
1500	1.823018	0
1510	1.822511	0
1520	1.822004	0
1530	1.821496	0
1540	1.820989	0
1550	1.820481	0
1560	1.819973	0
1570	1.819465	0
1580	1.818957	0
1590	1.818449	0
1600	1.81794	0
1610	1.817432	0
1620	1.816923	0
1630	1.816414	0
1640	1.815905	0
1650	1.815396	0
1660	1.814887	0
1670	1.814377	0
1680	1.813868	0
1690	1.813358	0
1700	1.812848	0

Table 9.4: Refractive index of alumina (Al_2O_3) [83].

Wavelength(nm)	**n**	**k**
300	1.807956	0
310	1.805038	0
320	1.802116	0
330	1.799672	0
340	1.797225	0
350	1.795147	0
360	1.793066	0
370	1.791275	0
380	1.789483	0
390	1.787923	0
400	1.786361	0
410	1.784988	0
420	1.783614	0
430	1.782395	0
440	1.781176	0
450	1.780086	0
460	1.778996	0
470	1.778015	0
480	1.777033	0
490	1.776145	0
500	1.775257	0
510	1.774449	0
520	1.77364	0
530	1.772901	0
540	1.772161	0
550	1.771483	0
560	1.770804	0
570	1.770178	0
580	1.769552	0
590	1.768973	0
600	1.768393	0
610	1.767856	0
620	1.767318	0
630	1.766818	0
640	1.766317	0
650	1.76585	0

Continued on next page

Table 9.4 – *Continued from previous page*

Wavelength(nm)	**n**	**k**
660	1.765383	0
670	1.764946	0
680	1.764508	0
690	1.764098	0
700	1.763688	0
710	1.763303	0
720	1.762918	0
730	1.762555	0
740	1.762191	0
750	1.761849	0
760	1.761506	0
770	1.761182	0
780	1.760858	0
790	1.760552	0
800	1.760245	0
810	1.759954	0
820	1.759663	0
830	1.759387	0
840	1.759111	0
850	1.758848	0
860	1.758585	0
870	1.758335	0
880	1.758085	0
890	1.757847	0
900	1.757608	0
910	1.75737	0
920	1.757131	0
930	1.756892	0
940	1.756654	0
950	1.756415	0
960	1.756176	0
970	1.755938	0
980	1.755699	0
990	1.75546	0
1000	1.755221	0
1010	1.754983	0
1020	1.754744	0
1030	1.754505	0

Continued on next page

Table 9.4 – *Continued from previous page*

Wavelength(nm)	**n**	**k**
1040	1.754266	0
1050	1.754027	0
1060	1.753788	0
1070	1.753549	0
1080	1.75331	0
1090	1.753071	0
1100	1.752831	0
1110	1.752592	0
1120	1.752353	0
1130	1.752114	0
1140	1.751875	0
1150	1.751635	0
1160	1.751396	0
1170	1.751157	0
1180	1.750917	0
1190	1.750678	0
1200	1.750438	0
1210	1.750199	0
1220	1.749959	0
1230	1.74972	0
1240	1.74948	0
1250	1.74924	0
1260	1.749001	0
1270	1.748761	0
1280	1.748521	0
1290	1.748282	0
1300	1.748042	0
1310	1.747802	0
1320	1.747562	0
1330	1.747322	0
1340	1.747082	0
1350	1.746842	0
1360	1.746602	0
1370	1.746362	0
1380	1.746122	0
1390	1.745882	0
1400	1.745642	0
1410	1.745402	0

Continued on next page

Table 9.4 – *Continued from previous page*

Wavelength(nm)	**n**	**k**
1420	1.745162	0
1430	1.744921	0
1440	1.744681	0
1450	1.744441	0
1460	1.744201	0
1470	1.74396	0
1480	1.74372	0
1490	1.743479	0
1500	1.743239	0
1510	1.742998	0
1520	1.742758	0
1530	1.742517	0
1540	1.742277	0
1550	1.742036	0
1560	1.741796	0
1570	1.741555	0
1580	1.741314	0
1590	1.741073	0
1600	1.740833	0
1610	1.740592	0
1620	1.740351	0
1630	1.74011	0
1640	1.739869	0
1650	1.739628	0
1660	1.739387	0
1670	1.739146	0
1680	1.738905	0
1690	1.738664	0
1700	1.738423	0

Table 9.5: Refractive index of amorphous carbon at 25°C [76].

Wavelength(nm)	**n**	**k**
400	2.175	1.206
433	2.258	1.102
467	2.323	1.025
500	2.321	0.991
533	2.331	0.981
567	2.337	0.977
600	2.343	0.982
633	2.356	0.986
667	2.371	1.019
700	2.434	1.005

Table 9.6: Refractive index of graphene [79].

Wavelength(nm)	**n**	**k**
200	1.45	0.200
250	1.43	2.400
300	3.35	2.000
350	3.25	1.100
400	2.70	1.150
450	2.69	1.200
500	2.695	1.270
550	2.694	1.340
600	2.698	1.410
650	2.730	1.480
700	2.780	1.550
750	2.830	1.620
800	2.850	1.690
850	2.870	1.760
900	2.930	1.810
950	2.960	1.860
1000	3.000	1.900

Table 9.7: Refractive index of soot at 25°C [76].

Wavelength(nm)	**n**	**k**
400	1.396	0.403
433	1.434	0.376
467	1.462	0.360
500	1.484	0.347
533	1.496	0.352
567	1.536	0.374
600	1.522	0.355
633	1.527	0.376
667	1.544	0.357
700	1.550	0.367

Table 9.8: Refractive index of graphite at 25°C [76].

Wavelength(nm)	**n**	**k**
400	2.377	1.656
433	2.529	1.528
467	2.637	1.422
500	2.641	1.386
533	2.648	1.383
567	2.649	1.395
600	2.656	1.394
633	2.684	1.399
667	2.717	1.433
700	2.767	1.438

Table 9.9: Refractive index of AEC [77].

Wavelength(nm)	**n**	**k**
124.0	1.66	0.795
137.8	1.7	0.713
155.0	1.71	0.656
177.1	1.7	0.628
206.6	1.7	0.646
248.0	1.73	0.712
310.0	1.84	0.808
326.3	1.9	0.91
344.4	1.92	0.92
364.7	2.0	0.92
388.4	2.06	0.91
413.3	2.11	0.9
442.8	2.17	0.89
478.9	2.24	0.88
516.6	2.3	0.87
563.6	2.38	0.82
619.9	2.43	0.75
688.8	2.43	0.7
774.9	2.33	0.71
885.6	2.24	0.8
1003.3	2.26	1.09
1240.0	2.63	1.47
1550.0	3.34	1.63
1771.0	3.67	1.6
2066.0	3.73	1.54

Table 9.10: Refractive index of SWCNT(High) [80].

Wavelength(nm)	**n**	**k**
270	1.42	0.176
300	1.43	0.1762
325	1.439	0.1764
350	1.44	0.1767
375	1.47	0.1769
400	1.52	0.1900
425	1.525	0.195
450	1.575	0.197
475	1.58	0.199
500	1.581	0.200
525	1.583	0.205
550	1.5835	0.210
575	1.584	0.215
600	1.5843	0.219
625	1.5844	0.223
650	1.5845	0.228
675	1.5846	0.233
700	1.5848	0.237
725	1.585	0.241
750	1.586	0.243
775	1.588	0.245
800	1.59	0.246
825	1.60	0.246
850	1.61	0.247
875	1.63	0.245
900	1.64	0.250

Table 9.11: Refractive index of SWCNT(Low) [80].

Wavelength(nm)	**n**	**k**
225	1.00775	1.001700
250	1.00795	1.001710
275	1.00900	1.001720
300	1.00805	1.001710
325	1.00890	1.001730
350	1.00950	1.001735
375	1.00100	1.001740
400	1.00100	1.001740
425	1.00100	1.001750
450	1.00100	1.001750
475	1.00100	1.001750
500	1.00100	1.001750
525	1.00125	1.001780
550	1.00125	1.001780
575	1.00125	1.001780
600	1.00125	1.001780
625	1.00125	1.001780
650	1.00125	1.001780
675	1.00125	1.001780
700	1.00125	1.001800
725	1.00135	1.001800
750	1.00125	1.001800
775	1.00125	1.001800
800	1.00180	1.001800
825	1.00180	1.001800
850	1.00180	1.001800
875	1.00180	1.001800
900	1.00180	1.001800